A Mystery of Muscle: Examining Mechanisms of Toxicity in Polyglutamine Disease

by

Samir Nath

A dissertation submitted in partial fulfillment
of the requirements for the degree of
Doctor of Philosophy
(Cellular and Molecular Biology)
in the University of Michigan
2020

Doctoral Committee:

Professor Andrew P. Lieberman, Chair
Professor Anthony Antonellis
Professor Yoichi Osawa
Assistant Professor Sriram Venneti

Samir Nath

nathsr@med.umich.edu

ORCID iD: 0000-0001-6336-7991

ACKNOWLEDGEMENTS

This dissertation is dedicated to several key individuals and groups who have collectively made this work possible. This work is far more a credit to others than myself, and to thank all involved adequately would require the length of this thesis.

First, it is dedicated to my wife, Kathleen. Her love and continuous support made the work described within these chapters possible. Throughout my thesis she has astounded me with her ability to quickly grasp the studies described within, listened patiently to every practice talk I have given, and sacrificed her own time and energy towards enabling my completion of this work. Without her, the work detailed in these chapters would not exist.

Second, it is dedicated to my parents whose love and sacrifice has enabled the years of education that have culminated in this thesis. They are a constant source of inspiration and motivation and I am grateful for all they have taught me. I would not be where I am without them.

Third, it is dedicated to the many friends who have been a constant source of joy and support. I have been continuously inspired by the community around me and am honored to be a member of it.

Fourth, it is dedicated to my mentor, Dr. Andrew Lieberman, whose guidance has been invaluable in performing the work within this thesis. His continuous mentorship has shaped both my world view and scientific thinking. His dedication to scientific excellence and mentoring the

next generation are aspects I aspire to provide for others, and he has been a constant role model for my own career. Without his support, the work herein would not exist.

Fifth, it is dedicated to the members of my thesis committee, who have provided mentorship, input and guidance throughout my thesis. This includes all current members listed above, and former member Dr. Sharlene Day, who have made significant intellectual contributions throughout the completion of this work.

Sixth, it is dedicated to the co-authors who have significantly contributed to the work within. This includes Dr. Sokol Todi and Gregory Marsh, who contributed the drosophila data in Chapter 3, Dr. Maria Pennuto, Caterina Marchioretti, and Dr. Gianni Soraru who together contributed the patient tissue data included in Chapter 4, and Dr. Gillian Bates, Samuel Jones, and Emily CE Danby who provided the R6/2 mouse tissue used in Chapter 4. I would additionally like to thank the contributors who have worked with me in the Lieberman lab.

Seventh, it is dedicated to the animals involved in the studies described within this work and in all scientific studies. Their sacrifice is ultimate, and it is given without compensation. Through time this sacrifice has saved countless human lives, and it is my hope that the sacrifices made to this thesis will contribute an additional building block towards developing therapies for those suffering from untreatable illnesses.

Finally, it is dedicated to the patient community. Their hope and support directly enabled the creation of many tools used within these pages. They are the motivating factor for my studies, and I dedicate my current and future work to repaying their incredible contributions.

TABLE OF CONTENTS

LIST OF FIGURES

LIST OF TABLES

ABSTRACT

Polyglutamine disorders encompass nine uniformly fatal diseases for which there are no disease course altering therapies. This group of related diseases share a key source: expansion of a CAG microsatellite repeat in genes which code for widely different proteins. Downstream of expansion, protein misfolding and oligomerization lead to gain-of-function proteotoxicity. Ultimately, this toxicity leads to disruption of a multitude of signaling pathways, altered homeostasis, and selective cell death. The first discovered polyglutamine disease is caused by an expansion of a CAG microsatellite repeat in the gene coding for androgen receptor and is called Kennedy's Disease or Spinobulbar Muscular Atrophy (SBMA). Patients with this repeat expansion develop progressive degeneration of the neuromuscular system and are ultimately wheelchair bound.

While the cause of SBMA is well-defined, the downstream consequences of receptor expansion remain poorly understood. Recently, several studies have implicated skeletal muscle as playing an important role in the pathogenesis of disease. However, despite two decades of study, the cause of muscle atrophy in SBMA remains poorly defined.

This thesis will first outline polyglutamine diseases with a focus on SBMA. In Chapter 2, I discuss the data characterizing protein quality control in polyglutamine disease with a focus on the ubiquitin-proteasome system (UPS), which is both an important therapeutic target and critical mediator of muscle atrophy downstream of other sources. In Chapter 3, this thesis provides primary data demonstrating the surprising finding of age-dependent proteasome impairment, suggesting the proteasome does not account for muscle atrophy in SBMA. In Chapter 4, this

thesis will delve examine potential sources of muscle atrophy in SBMA, implicating a key regulator of muscle hypertrophy as a novel therapeutic target in disease. In Chapter 5, the question of whether SBMA is accurately characterized as a neurodegenerative disease will be discussed, with primary data provided comparing changes in SBMA skeletal muscle to those caused by models of myopathy and neuropathy. Together, this data identifies a novel source of muscle atrophy downstream of polyglutamine proteins and defines several key questions for future studies.

CHAPTER I

Polyglutamine Proteins Drive a Family of Disease

1.1 Overview of Polyglutamine Disease

Polyglutamine (polyQ) diseases are a family of invariably fatal adult-onset neurodegenerative disorders [1, 2]. These diseases are characterized by chronic and progressive neurodegeneration of specific populations of neurons. All polyQ disorders are linked by one common etiology: expansion of a glutamine tract in a constitutively expressed protein.

The finding that these disorders are caused by a single mutation has led to a wealth of research seeking to understand the importance and function of polyQ tracts, which are long repetitive stretches of the amino acid glutamine. CAG repeats, which code for glutamine, are present in almost 300 genes in the human genome. Of those tracts, only 33 are present in protein coding regions. While the precise function of polyQ tracts remains poorly defined, current research suggests a role in stabilizing protein-protein interactions [3]. Increases in polyglutamine tract length have been implicated in at least nine distinct but related diseases [2]. Downstream of pathogenic expansion, polyQ proteins dysregulate several cellular signaling and quality control pathways [4-16]. Understanding the similarities and differences in these disorders is critical to developing tailored therapeutic strategies. The similarities between these diseases are readily apparent in their genetic causes and clinical presentation.

1.2 Polyglutamine Diseases Share Clinical Characteristics

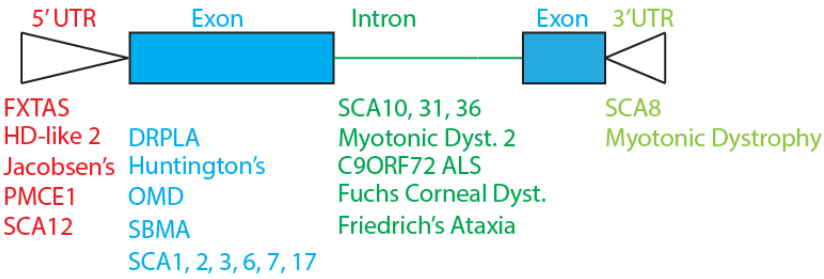

Figure 1. Location of microsatellite expansions by disease. Location of the microsatellite repeat in a gene is categorized by disease. 5'UTR = 5' Untranslated region, 3' UTR = 3' Untranslated Region, FXTAS = Fragile X Tremor Ataxia Syndrome, SCA = Spinocerebellar Ataxia, DRPLA = Dentatorubropallidoluysian Atrophy, SBMA = Spinobulbar Muscular Atrophy, HD = Huntington's Disease, PMCE = Progressive Myoclonic Epilepsy Type I, OMD = Oculopharyngeal Muscular Dystrophy.

In the thirty years since discovery, many pathogenic microsatellite expansions in a diverse array of genes have been identified. These expansions occur in all regions of a gene, including the 5' UTR, exons, introns, and the 3' UTR (Figure 1). In the case of polyglutamine expansion, nine different diseases were found to be caused by a CAG microsatellite expansion, which is found in a protein coding exonic region (Figure 1, blue). These diseases include Spinobulbar Muscular Atrophy (SBMA), Huntington's Disease, Spinocerebellar Ataxia Types 1, 2, 3, 6, 7, and 17, and Dentatorubropallidoluysian Atrophy [2].

Polyglutamine diseases share several key features. Most of these diseases occur in midlife, with earlier symptom onset correlating with increasing numbers of repeats. While symptom onset is repeat length dependent, rate of progression after onset is independent of repeat number [2]. This suggests that increasing repeat length promotes the pathogenic changes involved in disease onset, but once disease progression begins symptoms follow a predictable course.

These diseases also share instability of the microsatellite expansion, with paternal transmission trending towards further increased repeat expansions and anticipation [2, 17, 18].

Disease	Gene	Q Threshold
SBMA	Androgen receptor	38
HD	Huntingtin	36
DRPLA	Atrophin-1	49
SCA1	Ataxin-1	39
SCA2	Ataxin-2	32
SCA3	Ataxin-3	55
SCA6	Cav2.1	21
SCA7	Ataxin-7	38
SCA17	TATA-binding protein	45

Table 1. Polyglutamine expansion pathogenic threshold by gene.

Each of these diseases has a pathogenic threshold of repeat number, above which very high penetrance is seen (Table 1).

Finally, these diseases show misfolding of the protein product containing the expanded polyQ tract as well as its subsequent aggregation into intracellular inclusions [8, 19-22]. Downstream of this misfolding, several cellular pathways are disrupted, ultimately leading to cell death [4-16]. Because these expansions occur in widely differing proteins but lead to this panel of common features, a gain-of-function proteotoxic mechanism is thought to be responsible for disease [2, 18].

While gain of function is suggested as the cause of the neurodegenerative phenotype, polyQ expansion also leads to misfolding and impairment of the protein's normal function [4, 6, 14]. For example, expansion of the glutamine tract in androgen receptor leads to misfolding of the protein, impaired transactivation, and endocrine clinical features mimicking androgen insensitivity including gynecomastia and testicular atrophy [4, 6, 23]. PolyQ diseases are ideal candidates for pathogenic study downstream of a misfolded protein, as they represent monogenic, highly or completely penetrant illnesses. While the function of most proteins containing a polyQ tract expansion is not well characterized, SBMA is caused by expansion of the androgen receptor, which has a well understood canonical function. The well-characterized disease-causing protein makes it ideal for studying the complexities of disease pathophysiology. My thesis takes advantage of this established knowledge by using SBMA as a model of polyglutamine protein induced toxicity.

1.3 Spinobulbar Muscular Atrophy Clinical Manifestations

Spinal and bulbar muscular atrophy (SBMA) was the first disease found to be caused by expansion of a polyglutamine tract, which is contained in the androgen receptor (AR) gene [24]. Androgen receptor is encoded on the X chromosome, which leads to hemizygous male carriers. The disease phenotype is dependent on the presence of testosterone, the ligand for the androgen receptor [25]. As a result, females heterozygous or homozygous for the mutation do not develop overt disease. Downstream of this mutation, patients develop a robust phenotype in adulthood characterized by neuromuscular and endocrine changes. SBMA patients typically first present with tremor and limb weakness, often of the lower extremities. This motor phenotype is progressive and incorporates additional muscles over time [1, 26]. In addition to weakness, patients develop intense muscle cramps, fasciculations, dysarthria, and dysphagia [23]. Ultimately, patients lose ambulation and are wheelchair-bound. As is the case in other progressive neuromuscular diseases such as ALS, the predominant cause of death in these patients is aspiration pneumonia downstream of dysarthria and bulbar muscle weakness [23]. The mechanism of the neuromuscular phenotype is thought to be toxic gain-of-function of the polyglutamine protein, which will be discussed in depth in this and other chapters [2, 18].

In addition to the neuromuscular phenotype, SBMA patients show signs of androgen insensitivity, such as gynecomastia, testicular atrophy, and infertility [23]. These changes are also age-progressive but are thought to be due to androgen receptor misfolding. This misfolding leads to partial loss-of-function, which is a classic sign of androgen insensitivity. The duality of this phenotype has led to several studies on the role of testosterone, the ligand for androgen receptor, in disease pathogenesis. These studies have demonstrated that testosterone is necessary not only

for receptor transactivation, but plays a critical role in triggering polyQ AR misfolding and subsequent cellular toxicity [25, 27-29].

1.4 PolyQ AR Requires Testosterone for Toxicity

As there is a wealth of information about the canonical functions of AR, this protein makes an ideal candidate for studying downstream toxicity of polyglutamine expansion compared to its wild-type counterpart. Several studies have demonstrated that presence of the polyQ AR alone is insufficient for neuromuscular dysfunction. The polyQ protein requires binding of its ligand, testosterone, to initiate dimerization, nuclear translocation, misfolding, and toxicity [28, 30, 31]. This finding is further supported by studies demonstrating that castration of knock in male mice expressing endogenous levels of the polyQ expansion do not develop the neuromuscular phenotype. Further, adding back testosterone to castrated mice initiates the phenotype in these castrated mice [32]. Additionally, female knock in mice do not develop a neuromuscular phenotype [32]. Initially, it was postulated that due to its position on the X chromosome, the polyQ containing AR chromosome may be selectively inactivated in female cells. However, studies have demonstrated that there is no bias towards inactivation of the mutant allele carrying chromosome [33].

Further supporting the critical role of testosterone in pathogenesis, administration of testosterone to female mice leads to significant reductions in grip strength and an SBMA-like phenotype, demonstrating the need for both the mutant protein and its ligand to drive pathogenesis of disease [32]. These studies have led to several clinical trials examining the therapeutic efficacy of ligand inhibition.

1.5 Therapeutic Modulation of Testosterone in SBMA

SBMA patients are diagnosed by genetic test, but once diagnosed, there are no disease modifying FDA approved treatments [2]. At this time, several clinical trials have been conducted in SBMA populations to address the lack of therapies. Following the discovery that androgen receptor is the causative gene in SBMA, the anti-androgen leuprorelin was tested in SBMA patients. Leuprorelin is a Gonadotropin Releasing Hormone (GnRH) analogue which triggers the release of Leutenizing Hormone (LH) and Follicle Stimulating Hormone (FSH) from the pituitary. LH then stimulates androgen production in the testis. However, GnRH must work in a pulsatile manner to properly release LH and FSH, and when Leuprorelin is given continuously it disrupts this cycle, blocking their release and ultimately the production of androgens. Treatment of mouse models of SBMA with leuprorelin led to robust and almost complete rescue of the neuromuscular phenotype [25]. However, subsequent studies on leuprorelin in clinic have been variable, with some success in an initial phase 2 trial [34], but no significant effect in a subsequent multicenter phase 3 clinical trial [35].

Recently, an additional clinical trial on leuprorelin failed to find a statistically significant difference in the primary endpoint of barium swallow test, which measures bulbar muscle function [36]. However, these results came close to statistical significance in both centers and have led to approval for use in Japan.

There are several suggested reasons for the clear effect of leuprorelin in mice but not humans, including starting post-symptomatically in patients and pre-symptomatically in mice, lack of power to identify disease modifying effects, variability amongst the patient population increasing statistical noise, compensatory induction of AR isoforms which contain the glutamine tract and escape the need for testosterone-mediated transactivation as is seen in castration-

resistant prostate cancer, loss of anabolic effects in skeletal muscle, or a combination of these effects.

1.6 SBMA Patients Show Early Signs of Muscle Dysfunction

While it is known that ligand dependent protein misfolding and aggregation are critical toxicity in SBMA, the specific tissues which are affected and critical to pathogenesis have only recently been established. Among the tissues affected in SBMA, studies in the last decade have demonstrated that skeletal muscle is a critical target that contributes to disease pathogenesis. This concept is supported by clinical observations and data from experimental models. Muscle weakness is a prominent feature in SBMA, and predominantly affects the lower limbs and bulbar muscles [23, 37]. Subjects with SBMA exhibit evidence of muscle toxicity, including myopathic features on muscle biopsy and elevated serum creatine kinase levels that are higher than normally found in purely denervating diseases [38]. Moreover, muscle satellite cells cultured from SBMA patients show androgen-dependent impairment of fusion to form myotubes [39], indicating cell-autonomous toxicity in muscle.

Importantly, studies suggest signs of myopathy occur in advance of neuropathology in SBMA patients. Studies examining the marker of neuronal damage neurofilament light chain, which is elevated under conditions of neurodegeneration, found no increase in SBMA patient CSF, in contrast to ALS cases [38]. Importantly, the only biomarkers altered in SBMA patients were the markers of muscle dysfunction creatinine and creatine kinase [38]. This is further corroborated by a study examining neurofilament heavy chain with similar results [40]. Finally, skeletal muscle MRIs show strikingly different patterns between SBMA and ALS patients, with

SBMA patients showing a higher degree of fatty change in the skeletal muscle [41]. Together, this evidence suggests that SBMA patients have detectable myopathy in advance of detectable neuropathology, that muscle biomarkers correlated with disease severity while neuronal biomarkers do not, and that SBMA patient skeletal muscle is distinct from that of patients with pure motor neuron disease, such as ALS.

1.7 Knock-in Mice Expressing the PolyQ AR Show Early Signs of Myopathy Prior to Neuropathy

Supporting the notion that myopathy is an early disease manifestation, knock-in mice expressing the polyQ AR develop myopathy early in disease course [32]. These features include round fibers with internal nuclei and immunoreactive polyQ AR inclusions [32]. Additionally, muscle mass and diminished survival precede measurable neuropathology despite presence of the polyQ AR in both organs [32]. Together, this evidence was among the first to suggest that myopathy plays an early and important role in SBMA pathogenesis.

As the knock-in mouse was derived by using a humanized exon 1 containing the expanded polyQ tract, it could not be determined whether the neuromuscular phenotype was due to the expanded glutamine tract or the humanized exon 1. To address this concern, a control mouse, the AR21Q mouse, was generated using the same targeting vector with a normal number of glutamines. AR21Q mice do not develop a neuromuscular phenotype [42], demonstrating that the early myopathy of SBMA knock-in mice is due solely to the expanded glutamine tract. This data demonstrates that endogenous levels of polyglutamine androgen receptor leads to early

myopathic change in SBMA mice. As a result of these findings, studies have sought to determine what changes occur in skeletal muscle downstream of polyQ AR expression.

1.8 Pathophysiologic Changes in AR113Q Skeletal Muscle

Recent studies have sought to define pathophysiologic changes in skeletal muscle downstream of polyQ AR using the AR113Q knock-in mouse. In addition to early myopathy, recent studies have found impairments in neuromuscular transmission and deficits in end-plate potential, suggesting defects in skeletal muscle excitation machinery [43]. Surprisingly, AR113Q muscle remains innervated, though junctions show pathological fragmentation [44]. Lack of histologic denervation is surprising, as it is an early feature in other motor neuron diseases such as ALS [45]. However, this evidence suggests that neuromuscular junctions (NMJ) are impaired in SBMA and that pathological NMJ's may cause functional but not histologic denervation.

In addition to NMJ changes, AR113Q muscle shows robust, early change in metabolism. Recent publications have shown marked downregulation of glycolytic enzymes including Gapdh and Hk2 [46, 47]. These changes are accompanied by loss of the transcriptional regulator Nr4a1[46] and alterations in PGC1a signaling [47]. SBMA muscle also displayed altered levels of the metabolites fructose bisphosphate, pyruvate, NAD, and NADP, suggesting dramatic alterations in steady state metabolism [46]. Functionally, SBMA mice expend more energy compared to WT mice and lack the muscle hypertrophy expected from chronic exercise [46]. Together, these findings show a panel of changes occurring inside of skeletal muscle which are functionally relevant for the progressive neuromuscular phenotype.

1.9 Transgenic Mice Show Hormone Dependent Myopathy

Additional evidence for the role of skeletal muscle in SBMA pathogenesis has been provided by transgenic mouse models. Transgenic mice that overexpress the WT AR only in skeletal muscle show hormone-dependent myopathy and motor axon loss [48]. This suggests that at high enough levels in skeletal muscle, WT androgen receptor can trigger myopathy. Similar effects are seen in transgenic mice overexpressing polyQ AR only in muscle, demonstrating that expression in muscle alone can drive a myopathic component of disease [49]. Conversely, overexpression of polyQ AR in neurons alone did not lead to motor neuron death [49]. Together, this evidence demonstrates that skeletal muscle expression is critically important in disease pathogenesis.

1.10 Skeletal Muscle is a Primary Target of Toxicity in Mouse Models of Disease

Several studies have focused on skeletal muscle as a therapeutic target in SBMA. Expression of polyQ AR ubiquitously leads to a neuromuscular phenotype that is rescued when the polyQ protein is selectively deleted in muscle. These mice continue to express the polyQ protein in all other tissue, providing strong evidence that skeletal muscle plays a key role in pathogenesis. Simultaneously, our group has demonstrated that peripheral polyQ AR knockdown by antisense oligonucleotides (ASOs) dramatically ameliorates disease. These ASOs do not cross the blood brain barrier and only reduce levels of peripheral polyQ AR, demonstrating that removal of the CNS protein is not necessary for therapeutic benefit [50]. In support of this notion, administration of ASOs to the CNS showed no benefit in a transgenic model of SBMA [50]. Finally, overexpression of insulin-like growth factor-1, an important muscle trophic factor,

in skeletal muscle ameliorated the disease phenotype [51]. Importantly, a clinical trial of recombinant IGF-1 in SBMA patients led to increased muscle volume. These findings validate the notion that skeletal muscle is a primary therapeutic target in SBMA patients.

1.11 Remaining Questions in SBMA

While this body of evidence indicates an important role for skeletal muscle in the pathogenesis of neuromuscular degeneration in SBMA, the pathways that mediate the critical role of skeletal muscle remain largely unexplored. Of importance, the mechanism of muscle fiber atrophy in SBMA remains poorly defined. This thesis will identify multiple novel dysregulated pathways in skeletal muscle downstream of polyQ AR expression, as well as novel mediators of skeletal muscle atrophy downstream of the mutant protein. In chapter 2, I will discuss a potential role for protein quality control machinery in polyglutamine disease both in terms of dysregulation by polyglutamine proteins and as a therapeutic target. In chapter 3, my findings on implicating age-dependent impairment of the proteasome in SBMA for the first time will be discussed. In chapter 4, I define a novel mechanism of atrophy, MEF2 impairment, in SBMA and demonstrate it's potential as a therapeutic target. In chapter 5, I will compare transcriptomic data from SBMA and Huntington mouse models to models of myopathy and neuropathy as well as suggest future directions for research. It is my hope that this thesis will address fundamental questions about the pathophysiology of polyglutamine proteins in muscle and be used as a foundation for therapeutic strategies in disease.

References

1. Sobue, G., et al., *X-linked recessive bulbospinal neuronopathy. A clinicopathological study.* Brain : a journal of neurology, 1989. **112 (Pt 1)**: p. 209-232.
2. Lieberman, A.P., V.G. Shakkottai, and R.L. Albin, *Polyglutamine Repeats in Neurodegenerative Diseases.* Annu Rev Pathol, 2019. **14**: p. 1-27.
3. Schaefer, M.H., E.E. Wanker, and M.A. Andrade-Navarro, *Evolution and function of CAG/polyglutamine repeats in protein-protein interaction networks.* Nucleic Acids Res, 2012. **40**(10): p. 4273-87.
4. Mhatre, A.N., et al., *Reduced transcriptional regulatory competence of the androgen receptor in X-linked spinal and bulbar muscular atrophy.* Nature genetics, 1993. **5**(2): p. 184-188.
5. Chamberlain, N.L., E.D. Driver, and R.L. Miesfeld, *The length and location of CAG trinucleotide repeats in the androgen receptor N-terminal domain affect transactivation function.* Nucleic acids research, 1994. **22**(15): p. 3181-3186.
6. Kazemi-Esfarjani, P., M.A. Trifiro, and L. Pinsky, *Evidence for a repressive function of the long polyglutamine tract in the human androgen receptor: possible pathogenetic relevance for the (CAG)n-expanded neuronopathies.* Human molecular genetics, 1995. **4**(4): p. 523-527.
7. Mangiarini, L., et al., *Exon 1 of the HD gene with an expanded CAG repeat is sufficient to cause a progressive neurological phenotype in transgenic mice.* Cell, 1996. **87**(3): p. 493-506.
8. Cummings, C.J., et al., *Chaperone suppression of aggregation and altered subcellular proteasome localization imply protein misfolding in SCA1.* Nat Genet, 1998. **19**(2): p. 148-54.
9. Stenoien, D.L., et al., *Polyglutamine-expanded androgen receptors form aggregates that sequester heat shock proteins, proteasome components and SRC-1, and are suppressed by the HDJ-2 chaperone.* Hum Mol Genet, 1999. **8**(5): p. 731-41.
10. McCampbell, A., et al., *CREB-binding protein sequestration by expanded polyglutamine.* Human molecular genetics, 2000. **9**(14): p. 2197-2202.
11. Satyal, S.H., et al., *Polyglutamine aggregates alter protein folding homeostasis in Caenorhabditis elegans.* Proc Natl Acad Sci U S A, 2000. **97**(11): p. 5750-5.
12. Yvert, G., et al., *Expanded polyglutamines induce neurodegeneration and trans-neuronal alterations in cerebellum and retina of SCA7 transgenic mice.* Hum Mol Genet, 2000. **9**(17): p. 2491-506.
13. Jana, N.R., et al., *Altered proteasomal function due to the expression of polyglutamine-expanded truncated N-terminal huntingtin induces apoptosis by caspase activation through mitochondrial cytochrome c release.* Hum Mol Genet, 2001. **10**(10): p. 1049-59.
14. Lieberman, A.P., et al., *Altered transcriptional regulation in cells expressing the expanded polyglutamine androgen receptor.* Human molecular genetics, 2002. **11**(17): p. 1967-1976.
15. Szebenyi, G., et al., *Neuropathogenic forms of huntingtin and androgen receptor inhibit fast axonal transport.* Neuron, 2003. **40**(1): p. 41-52.

16. Morfini, G., et al., *JNK mediates pathogenic effects of polyglutamine-expanded androgen receptor on fast axonal transport.* Nature neuroscience, 2006. **9**(7): p. 907-916.
17. Zoghbi, H.Y. and H.T. Orr, *Glutamine repeats and neurodegeneration.* Annual review of neuroscience, 2000. **23**: p. 217-247.
18. Paulson, H., *Repeat expansion diseases.* Handb Clin Neurol, 2018. **147**: p. 105-123.
19. Abel, A., et al., *Expression of expanded repeat androgen receptor produces neurologic disease in transgenic mice.* Hum Mol Genet, 2001. **10**(2): p. 107-16.
20. Adachi, H., et al., *Heat shock protein 70 chaperone overexpression ameliorates phenotypes of the spinal and bulbar muscular atrophy transgenic mouse model by reducing nuclear-localized mutant androgen receptor protein.* The Journal of neuroscience : the official journal of the Society for Neuroscience, 2003. **23**(6): p. 2203-2211.
21. Adachi, H., et al., *CHIP overexpression reduces mutant androgen receptor protein and ameliorates phenotypes of the spinal and bulbar muscular atrophy transgenic mouse model.* The Journal of neuroscience : the official journal of the Society for Neuroscience, 2007. **27**(19): p. 5115-26.
22. Miller, V.M., et al., *CHIP suppresses polyglutamine aggregation and toxicity in vitro and in vivo.* J Neurosci, 2005. **25**(40): p. 9152-61.
23. Atsuta, N., et al., *Natural history of spinal and bulbar muscular atrophy (SBMA): a study of 223 Japanese patients.* Brain, 2006. **129**(Pt 6): p. 1446-55.
24. La Spada, A.R., et al., *Androgen receptor gene mutations in X-linked spinal and bulbar muscular atrophy.* Nature, 1991. **352**(6330): p. 77-79.
25. Katsuno, M., et al., *Leuprorelin rescues polyglutamine-dependent phenotypes in a transgenic mouse model of spinal and bulbar muscular atrophy.* Nat Med, 2003. **9**(6): p. 768-73.
26. Kennedy, W.R., M. Alter, and J.H. Sung, *Progressive proximal spinal and bulbar muscular atrophy of late onset. A sex-linked recessive trait.* Neurology, 1968. **18**(7): p. 671-680.
27. Adachi, H., et al., *Transgenic mice with an expanded CAG repeat controlled by the human AR promoter show polyglutamine nuclear inclusions and neuronal dysfunction without neuronal cell death.* Hum Mol Genet, 2001. **10**(10): p. 1039-48.
28. Walcott, J.L. and D.E. Merry, *Ligand promotes intranuclear inclusions in a novel cell model of spinal and bulbar muscular atrophy.* The Journal of biological chemistry, 2002. **277**(52): p. 50855-50859.
29. Takeyama, K.-i., et al., *Androgen-dependent neurodegeneration by polyglutamine-expanded human androgen receptor in Drosophila.* Neuron, 2002. **35**(5): p. 855-64.
30. Montie, H.L., et al., *Cytoplasmic retention of polyglutamine-expanded androgen receptor ameliorates disease via autophagy in a mouse model of spinal and bulbar muscular atrophy.* Hum Mol Genet, 2009. **18**(11): p. 1937-50.
31. Zboray, L., et al., *Preventing the Androgen Receptor N/C Interaction Delays Disease Onset in a Mouse Model of SBMA.* Cell Rep, 2015. **13**(10): p. 2312-23.
32. Yu, Z., et al., *Androgen-dependent pathology demonstrates myopathic contribution to the Kennedy disease phenotype in a mouse knock-in model.* The Journal of clinical investigation, 2006. **116**(10): p. 2663-2672.

33. Ishihara, H., et al., *Clinical features and skewed X-chromosome inactivation in female carriers of X-linked recessive spinal and bulbar muscular atrophy.* J Neurol, 2001. **248**(10): p. 856-60.
34. Banno, H., et al., *Phase 2 trial of leuprorelin in patients with spinal and bulbar muscular atrophy.* Ann Neurol, 2009. **65**(2): p. 140-50.
35. Katsuno, M., et al., *Efficacy and safety of leuprorelin in patients with spinal and bulbar muscular atrophy (JASMITT study): a multicentre, randomised, double-blind, placebo-controlled trial.* Lancet Neurol, 2010. **9**(9): p. 875-84.
36. Hashizume, A., et al., *Efficacy and safety of leuprorelin acetate for subjects with spinal and bulbar muscular atrophy: pooled analyses of two randomized-controlled trials.* J Neurol, 2019. **266**(5): p. 1211-1221.
37. Rhodes, L.E., et al., *Clinical features of spinal and bulbar muscular atrophy.* Brain, 2009. **132**(Pt 12): p. 3242-51.
38. Lombardi, V., et al., *Muscle and not neuronal biomarkers correlate with severity in spinal and bulbar muscular atrophy.* Neurology, 2019. **92**(11): p. e1205-e1211.
39. Malena, A., et al., *Androgen-dependent impairment of myogenesis in spinal and bulbar muscular atrophy.* Acta Neuropathol, 2013. **126**(1): p. 109-21.
40. Lombardi, V., et al., *Plasma pNfH levels differentiate SBMA from ALS.* J Neurol Neurosurg Psychiatry, 2020. **91**(2): p. 215-217.
41. Klickovic, U., et al., *Skeletal muscle MRI differentiates SBMA and ALS and correlates with disease severity.* Neurology, 2019. **93**(9): p. e895-e907.
42. Albertelli, M.A., et al., *Replacing the mouse androgen receptor with human alleles demonstrates glutamine tract length-dependent effects on physiology and tumorigenesis in mice.* Mol Endocrinol, 2006. **20**(6): p. 1248-60.
43. Xu, Y., et al., *Defects in Neuromuscular Transmission May Underlie Motor Dysfunction in Spinal and Bulbar Muscular Atrophy.* J Neurosci, 2016. **36**(18): p. 5094-106.
44. Poort, J.E., et al., *Neuromuscular junctions are pathological but not denervated in two mouse models of spinal bulbar muscular atrophy.* Hum Mol Genet, 2016. **25**(17): p. 3768-3783.
45. Philips, T. and J.D. Rothstein, *Rodent Models of Amyotrophic Lateral Sclerosis.* Curr Protoc Pharmacol, 2015. **69**: p. 5 67 1-5 67 21.
46. Giorgetti, E., et al., *Rescue of Metabolic Alterations in AR113Q Skeletal Muscle by Peripheral Androgen Receptor Gene Silencing.* Cell Rep, 2016. **17**(1): p. 125-36.
47. Rocchi, A., et al., *Glycolytic-to-oxidative fiber-type switch and mTOR signaling activation are early-onset features of SBMA muscle modified by high-fat diet.* Acta Neuropathol, 2016. **132**(1): p. 127-44.
48. Monks, D.A., et al., *Overexpression of wild-type androgen receptor in muscle recapitulates polyglutamine disease.* Proc Natl Acad Sci U S A, 2007. **104**(46): p. 18259-64.
49. Ramzan, F., et al., *Distinct Etiological Roles for Myocytes and Motor Neurons in a Mouse Model of Kennedy's Disease/Spinobulbar Muscular Atrophy.* J Neurosci, 2015. **35**(16): p. 6444-51.
50. Lieberman, A.P., et al., *Peripheral androgen receptor gene suppression rescues disease in mouse models of spinal and bulbar muscular atrophy.* Cell Rep, 2014. **7**(3): p. 774-84.
51. Palazzolo, I., et al., *Overexpression of IGF-1 in muscle attenuates disease in a mouse model of spinal and bulbar muscular atrophy.* Neuron, 2009. **63**(3): p. 316-28.

CHAPTER II

Protein Quality Control in Polyglutamine Disease

2.1 Abstract

Polyglutamine disorders are chronic, progressive neurodegenerative diseases caused by expansion of a glutamine tract in widely expressed genes. Despite excellent models of disease, a well-documented clinical history and progression, and established genetic causes, there are no FDA approved, disease modifying treatments for these disorders. Downstream of the mutant protein, several divergent pathways of toxicity have been identified over the last several decades, supporting the idea that targeting only one of these pathways of toxicity is unlikely to robustly alleviate disease progression. As a result, a vast body of research has focused on eliminating the mutant protein to broadly prevent downstream toxicity, either by silencing mutant protein expression or leveraging the endogenous protein quality control machinery. In the latter approach, a focus has been placed on four critical components of mutant protein degradation that are active in the nucleus, a key site of toxicity: disaggregation, ubiquitination, deubiquitination, and proteasomal activity. These machineries have unique functional components, but work together as a cellular defense system that can be successfully leveraged to alleviate disease phenotypes in several models of polyglutamine toxicity. This review will highlight recent advances in understanding both the potential and role of these components of the protein quality control machinery in polyglutamine disease pathophysiology.

2.2 Introduction

Polyglutamine (polyQ) diseases encompass nine untreatable and invariably fatal neurodegenerative diseases associated with protein misfolding and aggregation. The cause of this family of disease is expansion of a glutamine tract within widely differing proteins, leading to gain of function effects and a shared phenotype of adult-onset progressive neurodegeneration. There are no FDA approved disease modifying treatments for any polyQ disease despite their well-established genetic causes, carefully documented clinical history, and the availability of excellent genetic models that recapitulate aspects of the disease phenotype [1]. Work in these model systems over the last several decades has highlighted downstream toxic effects in a large number of pathways, including those regulating gene expression, axonal transport, mitochondrial function and energy metabolism [2-13]. These observations suggest that targeting any single pathway for therapeutic benefit may be incomplete and ineffective. As a consequence, strategies to rid cells of the mutant proteins have attracted considerable recent attention. Both reducing expression of the mutant protein using antisense oligonucleotides [12, 14, 15] and driving degradation of the mutant protein [16-21] lead to phenotypic rescue of multiple polyQ disease models, establishing removal of the mutant protein as a viable therapeutic strategy. This review will focus on pathways involved in mutant protein degradation, highlighting pathophysiologic changes and therapeutic approaches within the fields of ubiquitination, deubiquitinating enzymes, protein disaggregation, and proteasomal activity. Though misfolded proteins are also targeted for degradation through autophagy, several excellent recent reviews have detailed the

contribution of this pathway to their clearance and possible strategies for therapeutic manipulation [22-24].

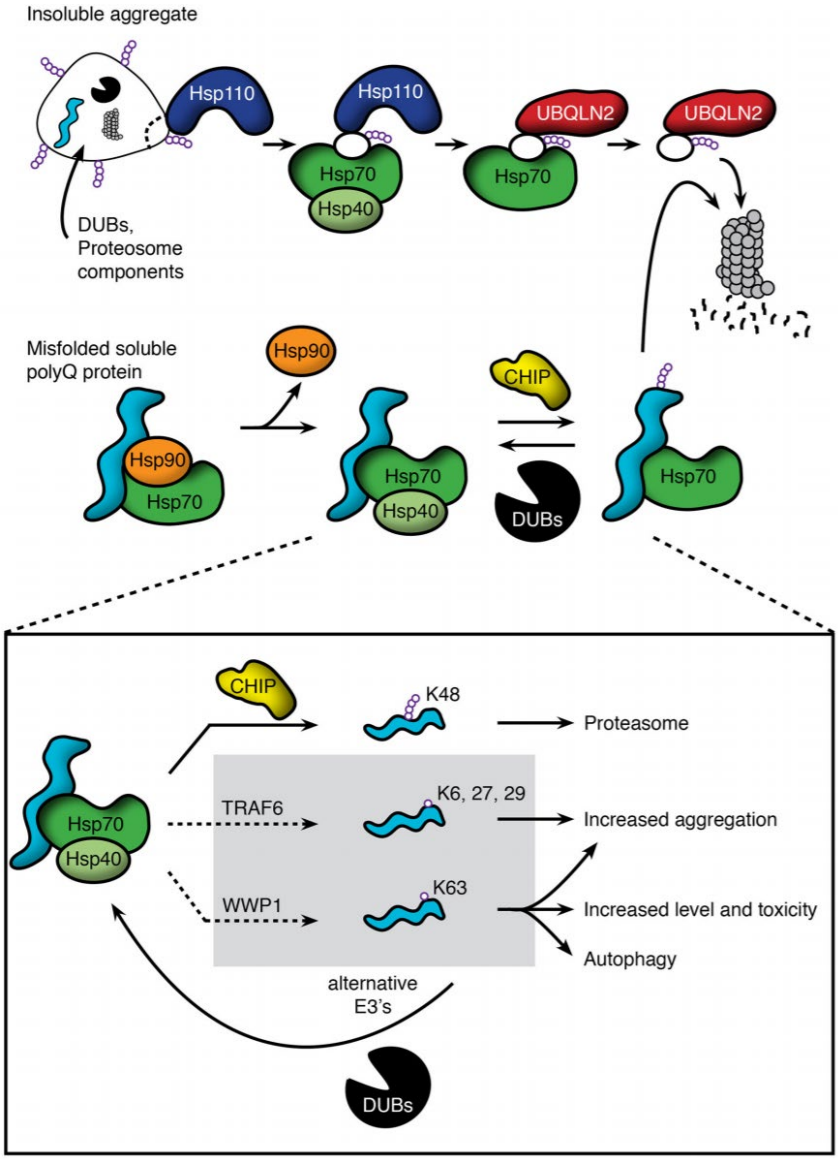

Figure 2. Pathways regulating polyglutamine protein degradation through the proteasome.

(Top) Insoluble protein aggregates are recognized by Hsp110, which acts to disaggregate and remove misfolded proteins. These substrates are then passed to the Hsp70/40 complex and subsequently bound by the ubiquitin-associated domain of UBQLN2. UBQLN2 traffics substrates to the proteasome, which recognizes UBQLN2's ubiquitin-like domain.
(Middle) Polyglutamine proteins that are clients of the Hsp90/Hsp70 based chaperone machinery include the androgen receptor and huntingtin. Soluble species interact with the chaperone machinery, but release Hsp90 upon misfolding. This allows substrate bound Hsp70/Hsp40 to recruit E3 ligases, such as CHIP, to promote polyubiquitination and proteasomal degradation. This action is opposed by deubiquitinating enzymes (DUBs), which can remove the polyubiquitin chains and send soluble polyQ proteins back into the cellular pool.
(Bottom) Though E3 ligases such as CHIP promote K48-linked polyubiquitination and proteasomal degradation, emerging evidence shows that other E3's can ubiquitinate using alternative lysine residues, leading to impairment of degradation, increased aggregation, and/or degradation through alternative pathways such as autophagy. For these ligases, DUBs may act in a beneficial manner to return polyglutamine proteins to the pool of proteins that can be polyubiquitinated through K48 linkages and degraded through the proteasome.

2.3 Ubiquitinating Enzymes (E3s) in PolyQ Diseases

A wealth of studies implicate the ubiquitination machinery as a potential therapeutic target in polyglutamine diseases. These enzymes serve a key role in targeting proteins for degradation both by the proteasome and autophagy [22, 25]. In the last decade, a great deal of focus has been placed on C-terminal Hsp70-interacting protein (CHIP), which acts as both a co-chaperone and an E3 ubiquitin ligase for misfolded proteins and plays a key role in facilitating their degradation [25].

CHIP's potential as a therapeutic target centers on its ability to promote ubiquitination and proteasomal degradation of client proteins of the Hsp90/Hsp70 based chaperone machinery [25-27]. In this machinery, Hsp90 and Hsp70 bind to client proteins in their native or near native conformations to regulate many aspects of proteostasis. The binding of Hsp90 to client proteins regulates hydrophobic protein clefts. Disease-causing mutations either destabilize clefts or introduce a second site of inherent instability that also binds chaperones. Interaction with Hsp90 stabilizes hydrophobic clefts; as mutant proteins unfold, interaction with Hsp90 is lost, leaving client-bound Hsp70 to recruit CHIP to promote ubiquitination [25] (Figure 2, middle). Notably, truncated fragments of disease-causing proteins that lack hydrophobic clefts present in the full-length protein may fail to interact with the Hsp90/Hsp70 based machinery. This is the case for an amino-terminal fragment of the polyQ androgen receptor that lacks the ligand-binding domain. The consequence is that degradation of this artificial construct is handled differently from the full-length protein and is largely mediated by autophagy [28].

In our model of chaperone machinery protein triage, Hsp70 binds client proteins and plays a critical role by recruiting CHIP to misfolded substrates, which in turn promotes ubiquitination and degradation of these proteins. The recruitment of CHIP may be influenced by

post-translational modifications of Hsp70, such as phosphorylation of a serine or threonine residue near the EEVD motif [29]. CHIP's ability to recognize and ubiquitinate Hsp90 clients depends on the binding cleft in the full-length protein. When CHIP substrates, such as nNOS [30], ErbB2 [27], and estrogen receptor [31], are manipulated by site-specific inhibitors within the ligand binding cleft, ubiquitination and degradation are increased [32-34], supporting the crucial role of the ligand binding cleft as a recognition motif for the Hsp70-CHIP complex.

Due to its ability to ubiquitinate client proteins, CHIP has been studied extensively in polyQ diseases. In Huntington disease models, CHIP overexpression suppresses aggregation and toxicity of the polyQ huntingtin protein both in non-neuronal cells and primary neurons. In contrast, haploinsufficiency of CHIP leads to accelerated disease in mice overexpressing polyQ huntingtin [35]. CHIP drives degradation of polyQ huntingtin by promoting ubiquitination and proteasomal degradation of the mutant protein, an action CHIP can also perform on ataxin-3, the causative protein in spinocerebellar ataxia type 3 (SCA3) [36]. Further, polyQ expansion of ataxin-3 leads to increased affinity for CHIP and decreased CHIP levels in SCA3 mice, suggesting a role for CHIP dysregulation in this polyQ diseases [37]. In spinal and bulbar muscular atrophy (SBMA), overexpression of CHIP leads to phenotypic rescue of a transgenic mouse model overexpressing polyQ AR. Importantly, this degradation is selective for the mutant receptor over the wild type protein, indicating a preference for misfolded substrates [17]. Recently, CHIP was identified as a causative gene for autosomal recessive cerebellar ataxia, further implicating it as a crucial protein in preventing neurodegeneration and regulating neuronal homeostasis [38].

There is likely functional redundancy between CHIP and other chaperone-dependent E3 ligases. In support of this notion, CHIP deletion in cells had no effect on degradation of the

polyQ androgen receptor or the glucocorticoid receptor, which are both known CHIP substrates [39]. To date no broadly overlapping E3s have been identified, raising the possibility that multiple E3 ligases are up-regulated in the setting of CHIP deletion.

Whereas E3s such as CHIP have been shown to play a protective role in polyQ disease, not all E3s fit this mold (Figure 2, bottom). TRAF6 is an E3 that is present in polyQ huntingtin aggregates and polyubiquitinates polyQ huntingtin using lysine residues K6, K27, and K29 within ubiquitin. In cellular models, this ubiquitination leads to increased aggregation of the polyQ protein without a change in WT huntingtin localization [40]. WWP1 is another E3 that colocalizes with polyQ huntingtin aggregates, and is upregulated in both mice and N2a cells expressing polyQ huntingtin. Interestingly, overexpression of WWP1 leads to increased polyQ huntingtin levels and toxicity. The toxic effects of WWP1 have been attributed to its ability to polyubiquitinate polyQ huntingtin at a K63 residue, leading to reduced proteasomal degradation of the mutant protein as well as increased toxicity in mouse and cellular models [41].

Together, this evidence provides a framework in which E3s such as CHIP to function together with molecular chaperones to both recognize and ubiquitinate misfolded protein substrates, leading to their proteasomal degradation. However, E3s must be considered on a case by case basis, as growing evidence supports the idea that non-K48 linked ubiquitination can have opposite and regulatory effects on cargo. We suggest that enhancing activity of canonical E3s such as CHIP while inhibiting other E3s such as TRAF6 and WWP1 may have cooperative therapeutic benefits to promote polyQ protein degradation.

2.4 Deubiquitinating Enzymes

Ubiquitination plays a key role in protein quality control. To counteract the activity of ubiquitin ligases, a system of checks and balances has been identified and characterized in the form of a network of deubiquitinating enzymes (DUBs). Over 90 DUBs have been identified within the human genome, each belonging to one of seven distinct families. These enzymes play diverse roles including altering protein function and impacting proteasomal degradation.

Recently, DUBs have emerged as attractive therapeutic targets in polyglutamine disorders. DUBs delay proteasomal degradation and their inhibition has been shown to enhance substrate degradation through the proteasome, demonstrating a pivotal role in diseases caused by misfolded protein accumulation [42, 43]. It is well established that DUBs interact with polyQ proteins, such as ataxin-1 [44], ataxin-3 [45], huntingtin [46], and androgen receptor [47-50]. However, polyQ proteins can also sequester DUBs, leading to their inactivation. For example, polyQ ataxin-7 sequesters USP22 into aggregates and inhibits its DUB activity [51]. DUBs can also regulate polyQ proteins, for example USP19b overexpression leads to an Hsp90-dependent increase in levels of both wild type and polyQ ataxin-3 as well as polyQ Htt in cellular models [45].

One DUB that has attracted considerable attention is USP14, which binds ubiquitinated substrates and facilitates opening of the proteasomal gate, allowing for selective and efficient substrate degradation [52]. Modulating the activity of this DUB has significant effects on substrate degradation. Overexpression of USP14 reduces polyQ huntingtin aggregation and protects against cell degeneration by inhibiting IRE1□ phosphorylation and blocking ER stress in PC6.3 cells [46]. In contrast, Lee et al. have shown that overexpression of USP14 leads to buildup of both wild type and polyQ ataxin-3 while pharmacologic inhibition of USP14 leads to

enhanced polyQ ataxin-3 and tau clearance in MEFs [42]. These contrary findings may be explained by cell line or protein specific differences, or effects on total ubiquitin pools in these cells as a result of modulating global deubiquitination. Nonetheless, they underscore the physiological importance of the USP family of DUBs.

DUBs not only modify the degradation and steady state levels of polyQ proteins, but also influence the function of their wild type counterparts. DUBs have been intensively studied in cancer, resulting in the identification of a number of enzymes that modulate activity of cancer causing genes. In particular, androgen receptor, mutations in which cause both prostate cancer and SBMA, is regulated in diverse ways by several DUBs. USP26 binds to androgen receptor through three nuclear receptor interaction motifs, and knockdown of USP26 leads to decreased AR activity in LnCaP and HEK293 cells [50]. USP10 is required for androgen receptor activated transcription of PSA and KLK3, and this role has been attributed to USP10's hormone-induced deubiquitylation of chromatin around AR responsive genes [53]. USP7 shows androgen-dependent association and deubiquitination of androgen receptor. This deubiquitination is essential for the androgen responsive binding to chromatin and subsequent transcriptional activation, a function that can also be performed by USP12 [47, 49]. The role of these enzymes in modulating polyQ AR function and toxicity has not yet been explored. As the physiologic function of many other polyQ disease causing proteins is not fully understood, how DUBs may affect their function remains an emerging field of investigation.

Underscoring the importance of DUBs to polyQ disease is SCA3, a disorder caused by expansion of a polyQ tract within the DUB ataxin-3. This DUB has many important cellular targets including p53. Interestingly, lack of polyQ ataxin-3's catalytic activity leads to increased toxicity in models of SCA3 [54, 55]. This effect may be due to loss of protein function or

buildup of the toxic protein, which is less readily recognized by p97 and inefficiently degraded by the proteasome [56]. Overall, this work on ataxin-3 and other DUBs shows that this family of proteins serves critical roles in modulating the function, localization and degradation of polyQ proteins, and represents an exciting new therapeutic target.

2.5 Disaggregation

Downstream of aggregation, a mechanism of disaggregation by which cells dismantle inclusions and degrade misfolded proteins has been characterized as functionally relevant to polyglutamine disease (Figure 2, top). A number of key components of the mammalian disaggregase machinery have been identified including heat shock protein 110 (Hsp110/Hsp104), ubiquilin-2 (UBQLN2), heat shock protein 70 (Hsp70), and heat shock protein 40 (Hsp40/DnaJ).

Hsp110 is a heat shock inducible protein first shown to play a key role in stress response and survival, a function that is conserved from bacteria to yeast and mammalian cells [57-59]. Hsp110 neither promotes proteolysis of nor protects the folded state of denatured luciferase, but mediates resolubilization of the aggregated protein [60]. The ability to disaggregate denatured luciferase is dependent on ATP and an intact nucleotide binding site, suggesting a role for ATP hydrolysis in disaggregation. This activity is also dependent on Ydj1, an Hsp40 which promotes ATP hydrolysis, and Ssa1, a yeast Hsp70, implicating other members of the heat shock protein family of chaperones in disaggregation [61].

Hsp110 has been implicated in blocking aggregation and toxicity of polyQ proteins. Overexpression of yeast Hsp104, an Hsp110 homologue, reduces aggregation of 72Q and 103Q

Htt, and surprisingly, deletion of Hsp104 eliminates aggregation almost entirely [62]. This finding parallels the effects of Hsp104 on the yeast prion psi+. These data support a model in which low levels of Hsp110 play a role in the recognition and seeding of prion-like aggregates, while high levels lead to recognition and solubulization of aggregated proteins [63, 64]. The role of Hsp110 in disaggregation of polyQ proteins has also been demonstrated in *C. elegans* expressing polyQ-GFP. In this system, overexpression of Hsp110 led to reduced aggregation and rescue of toxicity [65]. Further, overexpression of yeast Hsp104 and bacterial Gro-EL in Cos-7 and PC-12 cells reduced aggregation of polyQ Htt, supporting conserved disaggregase activity in mammalian cells [66]. Using sequential mass spectrometry in *S. cerevisiae*, a model of chaperone binding has started to emerge. Hsp70 and Hsp90 appear to function in initial recognition of polyQ proteins, and are released prior to aggregate maturation. Subsequent aggregate formation occurs prior to Hsp104 interaction, suggesting a preference of Hsp104 for the aggregated form [67].

In the last several years a new addition to the disaggregase machinery has been characterized, ubiquilin-2 (UBQLN2). UBQLN2, also known as hPLIC2, is encoded by an intronless gene and contains both a ubiquitin-like domain and a ubiquitin-associated domain [68]. Early studies showed that the ubiquitin-associated domain interacts with polyubiquitin chains on substrates, and the ubiquitin-like domain served to bring these substrates to and bind the proteasome. However, these studies also showed that overexpression of UBQLN2 interfered with proteasomal degradation, increasing the half-life of substrates such as p53 and IκBα [69, 70]. Several subsequent studies have corroborated impaired proteolysis downstream of UBQLN2 overexpression [71-73]. This relationship between substrate recognition and proteasomal inhibition suggests that UBQLN2 function is best studied at endogenous levels [74].

Consistent with these findings, Hjerpe et al. recently demonstrated a key role for UBQLN2 in the disaggregase machinery. Knockdown of UBQLN2 led to reduced survival and inability to clear insoluble ubiquitin aggregates after heat shock. Importantly, the clearance of insoluble aggregates was shown to be dependent on previously mentioned members of the disaggregase machinery including Hsp70 and Hsp110. The authors also showed that UBQLN2 colocalizes with polyQ Htt aggregates, and reduction of UBQLN2 led to increased aggregation [75].

The above evidence supports a model in which Hsp70/Hsp110 act to recognize and solubilize protein aggregates. UBQLN2 associates with client-bound Hsp70 and assists in shuttling aggregated components to the proteasome. One key remaining question is whether disaggregation alleviates toxicity in organismal models of polyglutamine disease, which will identify the importance of the disaggregation system for therapeutic strategies. Understanding how to therapeutically manipulate the disaggregase machinery is a worthwhile endeavor likely to lead to a better understanding of pathophysiology.

2.6 Proteasome Dysfunction in Polyglutamine Diseases

A wealth of evidence has linked the proteasome to several polyQ diseases, both as a therapeutic target and as a dysfunctional pathway downstream of mutant polyQ proteins. The 20S proteasome was first shown to co-localize with aggregates of polyQ ataxin-1 in both patients and transgenic mice. This same co-localization was later found in human SCA3 tissue, a mouse model expressing polyQ ataxin-7, HeLa cells expressing polyQ androgen receptor, and mice overexpressing truncated polyQ androgen receptor [76-80]. Interestingly, in human brain sections from SCA3 patients, only the 11S and 19S regulatory particles were found in inclusions,

suggesting differential recruitment of proteasomal components for misfolded aggregates [81]. Though proteasomes seem to co-localize with the majority of polyglutamine inclusions, they are not completely trapped, as some exchange of proteasomes within inclusions was observed using FRAP [82].

The proteasome also shows a preference for degrading misfolded polyQ proteins over their wild type counterparts, likely due to efficient targeting of mutant proteins for degradation. In MN1 cells expressing either 24Q or 65Q androgen receptor, the mutant protein demonstrates significantly reduced half-life, and this degradation is inhibited by the proteasome inhibitor lactacystin [7]. Similarly, in cells expressing 20Q and 76Q Htt, proteasome inhibition leads to greater buildup of the toxic, N-terminal polyQ Htt compared to wild type, and dramatically more buildup of the polyQ protein following proteasome inhibition compared to autophagy inhibition [83].

While the proteasome has been implicated in polyQ protein degradation, several studies have also shown impaired function in several disease models. In mice over-expressing N-terminal polyQ Htt, altered proteasome localization to aggregates was accompanied by an increase in half-life of the proteasome substrate p53 [84]. In cells over-expressing N-terminal polyQ Htt or □F508 CFTR (cystic fibrosis transmembrane conductance regulator), cells with aggregates had a significant impairment in proteasome activity compared to those lacking aggregates when function was measured by clearance of the fluorescent reporter protein GFPu [85]. Notably, the tight association of aggregation with the accumulation of GFPu was not reproduced in a mouse model of Huntington disease [86], raising the possibility that soluble misfolded species of the mutant protein might impair proteasome function in some model systems. When SH-SY5Y cells were stably transfected with polyQ-GFP, there was impaired

ability of the proteasome to compensate for heat shock-induced stress [87]. In cerebellar neurons expressing polyQ ataxin-7, proteasome function was significantly diminished, and this led to cytosolic accumulation and impaired activity of NF-kB, culminating in increased activation of caspase-9 [88]. The impairment in proteasome function downstream of polyQ proteins may be indirect, as studies in yeast and mammalian cells have demonstrated that accumulated substrates are less likely to be shuttled to the proteasome, potentially due to dysregulation of the key proteasome chaperone Sis1p or its mammalian orthologue DnaJB1 [89]. Together, this evidence suggests a role for proteasome impairment in models of polyglutamine diseases. Though cellular data has been very consistent in demonstrating proteasome dysregulation, in vivo studies have lacked consistent results [86, 90, 91]. For example, in R6/2 mice, which express an N-terminal fragment of polyQ Htt, the proteasome was significantly impaired in synapses of the striatum and in cultured neurons [92], but a similar effect was not seen at a global level within the brain [86] suggesting compartment specific differences. In support of this idea, reporter systems have demonstrated that proteasome activity is markedly lower in neurons compared to glia, potentially making them more sensitive to functional changes. Similarly, proteasome activity is lower in neuronal processes compared to the soma, and lower in the nucleus than the cytoplasm, reinforcing compartment specific differences that impact vulnerability to pathogenesis [93, 94].

Perhaps the most compelling evidence for proteasome dysfunction playing a key role in pathophysiology comes from successful attempts to modulate degradation through this pathway, resulting in reduced toxicity in disease models. Several excellent reviews have highlighted therapeutic strategies to promote degradation of mutant proteins through the proteasome, including Hsp90 inhibition [95] and Hsp70 modulation [25]. Importantly, some of these strategies alleviate polyQ toxicity in the absence of severe off-target effects, suggesting that they

warrant further exploration as therapeutic approaches for the broad treatment of polyQ disorders. The wealth of evidence implicating the proteasome as a therapeutic target, as well as its dysfunction and mislocalization in polyQ diseases, highlight its importance in the pathophysiology of disease.

2.7 Conclusions

Recent advances in our understanding of polyglutamine disease pathophysiology have shed light on several divergent pathways of toxicity downstream of the mutant protein [2-13]. As a result, a major focus of the field has been on either preventing synthesis of mutant proteins using antisense oligonucleotides [12, 14, 15] or enhancing degradation by leveraging endogenous cellular chaperone machinery [16-21]. The latter approach highlights the importance of ongoing research into the endogenous cellular machinery which acts to disaggregate, ubiquitinate, deubiquitinate, and degrade the mutant protein. Potential therapeutic targets have been identified within all of these key processes, and highlight the potential and viability of leveraging existing cell machineries to drive therapeutic strategies. We propose that a combination of approaches is likely necessary to limit polyglutamine protein toxicity while minimizing individual off target toxicities of therapeutics. The many advances highlighted in this review, as well as countless others in the fields of mutant gene silencing and trophic factor stimulation provide an optimistic outlook towards the future of disease treatments for polyglutamine disorders.

2.8 Acknowledgements

Work in the authors' laboratory was supported by the U. S. National Institutes of Health (R01 NS055746 to A.P.L., T32 GM007863 and T32 GM007315 to S.R.N.)

This chapter was published as a review article in *Frontiers in Molecular Neuroscience* [96].

References

1. Chua, J.P. and A.P. Lieberman, *Pathogenic mechanisms and therapeutic strategies in spinobulbar muscular atrophy.* CNS Neurol Disord Drug Targets, 2013. **12**(8): p. 1146-56.
2. Mhatre, A.N., et al., *Reduced transcriptional regulatory competence of the androgen receptor in X-linked spinal and bulbar muscular atrophy.* Nature genetics, 1993. **5**(2): p. 184-188.
3. Chamberlain, N.L., E.D. Driver, and R.L. Miesfeld, *The length and location of CAG trinucleotide repeats in the androgen receptor N-terminal domain affect transactivation function.* Nucleic acids research, 1994. **22**(15): p. 3181-3186.
4. Kazemi-Esfarjani, P., M.A. Trifiro, and L. Pinsky, *Evidence for a repressive function of the long polyglutamine tract in the human androgen receptor: possible pathogenetic relevance for the (CAG)n-expanded neuronopathies.* Human molecular genetics, 1995. **4**(4): p. 523-527.
5. Irvine, R.A., et al., *Inhibition of p160-mediated coactivation with increasing androgen receptor polyglutamine length.* Human molecular genetics, 2000. **9**(2): p. 267-274.
6. McCampbell, A., et al., *CREB-binding protein sequestration by expanded polyglutamine.* Human molecular genetics, 2000. **9**(14): p. 2197-2202.
7. Lieberman, A.P., et al., *Altered transcriptional regulation in cells expressing the expanded polyglutamine androgen receptor.* Human molecular genetics, 2002. **11**(17): p. 1967-1976.
8. Szebenyi, G., et al., *Neuropathogenic forms of huntingtin and androgen receptor inhibit fast axonal transport.* Neuron, 2003. **40**(1): p. 41-52.
9. Morfini, G., et al., *JNK mediates pathogenic effects of polyglutamine-expanded androgen receptor on fast axonal transport.* Nature neuroscience, 2006. **9**(7): p. 907-916.
10. Ranganathan, S., et al., *Mitochondrial abnormalities in spinal and bulbar muscular atrophy.* Human molecular genetics, 2009. **18**(1): p. 27-42.
11. Kemp, M.Q., et al., *Impaired motoneuronal retrograde transport in two models of SBMA implicates two sites of androgen action.* Human molecular genetics, 2011. **20**(22): p. 4475-4490.
12. Giorgetti, E., et al., *Rescue of Metabolic Alterations in AR113Q Skeletal Muscle by Peripheral Androgen Receptor Gene Silencing.* Cell Rep, 2016. **17**(1): p. 125-36.
13. Rocchi, A., et al., *Glycolytic-to-oxidative fiber-type switch and mTOR signaling activation are early-onset features of SBMA muscle modified by high-fat diet.* Acta Neuropathol, 2016. **132**(1): p. 127-44.
14. Sahashi, K., et al., *Silencing neuronal mutant androgen receptor in a mouse model of spinal and bulbar muscular atrophy.* Hum Mol Genet, 2015. **24**(21): p. 5985-94.
15. Lieberman, A.P., et al., *Peripheral androgen receptor gene suppression rescues disease in mouse models of spinal and bulbar muscular atrophy.* Cell Rep, 2014. **7**(3): p. 774-84.
16. Adachi, H., et al., *Heat shock protein 70 chaperone overexpression ameliorates phenotypes of the spinal and bulbar muscular atrophy transgenic mouse model by reducing nuclear-localized mutant androgen receptor protein.* The Journal of neuroscience : the official journal of the Society for Neuroscience, 2003. **23**(6): p. 2203-2211.

17. Adachi, H., et al., *CHIP overexpression reduces mutant androgen receptor protein and ameliorates phenotypes of the spinal and bulbar muscular atrophy transgenic mouse model.* The Journal of neuroscience : the official journal of the Society for Neuroscience, 2007. **27**(19): p. 5115-26.
18. Tokui, K., et al., *DMAG ameliorates polyglutamine-mediated motor neuron degeneration through well-preserved proteasome function in a SBMA model mouse.* Hum Mol Genet, 2008.
19. Sittler, A., et al., *Geldanamycin activates a heat shock response and inhibits huntingtin aggregation in a cell culture model of Huntington's disease.* Hum Mol Genet, 2001. **10**(12): p. 1307-15.
20. Wang, A.M., et al., *Activation of Hsp70 reduces neurotoxicity by promoting polyglutamine protein degradation.* Nature chemical biology, 2013. **9**(2): p. 112-118.
21. Silva-Fernandes, A., et al., *Chronic treatment with 17-DMAG improves balance and coordination in a new mouse model of Machado-Joseph disease.* Neurotherapeutics, 2014. **11**(2): p. 433-49.
22. Rusmini, P., et al., *The Role of the Protein Quality Control System in SBMA.* J Mol Neurosci, 2016. **58**(3): p. 348-64.
23. Martin, D.D., et al., *Autophagy in Huntington disease and huntingtin in autophagy.* Trends Neurosci, 2015. **38**(1): p. 26-35.
24. Rusmini, P., et al., *Aberrant Autophagic Response in The Muscle of A Knock-in Mouse Model of Spinal and Bulbar Muscular Atrophy.* Sci Rep, 2015. **5**: p. 15174.
25. Pratt, W.B., et al., *Targeting Hsp90/Hsp70-based protein quality control for treatment of adult onset neurodegenerative diseases.* Annu Rev Pharmacol Toxicol, 2015. **55**: p. 353-71.
26. Chung, C., et al., *The E3 ubiquitin ligase CHIP selectively regulates mutant epidermal growth factor receptor by ubiquitination and degradation.* Biochem Biophys Res Commun, 2016. **479**(2): p. 152-158.
27. Zhou, P., et al., *ErbB2 degradation mediated by the co-chaperone protein CHIP.* J Biol Chem, 2003. **278**(16): p. 13829-37.
28. Wang, A.M., et al., *Inhibition of hsp70 by methylene blue affects signaling protein function and ubiquitination and modulates polyglutamine protein degradation.* The Journal of biological chemistry, 2010. **285**(21): p. 15714-15723.
29. VanPelt, J. and R.C. Page, *Unraveling the CHIP:Hsp70 complex as an information processor for protein quality control.* Biochim Biophys Acta, 2016.
30. Peng, H.M., et al., *Ubiquitylation of neuronal nitric-oxide synthase by CHIP, a chaperone-dependent E3 ligase.* J Biol Chem, 2004. **279**(51): p. 52970-7.
31. Fan, M., A. Park, and K.P. Nephew, *CHIP (carboxyl terminus of Hsc70-interacting protein) promotes basal and geldanamycin-induced degradation of estrogen receptor-alpha.* Mol Endocrinol, 2005. **19**(12): p. 2901-14.
32. Peng, H.M., et al., *Dynamic cycling with Hsp90 stabilizes neuronal nitric oxide synthase through calmodulin-dependent inhibition of ubiquitination.* Biochemistry, 2009. **48**(35): p. 8483-90.
33. Citri, A., et al., *Drug-induced ubiquitylation and degradation of ErbB receptor tyrosine kinases: implications for cancer therapy.* EMBO J, 2002. **21**(10): p. 2407-17.

34. Wijayaratne, A.L. and D.P. McDonnell, *The human estrogen receptor-alpha is a ubiquitinated protein whose stability is affected differentially by agonists, antagonists, and selective estrogen receptor modulators.* J Biol Chem, 2001. **276**(38): p. 35684-92.
35. Miller, V.M., et al., *CHIP suppresses polyglutamine aggregation and toxicity in vitro and in vivo.* J Neurosci, 2005. **25**(40): p. 9152-61.
36. Jana, N.R., et al., *Co-chaperone CHIP associates with expanded polyglutamine protein and promotes their degradation by proteasomes.* J Biol Chem, 2005. **280**(12): p. 11635-40.
37. Scaglione, K.M., et al., *Ube2w and ataxin-3 coordinately regulate the ubiquitin ligase CHIP.* Mol Cell, 2011. **43**(4): p. 599-612.
38. Shi, Y., et al., *Identification of CHIP as a novel causative gene for autosomal recessive cerebellar ataxia.* PLoS One, 2013. **8**(12): p. e81884.
39. Morishima, Y., et al., *CHIP deletion reveals functional redundancy of E3 ligases in promoting degradation of both signaling proteins and expanded glutamine proteins.* Human molecular genetics, 2008. **17**(24): p. 3942-52.
40. Zucchelli, S., et al., *Tumor necrosis factor receptor-associated factor 6 (TRAF6) associates with huntingtin protein and promotes its atypical ubiquitination to enhance aggregate formation.* J Biol Chem, 2011. **286**(28): p. 25108-17.
41. Lin, L., et al., *Atypical ubiquitination by E3 ligase WWP1 inhibits the proteasome-mediated degradation of mutant huntingtin.* Brain Res, 2016. **1643**: p. 103-12.
42. Lee, B.H., et al., *Enhancement of proteasome activity by a small-molecule inhibitor of USP14.* Nature, 2010. **467**(7312): p. 179-84.
43. Hanna, J., et al., *Deubiquitinating enzyme Ubp6 functions noncatalytically to delay proteasomal degradation.* Cell, 2006. **127**(1): p. 99-111.
44. Hong, S., et al., *USP7, a ubiquitin-specific protease, interacts with ataxin-1, the SCA1 gene product.* Mol Cell Neurosci, 2002. **20**(2): p. 298-306.
45. He, W.T., et al., *Cytoplasmic Ubiquitin-Specific Protease 19 (USP19) Modulates Aggregation of Polyglutamine-Expanded Ataxin-3 and Huntingtin through the HSP90 Chaperone.* PLoS One, 2016. **11**(1): p. e0147515.
46. Hyrskyluoto, A., et al., *Ubiquitin-specific protease-14 reduces cellular aggregates and protects against mutant huntingtin-induced cell degeneration: involvement of the proteasome and ER stress-activated kinase IRE1alpha.* Hum Mol Genet, 2014. **23**(22): p. 5928-39.
47. Chen, S.T., et al., *The Deubiquitinating Enzyme USP7 Regulates Androgen Receptor Activity by Modulating Its Binding to Chromatin.* J Biol Chem, 2015. **290**(35): p. 21713-23.
48. Schrecengost, R.S., et al., *USP22 regulates oncogenic signaling pathways to drive lethal cancer progression.* Cancer Res, 2014. **74**(1): p. 272-86.
49. Burska, U.L., et al., *Deubiquitinating enzyme Usp12 is a novel co-activator of the androgen receptor.* J Biol Chem, 2013. **288**(45): p. 32641-50.
50. Dirac, A.M. and R. Bernards, *The deubiquitinating enzyme USP26 is a regulator of androgen receptor signaling.* Mol Cancer Res, 2010. **8**(6): p. 844-54.
51. Yang, H., et al., *Aggregation of Polyglutamine-expanded Ataxin 7 Protein Specifically Sequesters Ubiquitin-specific Protease 22 and Deteriorates Its Deubiquitinating Function in the Spt-Ada-Gcn5-Acetyltransferase (SAGA) Complex.* J Biol Chem, 2015. **290**(36): p. 21996-2004.

52. Peth, A., H.C. Besche, and A.L. Goldberg, *Ubiquitinated proteins activate the proteasome by binding to Usp14/Ubp6, which causes 20S gate opening.* Mol Cell, 2009. **36**(5): p. 794-804.
53. Draker, R., E. Sarcinella, and P. Cheung, *USP10 deubiquitylates the histone variant H2A.Z and both are required for androgen receptor-mediated gene activation.* Nucleic Acids Res, 2011. **39**(9): p. 3529-42.
54. Warrick, J.M., et al., *Ataxin-3 suppresses polyglutamine neurodegeneration in Drosophila by a ubiquitin-associated mechanism.* Mol Cell, 2005. **18**(1): p. 37-48.
55. Todi, S.V., et al., *Activity and cellular functions of the deubiquitinating enzyme and polyglutamine disease protein ataxin-3 are regulated by ubiquitination at lysine 117.* J Biol Chem, 2010. **285**(50): p. 39303-13.
56. Todi, S.V., et al., *Cellular turnover of the polyglutamine disease protein ataxin-3 is regulated by its catalytic activity.* J Biol Chem, 2007. **282**(40): p. 29348-58.
57. Sanchez, Y. and S.L. Lindquist, *HSP104 required for induced thermotolerance.* Science, 1990. **248**(4959): p. 1112-5.
58. Sanchez, Y., et al., *Hsp104 is required for tolerance to many forms of stress.* EMBO J, 1992. **11**(6): p. 2357-64.
59. Weber-Ban, E.U., et al., *Global unfolding of a substrate protein by the Hsp100 chaperone ClpA.* Nature, 1999. **401**(6748): p. 90-3.
60. Parsell, D.A., et al., *Protein disaggregation mediated by heat-shock protein Hsp104.* Nature, 1994. **372**(6505): p. 475-8.
61. Glover, J.R. and S. Lindquist, *Hsp104, Hsp70, and Hsp40: a novel chaperone system that rescues previously aggregated proteins.* Cell, 1998. **94**(1): p. 73-82.
62. Krobitsch, S. and S. Lindquist, *Aggregation of huntingtin in yeast varies with the length of the polyglutamine expansion and the expression of chaperone proteins.* Proc Natl Acad Sci U S A, 2000. **97**(4): p. 1589-94.
63. Chernoff, Y.O., et al., *Role of the chaperone protein Hsp104 in propagation of the yeast prion-like factor [psi+].* Science, 1995. **268**(5212): p. 880-4.
64. Patino, M.M., et al., *Support for the prion hypothesis for inheritance of a phenotypic trait in yeast.* Science, 1996. **273**(5275): p. 622-6.
65. Satyal, S.H., et al., *Polyglutamine aggregates alter protein folding homeostasis in Caenorhabditis elegans.* Proc Natl Acad Sci U S A, 2000. **97**(11): p. 5750-5.
66. Carmichael, J., C. Vacher, and D.C. Rubinsztein, *The bacterial chaperonin GroEL requires GroES to reduce aggregation and cell death in a COS-7 cell model of Huntington's disease.* Neurosci Lett, 2002. **330**(3): p. 270-4.
67. Walter, G.M., et al., *Ordered assembly of heat shock proteins, Hsp26, Hsp70, Hsp90, and Hsp104, on expanded polyglutamine fragments revealed by chemical probes.* J Biol Chem, 2011. **286**(47): p. 40486-93.
68. Deng, H.X., et al., *Mutations in UBQLN2 cause dominant X-linked juvenile and adult-onset ALS and ALS/dementia.* Nature, 2011. **477**(7363): p. 211-5.
69. Kleijnen, M.F., et al., *The hPLIC proteins may provide a link between the ubiquitination machinery and the proteasome.* Mol Cell, 2000. **6**(2): p. 409-19.
70. Kleijnen, M.F., R.M. Alarcon, and P.M. Howley, *The ubiquitin-associated domain of hPLIC-2 interacts with the proteasome.* Mol Biol Cell, 2003. **14**(9): p. 3868-75.
71. Massey, L.K., et al., *Overexpression of ubiquilin decreases ubiquitination and degradation of presenilin proteins.* J Alzheimers Dis, 2004. **6**(1): p. 79-92.

72. Raasi, S. and C.M. Pickart, *Rad23 ubiquitin-associated domains (UBA) inhibit 26 S proteasome-catalyzed proteolysis by sequestering lysine 48-linked polyubiquitin chains.* J Biol Chem, 2003. **278**(11): p. 8951-9.
73. Chen, L. and K. Madura, *Rad23 promotes the targeting of proteolytic substrates to the proteasome.* Mol Cell Biol, 2002. **22**(13): p. 4902-13.
74. Verma, R., et al., *Multiubiquitin chain receptors define a layer of substrate selectivity in the ubiquitin-proteasome system.* Cell, 2004. **118**(1): p. 99-110.
75. Hjerpe, R., et al., *UBQLN2 Mediates Autophagy-Independent Protein Aggregate Clearance by the Proteasome.* Cell, 2016. **166**(4): p. 935-49.
76. Chai, Y., et al., *Evidence for proteasome involvement in polyglutamine disease: localization to nuclear inclusions in SCA3/MJD and suppression of polyglutamine aggregation in vitro.* Hum Mol Genet, 1999. **8**(4): p. 673-82.
77. Cummings, C.J., et al., *Chaperone suppression of aggregation and altered subcellular proteasome localization imply protein misfolding in SCA1.* Nat Genet, 1998. **19**(2): p. 148-54.
78. Stenoien, D.L., et al., *Polyglutamine-expanded androgen receptors form aggregates that sequester heat shock proteins, proteasome components and SRC-1, and are suppressed by the HDJ-2 chaperone.* Hum Mol Genet, 1999. **8**(5): p. 731-41.
79. Yvert, G., et al., *Expanded polyglutamines induce neurodegeneration and trans-neuronal alterations in cerebellum and retina of SCA7 transgenic mice.* Hum Mol Genet, 2000. **9**(17): p. 2491-506.
80. Abel, A., et al., *Expression of expanded repeat androgen receptor produces neurologic disease in transgenic mice.* Hum Mol Genet, 2001. **10**(2): p. 107-16.
81. Schmidt, T., et al., *Protein surveillance machinery in brains with spinocerebellar ataxia type 3: redistribution and differential recruitment of 26S proteasome subunits and chaperones to neuronal intranuclear inclusions.* Ann Neurol, 2002. **51**(3): p. 302-10.
82. Stenoien, D.L., M. Mielke, and M.A. Mancini, *Intranuclear ataxin1 inclusions contain both fast- and slow-exchanging components.* Nat Cell Biol, 2002. **4**(10): p. 806-10.
83. Li, X., et al., *Inhibiting the ubiquitin-proteasome system leads to preferential accumulation of toxic N-terminal mutant huntingtin fragments.* Hum Mol Genet, 2010. **19**(12): p. 2445-55.
84. Jana, N.R., et al., *Altered proteasomal function due to the expression of polyglutamine-expanded truncated N-terminal huntingtin induces apoptosis by caspase activation through mitochondrial cytochrome c release.* Hum Mol Genet, 2001. **10**(10): p. 1049-59.
85. Bence, N.F., R.M. Sampat, and R.R. Kopito, *Impairment of the ubiquitin-proteasome system by protein aggregation.* Science, 2001. **292**(5521): p. 1552-5.
86. Bett, J.S., et al., *The ubiquitin-proteasome reporter GFPu does not accumulate in neurons of the R6/2 transgenic mouse model of Huntington's disease.* PLoS One, 2009. **4**(4): p. e5128.
87. Ding, Q., et al., *Polyglutamine expansion, protein aggregation, proteasome activity, and neural survival.* J Biol Chem, 2002. **277**(16): p. 13935-42.
88. Wang, H.L., et al., *Polyglutamine-expanded ataxin-7 decreases nuclear translocation of NF-kappaB p65 and impairs NF-kappaB activity by inhibiting proteasome activity of cerebellar neurons.* Cell Signal, 2007. **19**(3): p. 573-81.
89. Park, S.H., et al., *PolyQ proteins interfere with nuclear degradation of cytosolic proteins by sequestering the Sis1p chaperone.* Cell, 2013. **154**(1): p. 134-45.

90. Bennett, E.J., et al., *Global changes to the ubiquitin system in Huntington's disease.* Nature, 2007. **448**(7154): p. 704-8.
91. Bowman, A.B., et al., *Neuronal dysfunction in a polyglutamine disease model occurs in the absence of ubiquitin-proteasome system impairment and inversely correlates with the degree of nuclear inclusion formation.* Hum Mol Genet, 2005. **14**(5): p. 679-91.
92. Wang, J., et al., *Impaired ubiquitin-proteasome system activity in the synapses of Huntington's disease mice.* J Cell Biol, 2008. **180**(6): p. 1177-89.
93. Tydlacka, S., et al., *Differential activities of the ubiquitin-proteasome system in neurons versus glia may account for the preferential accumulation of misfolded proteins in neurons.* J Neurosci, 2008. **28**(49): p. 13285-95.
94. Zhao, T., et al., *Compartment-Dependent Degradation of Mutant Huntingtin Accounts for Its Preferential Accumulation in Neuronal Processes.* J Neurosci, 2016. **36**(32): p. 8317-28.
95. Reis, S.D., B.R. Pinho, and J.M. Oliveira, *Modulation of Molecular Chaperones in Huntington's Disease and Other Polyglutamine Disorders.* Mol Neurobiol, 2016.
96. Nath, S.R. and A.P. Lieberman, *The Ubiquitination, Disaggregation and Proteasomal Degradation Machineries in Polyglutamine Disease.* Front Mol Neurosci, 2017. **10**: p. 78.

CHAPTER 3

Androgen Receptor Polyglutamine Expansion Drives Age-Dependent Quality Control Defects and Muscle Dysfunction.

3.1 Abstract

Skeletal muscle has emerged as a critical, disease-relevant target tissue in spinal and bulbar muscular atrophy, a degenerative disorder of the neuromuscular system caused by a CAG/polyglutamine (polyQ) expansion in the androgen receptor (AR) gene. Here, we used RNA-sequencing (RNA-Seq) to identify pathways that are disrupted in diseased muscle using AR113Q knockin mice. This analysis unexpectedly identified substantially diminished expression of numerous ubiquitin/proteasome pathway genes in AR113Q muscle, encoding approximately 30% of proteasome subunits and 20% of E2 ubiquitin conjugases. These changes were age, hormone, and glutamine length dependent and arose due to a toxic gain of function conferred by the mutation. Moreover, altered gene expression was associated with decreased levels of the proteasome transcription factor NRF1 and its activator DDI2 and resulted in diminished proteasome activity. Ubiquitinated ADRM1 was detected in AR113Q muscle, indicating the occurrence of stalled proteasomes in mutant mice. Finally, diminished expression of Drosophila orthologues of NRF1 or ADRM1 promoted the accumulation of polyQ AR protein and increased toxicity. Collectively, these data indicate that AR113Q muscle develops progressive proteasome dysfunction that leads to the impairment of quality control and the

accumulation of polyQ AR protein, key features that contribute to the age-dependent onset and progression of this disorder.

3.2 Introduction

Degeneration of the neuromuscular system is characteristic of the age-dependent phenotype that manifests in subjects with spinal and bulbar muscular atrophy (SBMA), a CAG/polyglutamine (polyQ) expansion disorder caused by a mutation in the androgen receptor (AR) gene [1-4]. The polyQ AR undergoes hormone-dependent nuclear translocation and protein unfolding, steps that are essential to disease pathogenesis. Expansion of the AR's polyQ tract both impairs its normal function as a transcriptional regulator and leads to ligand-dependent proteotoxicity. These features result in the disruption of multiple pathways that are critical for normal cellular function [5-12].

Among the tissues affected in SBMA, skeletal muscle is a critical target that contributes to disease pathogenesis. This concept is supported by clinical observations and data from experimental models. SBMA subjects exhibit evidence of muscle toxicity, including myopathic features on muscle biopsy and elevated serum creatine kinase levels that are higher than normally found in purely denervating diseases [13-15]. Moreover, muscle satellite cells cultured from SBMA patients show androgen-dependent impairment of fusion to form myotubes [16], indicating cell autonomous toxicity in muscle. Supporting the notion that myopathy is an early disease manifestation, knock-in mice expressing the polyQ AR develop myopathy months prior to spinal cord pathology [17]. Further support for the role of muscle in disease pathogenesis are data from transgenic mice that over-express the wild type AR only in skeletal muscle and show

hormone-dependent myopathy and motor axon loss; similar effects are seen in transgenic mice over-expressing polyQ AR only in muscle [18]. Notably, the phenotypic severity of SBMA transgenic mice is ameliorated by over-expression of insulin-like growth factor-1 in muscle [19]. That muscle contributes to the SBMA phenotype and provides a therapeutic target is further corroborated by studies showing that peripheral polyQ AR knockdown by antisense oligonucleotides or conditional gene deletion in skeletal muscle rescues disease in mice [20, 21].

While this body of evidence indicates an important role for skeletal muscle in the pathogenesis of neuromuscular degeneration in SBMA, little is known about the pathways that contribute to this process. Here, we used an unbiased approach to identify gene expression changes in skeletal muscle from AR113Q mice, a knock-in mouse model that displays a hormone-dependent phenotype characterized by diminished body weight, impaired strength and shortened lifespan [17]. This analysis unexpectedly uncovered decreased expression of numerous genes encoding components of the ubiquitin proteasome pathway. We demonstrate that these changes are age-, hormone-, and glutamine tract length-dependent, occur in multiple disease-relevant muscles, and are associated with diminished proteasome function. Our analysis identifies progressive impairment of a critical protein quality control pathway in SBMA mice, a feature that likely contributes to the age-dependence of this disorder.

3.3 Results

3.3.1 Age-Dependent Diminished Expression of Ubiquitin-Proteasome Pathway Genes in AR113Q Skeletal Muscle

To identify novel pathways disrupted by the polyQ AR that contribute to skeletal muscle pathology, we performed RNA-Seq on the levator ani/bulbocavernosus (LABC) muscle from littermate wild type and AR113Q males at 14 weeks of age. The LABC is a pelvic floor muscle that was selected because of its sensitivity to polyQ AR toxicity owing to its high level of AR expression. As such, this muscle is markedly atrophic in sexually mature AR113Q males at a young age (Fig 3.1A). Our analysis uncovered a large number of gene expression changes in mutant muscle, including many impacting regulators of cellular energy metabolism including GAPDH, HK2, PGK1, ALDOA, and PGAM2 (Supplemental Table 1), as has been previously reported [9, 22, 23]. Unexpectedly, we also uncovered diminished expression of numerous components of the ubiquitin-proteasome pathway in mutant muscle. These changes involved ~30% of constitutive proteasome subunits and 20% of E2 ubiquitin conjugating enzymes, all of which were reduced in expression in the 14 week LABC from AR113Q males (Fig 3.1B, Supplemental Tables 1, 2); many more subunits trended towards reduced expression but did not reach statistical significance. In contrast, no proteasome subunits were increased in expression, including immunoproteasome subunits and assembly chaperones. Importantly, the observed changes included several key subunits, such as ubiquitin receptors, proteolytic subunits and assembly scaffold proteins.

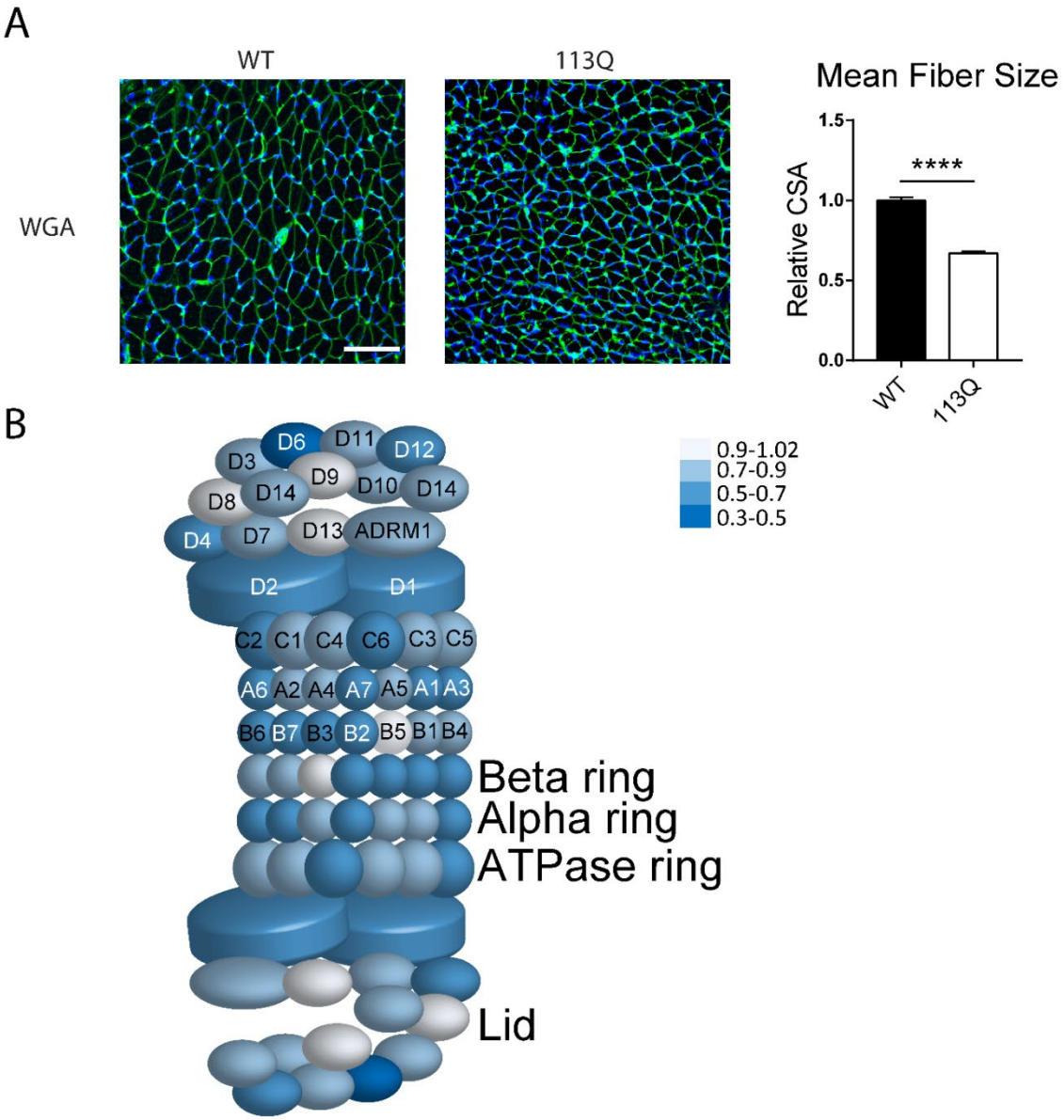

Figure 3.1. Decreased expression of ubiquitin proteasome pathway genes in AR113Q muscle.

A. LABC muscle from 14 wk WT or AR113Q males stained by FITC-wheat germ agglutinin (WGA) to highlight muscle fibers. Scale bar = 100 µm. Fiber size quantified at right and expressed as relative cross sectional area (CSA). Data are mean ± S.E.M. n=3 mice/genotype. ****p<0.0001 by Student t-test. **B.** Diagram of the 26S proteasome, highlighting subunits of the 20S core and the 19S lid. Genes with reduced expression in 14 wk LABC of AR113Q vs WT mice were identified by RNA-Seq and are color coded in blue according to fold change. Those that met a significance threshold of <0.67 fold change are marked with white text labels.

We confirmed in an independent cohort of AR113Q males that proteasome subunits PSMA7, a 20S core scaffold protein [24, 25], and PSMD6, a regulatory subunit of the lid [26], and the ubiquitin conjugase UBE2T were reduced in expression in the 14 week LABC (Fig 3.3, LABC). We also aged a cohort of AR113Q and wild type littermates to 52 weeks, at which point mutant males exhibited a robust phenotype characterized by significantly diminished body weight, grip strength, and limb muscle mass (Fig 3.2).

These mice continued to display significantly decreased expression of PSMA7, PSMD6 and UBE2T in the LABC (Fig 2, LABC). Furthermore, we found that these same gene expression changes also occurred in other disease relevant skeletal muscles, including the quadriceps and tibialis anterior, in an age-dependent manner (Fig 3.3, Quad, TA). Notably, these changes were not detected in 52- week lumbar spinal cord, the site which innervates these muscles,

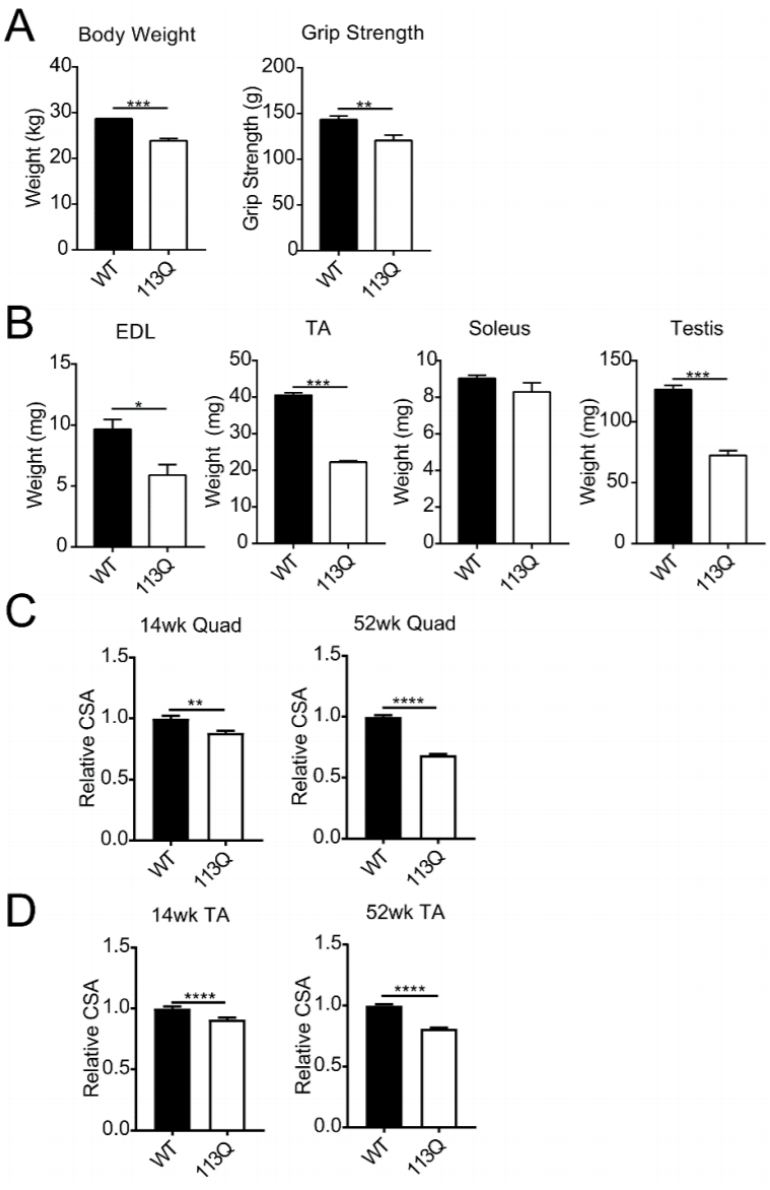

Figure 3.2. AR113Q mice display a robust phenotype at 52 wks. A. 52 wk AR113Q males show significant reduction in body weight (left, n=3/group) and grip strength (right, n=6/group). Data are mean ± S.E.M. **p

suggesting that the gene expression changes were most severe in skeletal muscles of AR113Q mice (Fig 2, Lumbar SC).

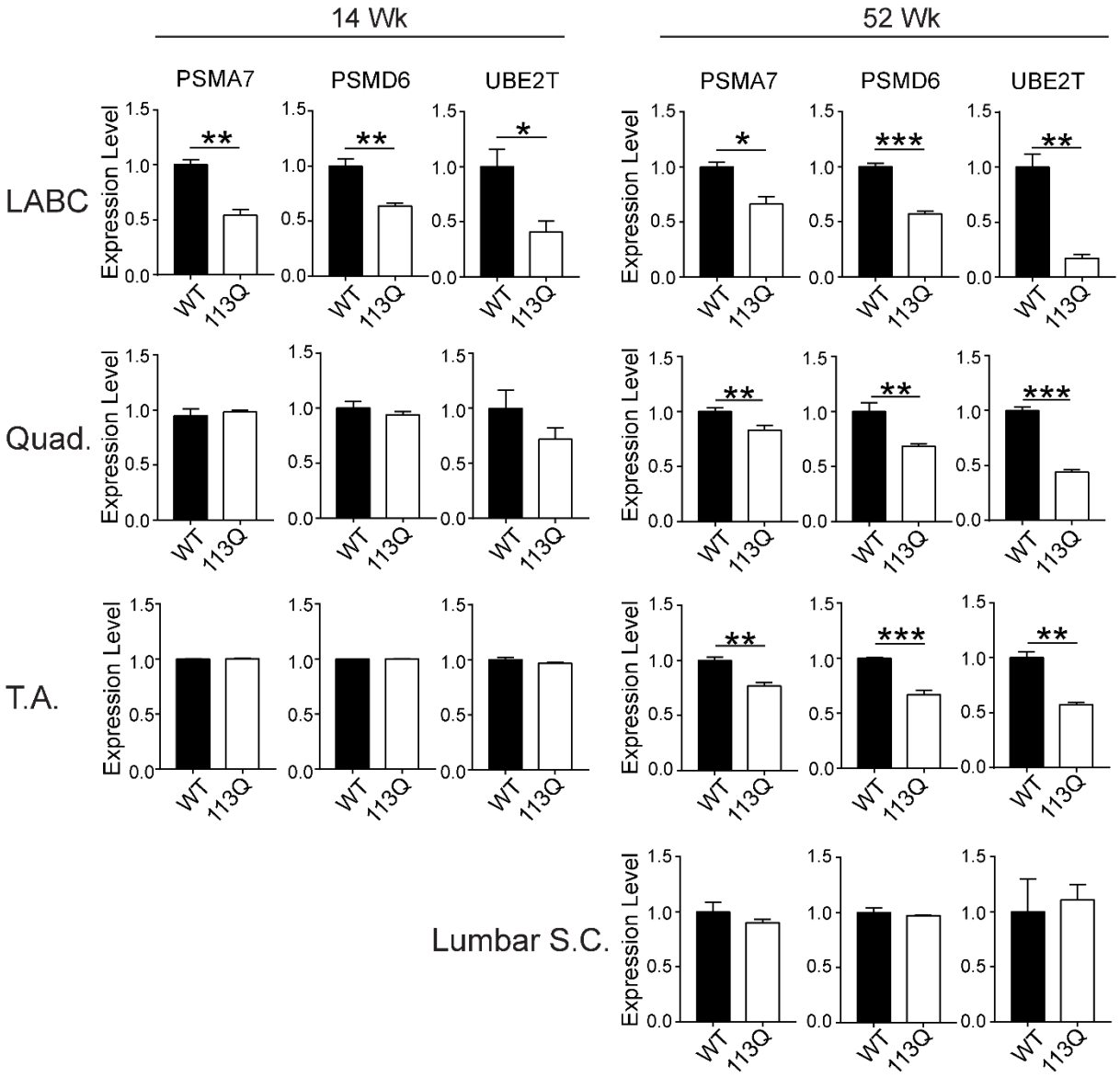

Figure 3.3. Decreased expression of ubiquitin proteasome pathway genes is age-dependent. Relative expression of proteasome genes *Psma7* and *Psmd6* and the ubiquitin conjugase *Ube2T* was determined in WT or AR113Q mice at 14 or 52 wks by qPCR. Shown are data from LABC (n=3 mice/genotype), quadriceps (quad) (14wk: n=3mice/genotype, 52wk: n=6 mice/genotype), tibialis anterior (TA) (n=3 mice/genotype) and lumbar spinal cord (SC) (n=3 mice/genotype). Data are mean ± S.E.M. *p<0.05, **p<0.01, ***p<0.001 by t-test.

3.3.2 Gene Expression Changes are PolyQ Length-Dependent and Mediated by a Toxic Gain-of-Function

Pathologic expansion of the androgen receptor's polyQ tract leads to both a partial loss of normal function and ligand-dependent proteotoxicity. We sought to determine the extent to which these two consequences of the mutation contribute to age-dependent loss of ubiquitin proteasome pathway gene expression. To address this question, we first determined whether changes in gene expression were solely dependent upon the length of AR's polyQ tract. To accomplish this, we compared gene expression in two lines of knock-in mice generated using the same targeting vector except for the length of the CAG repeat [27, 28]. Whereas AR113Q mice develop age-dependent neuromuscular pathology, AR21Q males are similar to wild type littermates [17]. Expression of PSMA7, PSMD6 and UBE2T was significantly decreased in 14 week LABC of AR113Q versus AR21Q males, establishing that these changes are dependent upon the length of the polyQ tract (Fig 3.4A).

To probe how polyQ AR alters gene expression, we asked whether these changes represent a loss of normal AR signaling or a gain of a new, toxic function. To answer this question, we first examined the effect of surgical castration in wild type males. This intervention leads to loss of testosterone production and consequently eliminates ligand-dependent AR signaling. Castration alone had no effect on expression of the proteasome genes PSMA7 and PSMD6 and slightly increased expression of UBE2T (Fig 3.4B), indicating that loss of AR signaling was not sufficient to account for gene expression changes characteristic of AR113Q muscle.

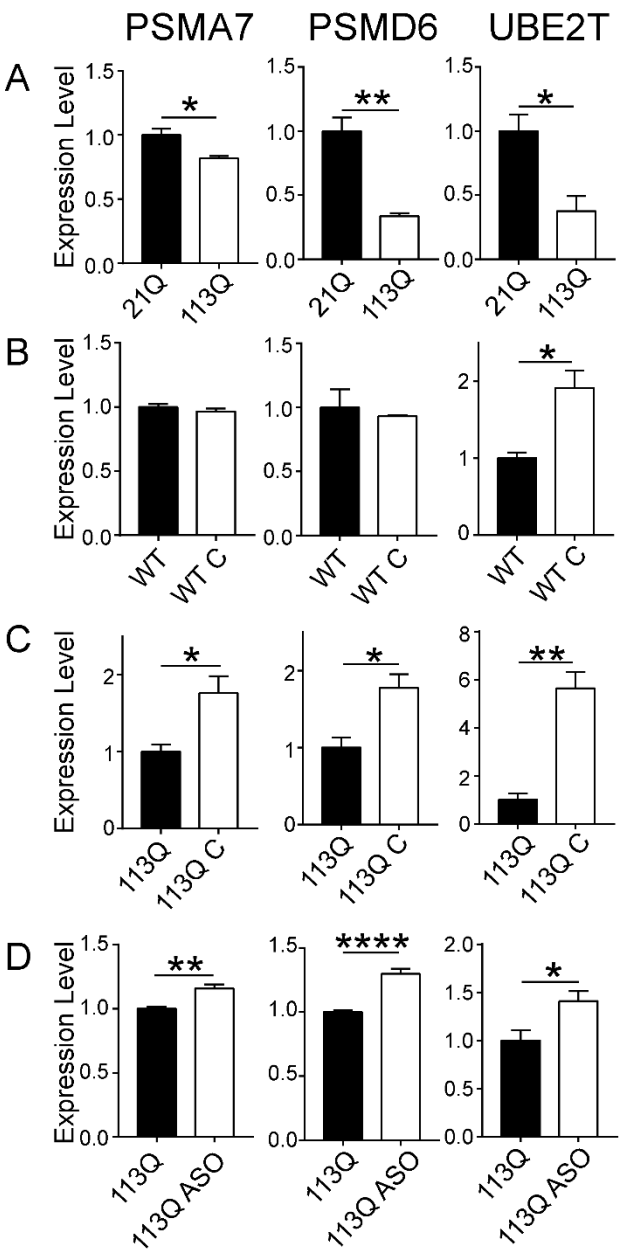

Figure 3.4. Ubiquitin proteasome pathway gene expression changes are hormone- and glutamine-length dependent. A. Relative expression of *Psma7, Psmd6* and *Ube2T* was determined in LABC from 14 wk AR21Q or AR113Q mice by qPCR. Data are mean ± S.E.M. n=3mice/genotype. **B., C.** WT (panel B) and AR113Q (panel C) males were surgically castrated (C) at 5-6 wks, then aged to 14 wks. Gene expression in LABC was determined by qPCR and compared to noncastrated littermates. Data are mean ± S.E.M. n=3mice/genotype. **D.** AR113Q males were treated with AR targeted ASO or vehicle from 6 – 26 wks. Gene expression in quadriceps was determined by qPCR. Data are mean ± S.E.M. n=3-4mice/genotype. **A-D.** *p<0.05, **p<0.01, ****p<0.0001 by t-test.

In contrast to effects in wild type males, surgical castration of AR113Q males significantly rescued gene expression exchanges (Fig 3.4C). These findings are consistent with

other manifestations of the neuromuscular phenotype of AR113Q males that are dependent upon both polyQ AR and its ligand testosterone [17], reflecting ligand-dependent proteotoxicity. The essential role of polyQ AR expression in muscle to effect these changes was verified by subcutaneous administration of AR-targeted antisense oligonucleotides (ASO). Treatment of AR113Q mice with ASOs from age 6 to 26 weeks rescues disease phenotypes and diminishes polyQ AR expression in skeletal muscle but not spinal cord [20]. This treatment also increased expression of PSMA7, PSMD6 and UBE2T in quadriceps muscle of mutant males (Fig 3.4D). Collectively, these data show that diminished expression of ubiquitin-proteasome pathway genes is polyglutamine length-dependent and mediated by a toxic gain-of-function.

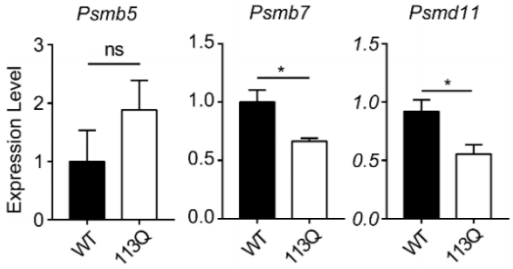

Figure 3.5. Proteasome gene expression in AR113Q LABC at 14 wk. Relative expression of Psmb5, Psmb7 and Psmb11 was determined in LABC of wild type or AR113Q mice at 14 wk by qPCR. Data are mean ± S.E.M. n=3 mice/genotype. *p<0.05 by t-test

3.3.3 Loss of Proteasome Subunits is Associated with Diminished Proteasome Transcriptional Machinery

Coincident with diminished gene expression, we found that AR113Q muscle showed robust and significant reduction in several proteasome subunits when analyzed by western blot. Subunits altered in 14 week LABC included PSMB7, the trypsin-like subunit [29], PSMB5, the chymotrypsin-like subunit [29], PSMD11, which functions as a regulatory link between the ATPase ring and 20S core [30], and PSMA7, a scaffold protein and contributor to the size gate of the proteasome [24, 25] (Fig 3.6A). We further confirmed changes in PSMB5 and PSMB7 protein levels in 52- week quadriceps muscle (Fig 3.6B). Notably, all proteasome subunits that

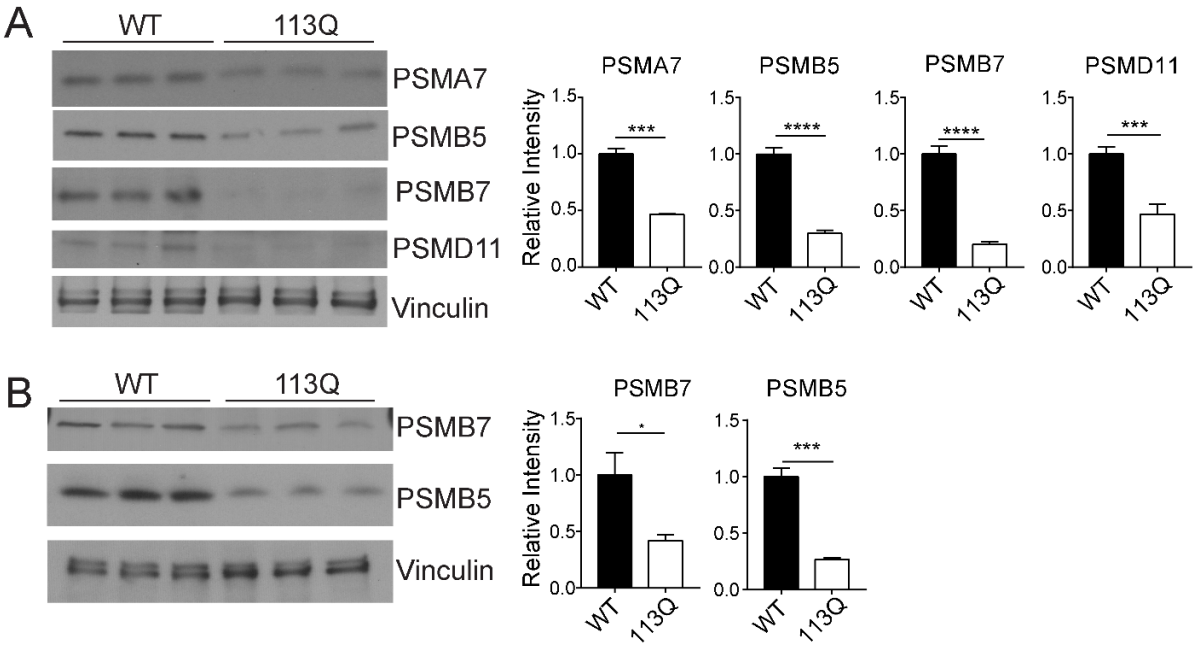

Figure 3.6. Proteasome subunits are decreased in AR113Q muscle. A., B. LABC (panel A) was harvested at 14 wks and quadriceps (panel B) at 52 wks from WT and AR113Q mice. Samples were analyzed by western blot for indicated proteasome subunits. Vinculin controls for loading. Quantified at right. Data are mean ± S.E.M. n=6-7 mice/genotype (LABC) and n=3mice/genotype (quad). *p<0.05, ***p<0.001, ****p<0.0001 by t-test.

were found to be down-regulated at the protein level also showed reduced mRNA expression, except for PSMB5 (Fig 3.5). The finding that this subunit was decreased at the protein but not mRNA level raises the possibility that the level of the entire proteasome machinery may be diminished in mutant muscle.

Given the broad loss of proteasome subunit expression, we hypothesized that critical transcriptional activators of proteasome genes are altered in AR113Q muscle. To test this notion, we examined the best characterized proteasome transcription factor, nuclear factor erythroid 2 like 1 (Nrf1/NFE2L1) [31]. We found a robust loss of the 95 kDa form of Nrf1 in both 14 week LABC (Fig 3.7A) and 52 week quadriceps muscle (Fig 5B) from AR113Q males. This observation was confirmed using a second anti-Nrf1 antibody (Fig 3.8). Notably, the 95 kDa Nrf1 species is the cleaved and active form of this transcription factor [32], and the changes we observed in AR113Q mice occurred in the absence of changes in Nrf1/NFE2L1 gene expression

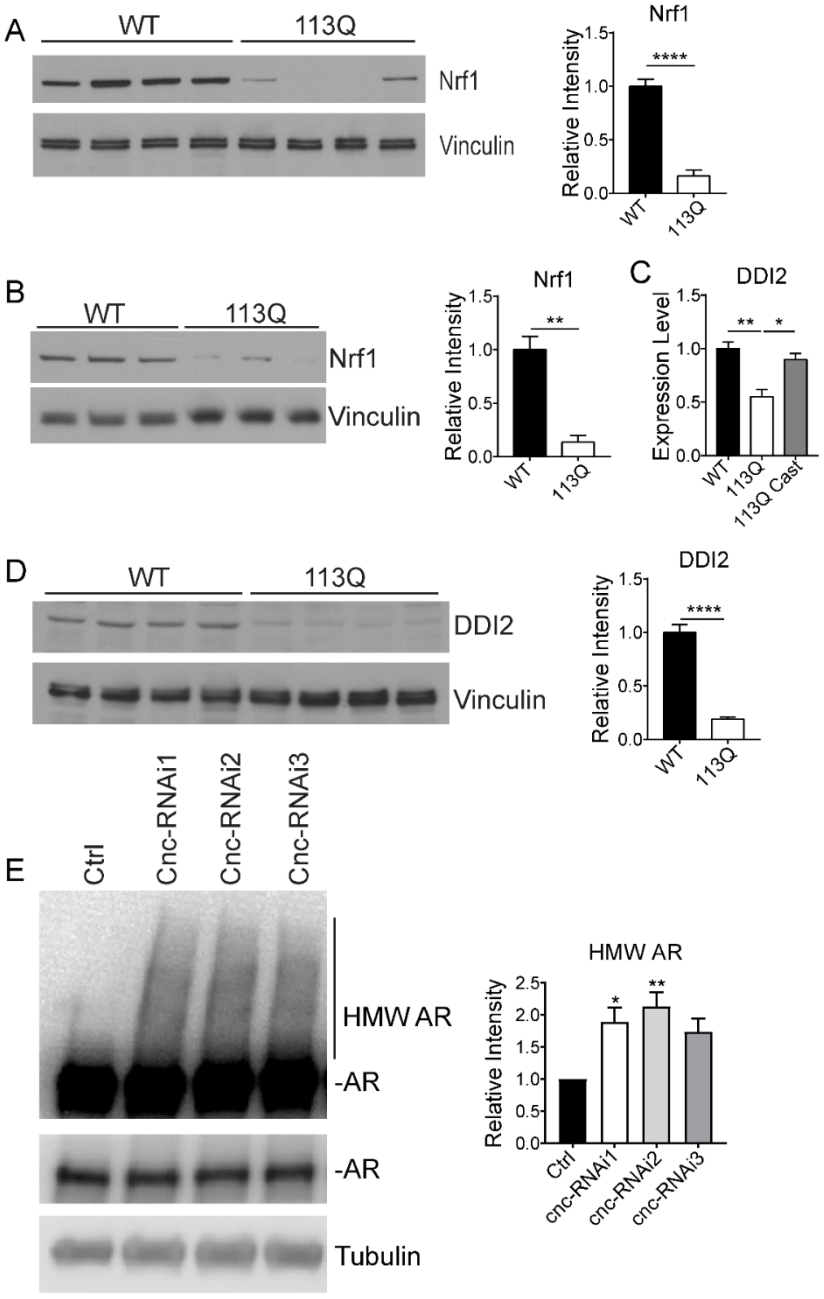

Figure 3.7. Nrf1 and DDI2 are reduced in AR113Q muscle, and reduction of Nrf1 leads to a buildup of polyQ AR in vivo. A., B. Lysates from 14 wk LABC (panel A) or 52 wk quadriceps (panel B) were probed by western blot for expression of the proteasome transcription factor Nrf1 (NFE2L1). Vinculin controls for loading. Quantified at right. Data are mean ± S.E.M. n=3 mice/genotype (Quad) and 4 mice/genotype (LABC). **p<0.01, ****p<0.0001 by t-test. **C.** Expression of DDI2 mRNA was quantified in 14 wk LABC from WT, AR113Q and castrated AR113Q mice by qPCR. Data are mean ± S.E.M. n=3 mice/genotype. *p<0.05, **p<0.01 by t-test. **D.** Lysates from 14wk LABC were probed by western blot for expression of DDI2. Vinculin controls for loading. Quantified at right. Data are mean ± S.E.M. n=4 mice/genotype. ****p<0.0001 by t-test. **E.** *Drosophila* expressing AR52Q under control of the GMR-gal4 promoter were crossed to 3 independent lines expressing RNAi targeted towards cap'n'collar (cnc), the Nrf1 orthologue. Levels of AR were analyzed by western blot. Tubulin controls for loading. Relative intensity of high MW (HMW) AR species quantified at right. Data are mean ± S.E.M. n=5 biological replicates/group. *p<0.05, **p<0.01 by one-way ANOVA with Tukey's post-hoc test.

species are lost in disease. Recent work from multiple groups has demonstrated that the mammalian aspartyl protease DDI2 and its *C. elegans* orthologue SKN-1A cleave Nrf1 from the ER membrane to allow nuclear translocation and transcription of proteasomal genes [33, 34]. Intriguigly, both mRNA and protein levels of DDI2 were diminished in the 14 week LABC of AR113Q mice (Fig 3.7C, D). Furthermore, the loss of DDI2 gene expression was rescued by surgical castration, similar to proteasome gene expression changes, suggesting that diminished DDI2 may contribute to decreased 95 kDa Nrf1 species in AR113Q muscle.

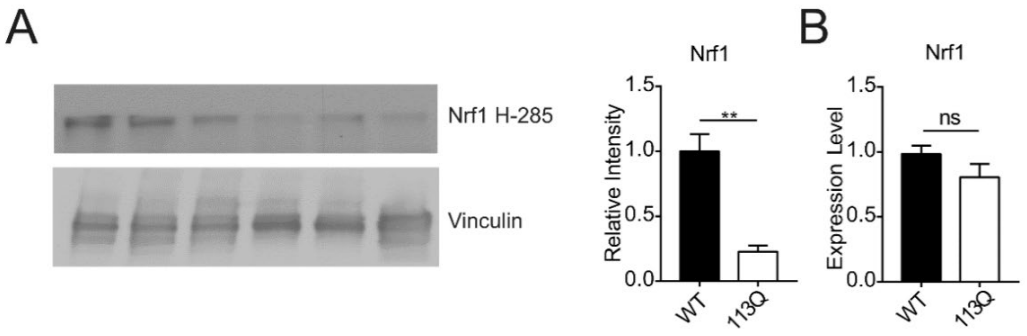

Figure 3.8. NRF1 is reduced in the 14 wk AR113Q LABC. A. 14 wk LABC from wild type or AR113Q males was probed by western blot for Nrf1 using the H-285 antibody. Quantified at right. Data are mean ± S.E.M. n=3 mice/genotype. **p<0.01 by t-test B. Relative expression of NRF1 (NFE2L1) was determined in LABC of WT or AR113Q mice at 14 wk by qPCR. Data are mean ± S.E.M. n=3 mice/genotype. Not significant (ns) by t-test.

To determine whether loss of the proteasome transcriptional machinery is sufficient to alter steady state levels of polyQ AR, we used a well-characterized *Drosophila* model expressing AR52Q under the control of the GMR-Gal4 promoter [35]. We crossed this model to three independent lines expressing RNAi towards cap'n'collar, the fly orthologue of Nrf1 [36]. Cap'n'collar knockdown causes diminished expression of proteasome genes in flies [36]. Target knockdown was confirmed by quantitative PCR (qPCR) (Fig 3.9). This manipulation resulted in significant accumulation of high molecular weight polyQ AR species in two of three lines, with the third line yielding results that trended similarly (p=0.06) (Fig 3.7E). We conclude that loss of Nrf1 impairs polyQ AR clearance *in vivo*. This accumulation of polyQ AR protein was

accompanied by evidence of enhanced toxicity (Fig 3.9D). We conclude that loss of NRF1 impairs polyQ AR clearance in vivo and that this accumulation contributes to age-dependent toxicity in vivo.

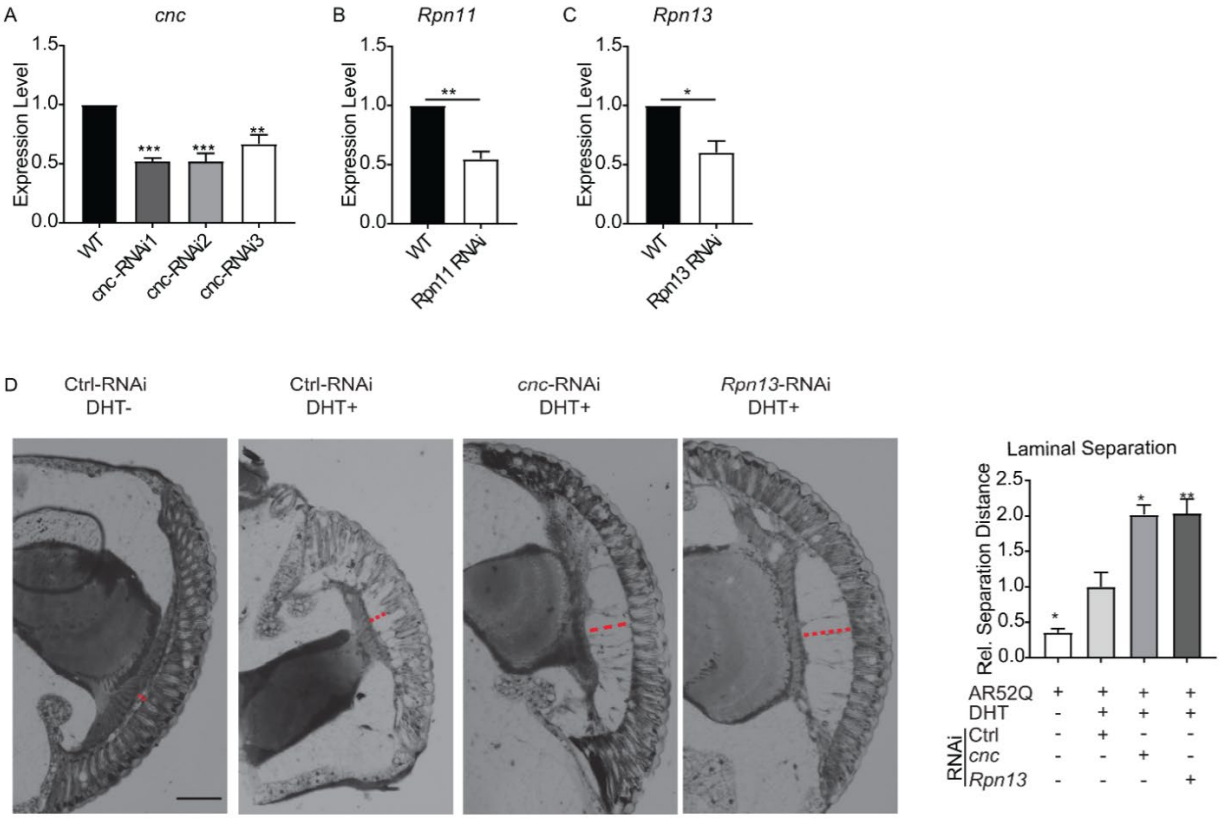

Figure 3.9. Cnc knockdown leads to enhanced toxicity in drosophila. A. Relative cnc expression in WT and cnc RNAi Drosophila lines was measured by qPCR. Data are mean ± S.E.M. n=3 biological replicates/group. **p<0.01, ***p<0.001 by one-way ANOVA with Tukey's post-hoc test. B. Relative Rpn11 expression in WT and Rpn11 RNAi Drosophila lines was measured by qPCR. Data are mean ± S.E.M. n=3 biological replicates/group. **p<0.01 by t-test C. Relative Rpn13 expression in WT and Rpn13 RNAi Drosophila lines was measured by qPCR. Data are mean ± S.E.M. n=3 biological replicates/group. *p<0.05, **p<0.01 by one-way ANOVA with Tukey's posthoc test.

3.3.4 Proteasome Activity is Diminished in AR113Q mice

Following our results demonstrating reduced level of Nrf1, DDI2 and proteasome subunits, we hypothesized that AR113Q muscle exhibits decreased proteasome activity. To test the functional status of the proteasome, we employed the activity based probe Me_4BodipyFL-Ahx_3Leu_3VS. This fluorescent probe binds the active site of catalytic proteasome subunits, allowing detection of changes in constitutive proteasome subunits as well as induction of the

immunoproteasome [37, 38]. We initially confirmed that signal in this assay was inhibited by MG132, a small molecule that similarly binds catalytic sites to inhibit proteasome activity and thereby competes for binding by the activity based probe (Fig 3.10). Using this assay, we found relatively little difference in proteasome activity in quadriceps muscle at 14 weeks, but significant age-dependent loss of active PSMB5 and PSMB6/7 bands in 52-week quadriceps of AR113Q mice (Fig 3.11A, B). These changes were not associated with the appearance of additional bands that might suggest induction of the immunoproteasome. Corroborating these findings in 52-week quadriceps muscle, we observed a significant reduction in chymotrypsin-like activity of the proteasome as measured by cleavage of the fluorogenic substrate Suc-AMC-LLVY (Fig 6C).

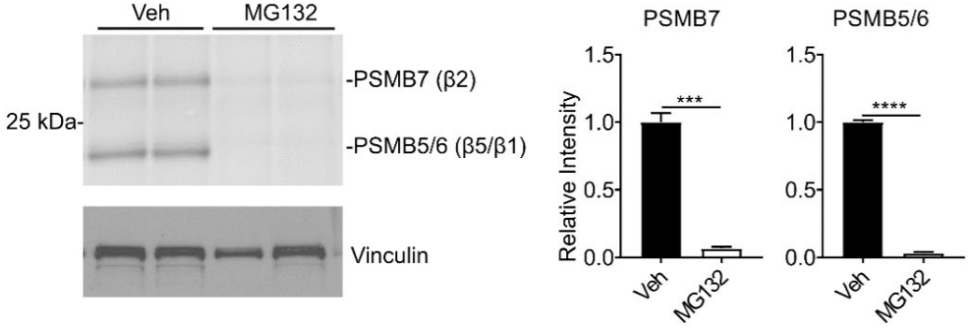

Figure 3.10. Signal from activity based probe is inhibited by MG132. 14 wk quadriceps from wild type mice were lysed in HR buffer and incubated with a BODIPY-labeled activity based probe in the absence (Veh) or presence of 25 μM MG132. Co-incubation with MG132 significantly reduced the level of active proteasomes. Data was normalized to vinculin and quantified at right. Data are mean ± S.E.M. n=3 mice/group. ***p<0.001, ****p<0.0001 by t-test.

To assess the consequence of diminished functional proteasomes on polyQ AR clearance, we used PC12 cells stably expressing AR112Q under the control of a TetOn promoter [39]. Inhibition of the proteasome by epoxomicin led to the accumulation of high molecular weight polyQ AR (Fig 3.11D), suggestive of ubiquitinated or aggregated species and paralleling our findings in *Drosophila* following knockdown of cap'n'collar (Fig 3.7E). Furthermore, inhibition

of ubiquitination by MLN7243, a small molecule inhibitor of E1 ubiquitin activating enzymes [40], led to accumulation of AR112Q monomer, demonstrating the importance of ubiquitination and an intact proteasome on polyQ AR clearance (Fig 3.11E).

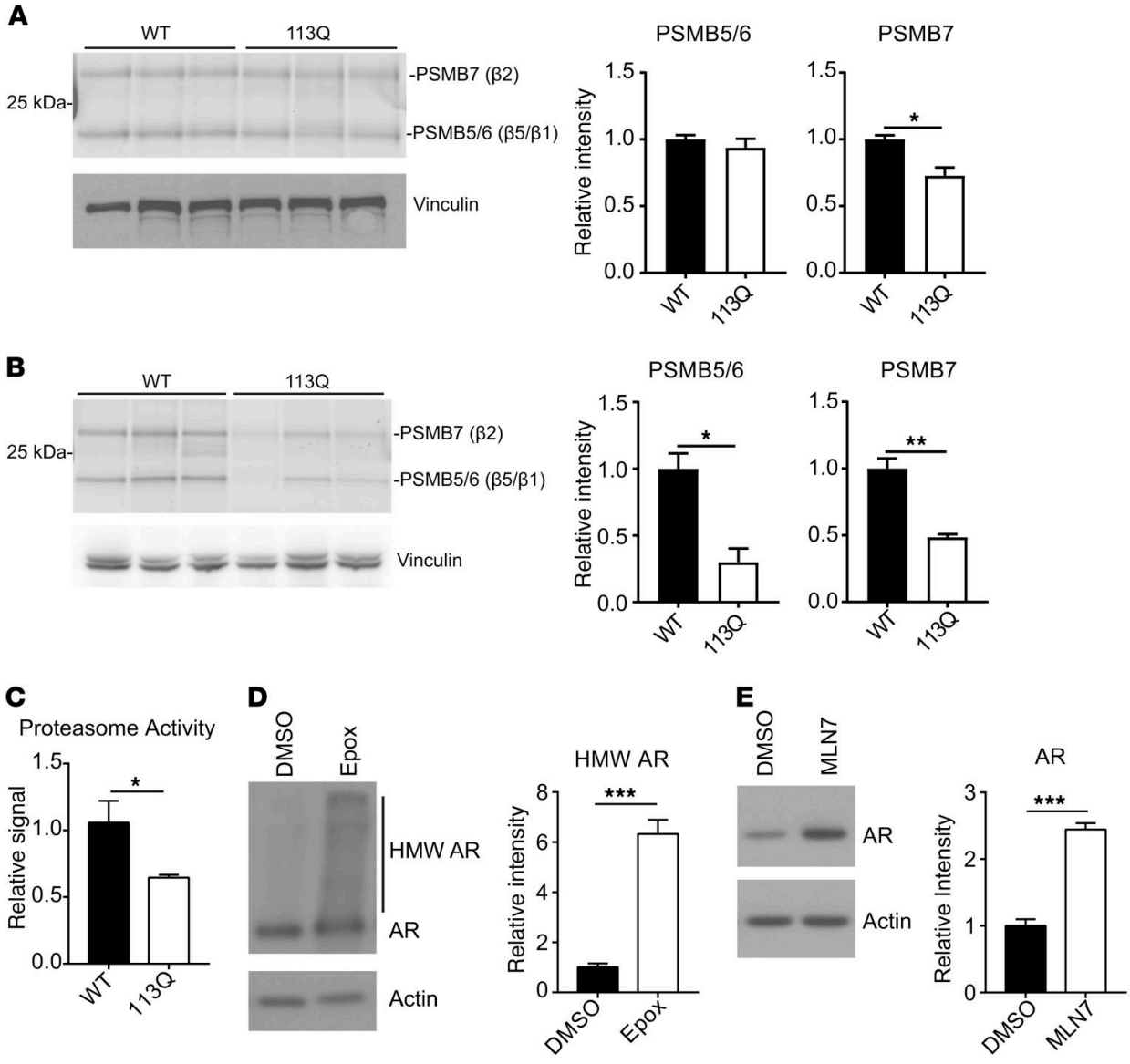

Figure 3.11. Proteasome activity is diminished in AR113Q muscle. A., B. Lysates from14 wk (panel A) and 52 wk (panel B) quadriceps were incubated with a BODIPY-labeled activity based probe, then resolved by SDS-PAGE. Quantified at right. Data are mean ± S.E.M. n=3 mice/genotype. *p<0.05, **p<0.01 by t-test. **C.** Lysates from quadriceps were prepared from 52 wk WT and AR113Q mice and probed for chymotrypsin-like activity of the proteasome by cleavage of AMC-Suc-LLVY. Data are mean ± S.E.M. n=3 mice/genotype. *p<0.05 by t-test. **D, E.** PC12 cells were induced to express AR112Q for 48h in the presence of 10 nM R1881, then washed with PBS and incubated with 100 nM epoxomicin (Epox), 1uM MLN7243 (MLN7) or vehicle (DMSO) for 18h, as indicated. AR levels were determined by western blot. Quantified at right. Data are mean ± S.E.M. n=3 biological replicates. ***p<0.001 by t-test.

3.3.5 Proteasome Lid Modifications Suggest Impairment of PolyQ AR Degradation

The importance of ubiquitination for polyQ AR clearance prompted us to examine the proteasome subunits responsible for binding ubiquitinated substrates in AR113Q muscle. Ubiquitination of the proteasome's ubiquitin receptor ADRM1/Rpn13 has been shown to occur, causing blockade of ubiquitin-dependent degradation and leading to a buildup of "stalled" proteasomes [41]. To assess whether this occurs in AR113Q mice, we examined ADRM1 protein in WT and AR113Q 14 week LABC and 52 week quadriceps. Strikingly, we found evidence of high molecular weight bands and diminished ADRM1 monomer in these mutant muscles (Fig 3.12A, Fig 3.13A). To confirm that high molecular weight ADRM1 bands reflected ubiquitinated species, samples were incubated with the deubiquitinating (DUB) enzyme USP2 in the absence or presence of the DUB inhibitor N-ethylmaleimide (NEM). This treatment reduced the high molecular weight bands to the monomer only in the absence of NEM (Fig 3.13B, Fig 3.12B), indicating that ubiquitinated ADRM1 had accumulated in AR113Q muscle. We further confirmed ADRM1 ubiquitination in AR113Q muscle by ADRM1 IP, followed by Western blot for ubiquitin (Fig 3.12C).

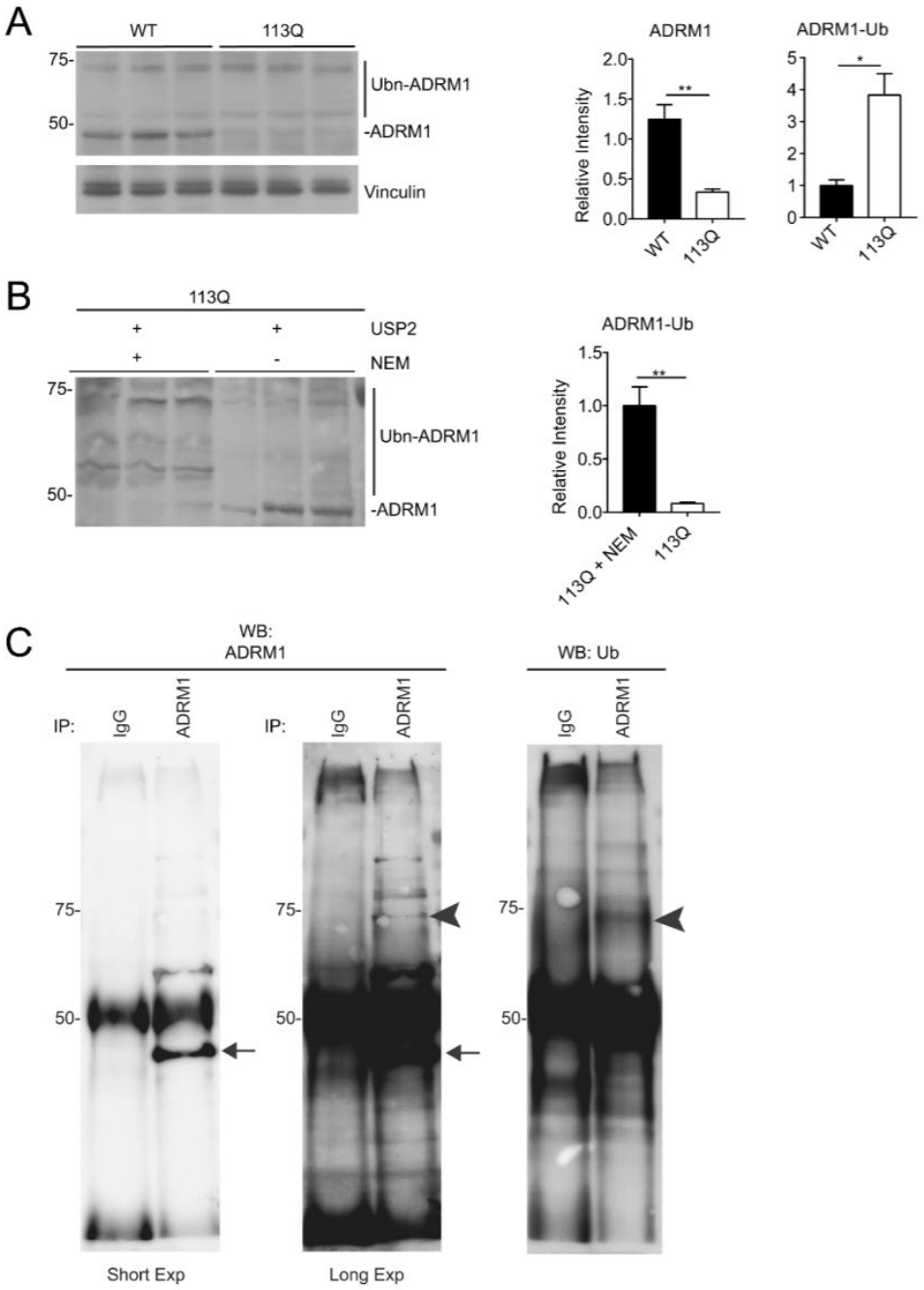

Figure 3.12. ADRM1 is ubiquitinated in AR113Q LABC A. Lysates of 14 wk LABC were probed by western blot for ADRM1. Vinculin controls for loading; quantified at right. Data are mean ± S.E.M. n=3 mice/genotype. *p<0.05, **p<0.01 by t-test. B. Lysates of 14 wk LABC were incubated with the catalytic domain of USP2 in the absence or presence of10 μM of the deubiquitinase inhibitor NEM, as indicated, and then analyzed by western blot. High molecular weight species were normalized to level of ADRM1 monomer. Quantified at right. n=3 mice/genotype. **p<0.01 by t-test. C. Lysates of AR113Q 52 wk gastrocnemius muscle were immunoprecipitated with either ADRM1 antibody or control IgG. Arrow indicates endogenous, unmodified ADRM1; arrowhead indicates endogenous high molecular weight ADRM1 species identified by western blot for ADRM1 or ubiquitin. Dense ~50 KDa band represents immunoglobulin heavy chain.

To assess the functional importance of this proteasome subunit in polyQ AR clearance, we used *Drosophila* expressing AR52Q under the control of the GMR-Gal4 promoter [35]. We crossed this line to flies expressing RNAi towards Rpn13/ADRM1. Flies expressing RNAi towards Rpn11, a well-characterized DUB associated with the proteasome that removes ubiquitin chains and allows for substrate entrance [42], was used as a positive control. We found that knockdown of either Rpn13/ADRM1 or Rpn11 led to an accumulation of high molecular weight polyQ AR in vivo (Fig 3.13C), similar to the effects of cap'n'collar knockdown (Figure 3.7E). Further, treatment of PC12 cells expressing AR112Q with RA190, a small molecule that inhibits Rpn13 [43], yielded similar results (Figure 3.13D), emphasizing the role of the proteasome lid in polyQ AR degradation. Collectively, our results demonstrate that impairment of the proteasome occurs by multiple mechanisms *in vivo*, including transcriptional silencing and post-translational

modification, and that the loss of functional proteasomes leads to the accumulation of the toxic, mutant protein.

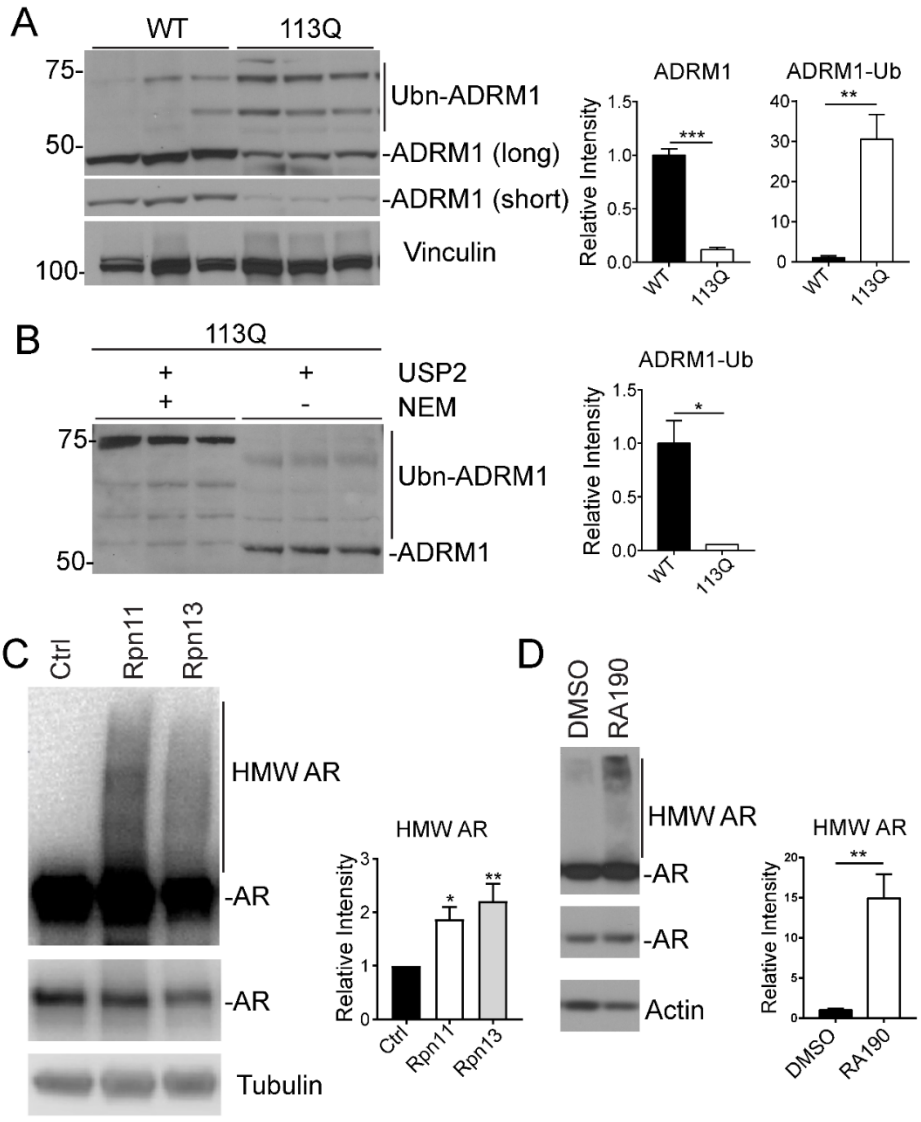

Figure 3.13. ADRM1 is ubiquitinated in 113Q mouse muscle. A. Lysates of 52 wk quadriceps were probed by western blot for ADRM1. Vinculin controls for loading; quantified at right. Data are mean ± S.E.M. n=3 mice/genotype. **p<0.01, ***p<0.001 by t-test. **B.** Lysates of 52 wk quadriceps were incubated with the catalytic domain of USP2 in the absence or presence of 10 μM NEM, as indicated, and then analyzed by western blot. High molecular weight species were normalized to level of ADRM1 monomer. Quantified at right. n=3 mice/genotype. *p<0.05 by t-test. **C.** *Drosophila* expressing AR52Q under control of the GMR-Gal4 promoter were crossed to lines expressing RNAi against Rpn11 or Rpn13/ADRM1. Levels of AR were analyzed by western blot. Tubulin controls for loading. Relative intensity of high MW (HMW) AR species quantified at right. *p<0.05, **p<0.01 by one-way ANOVA with Tukey's post-hoc test. **D.** PC12 cells were induced to express AR112Q for 72h in the presence of 10 nM R1881, then washed with PBS and treated with DMSO or 3 μM RA190 to inhibit Rpn13/ADRM1 for 18h. Data are mean ± S.E.M. n=3 biological replicates. **p<0.01 by t-test.

3.4 Discussion

Here we sought to identify key pathways that contribute to SBMA pathogenesis by using an unbiased analysis of gene expression changes. To accomplish this, we performed RNA-Seq on the levator ani/bulbocavernosus muscle, a pelvic floor muscle. This muscle expresses high levels of polyQ AR and is severely atrophic in AR113Q males, a mouse model of SBMA generated through gene targeting [17, 27]. Our focus on skeletal muscle builds on recent data from SBMA patients and model systems that polyQ AR expression in peripheral tissues, particularly skeletal muscle, is a critical contributor to the disease phenotype [4, 20, 21]. Our analysis identified significant down-regulation of genes encoding components of the ubiquitin proteasome pathway, including ~30% of proteasome subunits and ~20% of E2 ubiquitin conjugating enzymes. Dysregulation of this pathway was of particular interest since prior studies have established that quality control decisions regulating degradation of the polyQ AR are tightly controlled by the Hsp90/Hsp70-based chaperone machinery [44]. Importantly, targeting this pathway promotes clearance of the polyQ AR by the proteasome and alleviates the disease phenotype in SBMA models [45-50]. Our findings establish that proteasome function diminishes with age in multiple disease-relevant skeletal muscles from AR113Q mice. This identifies a progressive impairment of the proteostasis machinery that likely contributes to the age-dependent phenotype characteristic of this disorder.

The occurrence of proteasome dysfunction in AR113Q muscle was unanticipated, as skeletal muscle atrophy that follows other injuries, including surgical denervation, fasting, tumor bearing, uremia and diabetes, are all associated with a significant up-regulation of proteasome subunits [51]. Notably, SBMA is distinguished from these other states by the accumulation of a toxic, misfolded protein in diseased muscle. That the impairment of proteasome function is

closely tied to this pathology is demonstrated by the observation that gene expression changes occur as a consequence of a gain-of-function conferred by the polyQ tract expansion (Fig 3). These gene expression changes result in diminished functionally active proteasomes (Fig 6) and an accumulation of stalled proteasomes characterized by the ubiquitination of ADRM1, a proteasome subunit responsible for binding ubiquitinated substrates (Fig 7). We demonstrate that changes in proteasome function impair clearance of the polyQ AR in well-established cellular and *Drosophila* models of SBMA (Figs 5, 7), indicating the importance of quality control defects to disease. Notably, prior studies have demonstrated up-regulation of macroautophagy in AR113Q and SBMA patient muscle [52, 53], a compensatory response that is likely aimed at maintaining organ system homeostasis in the setting of diminished proteasome function.

The extent to which proteasome dysfunction occurs in the polyglutamine diseases has been controversial, as previous findings *in vivo* have lacked consistency and reproducibility [54]. In SBMA, proteasome activity was previously studied in transgenic mice over-expressing AR97Q. While accumulation of the proteasome reporter substrate GFP-Ub was noted, this finding was attributed to increased GFP-Ub gene expression as measured relative to the loading control GAPDH [47]. However, recent studies have demonstrated marked down-regulation of glycolytic enzymes, including GAPDH, in muscle from SBMA mice and patients as a component of a previously unappreciated metabolic shift [22, 23]. Our current analysis takes into account these changes and demonstrates diminished proteasome mRNA and protein levels, along with impaired function in AR113Q muscle.

The consequences of expansion of the AR's polyQ tract are complex, with a resulting partial loss-of-function impairing transcriptional regulation of AR target genes, and ligand-dependent proteotoxicity disrupting several critical downstream pathways [1-4]. Both of these

effects are likely to contribute to the SBMA phenotype. In fact, restoring transcriptional regulatory activity to the polyQ AR by disrupting its SUMOylation (AR113Q KRKR mice) rescues exercise capacity and extends lifespan without altering protein aggregation or rescuing muscle atrophy [55]. In contrast, the effects on proteasome function characterized here are independent of the partial loss-of-function conferred by the polyQ tract expansion. This conclusion is supported by the fact that the changes in ubiquitin-proteasome pathway genes in AR113Q mice persist in skeletal muscle from AR113Q KRKR mutants (data not shown).

Collectively, our data demonstrate that the proteasome is impaired in AR113Q muscles by a multifactorial process, including loss of the transcriptional machinery that promotes gene expression, diminished catalytic activity, and the occurrence of post-translational modifications to proteasome subunits that impair binding of ubiquitinated substrates. These findings represent, to our knowledge, the first demonstration of DDI2 and ADRM1 alterations in a mouse model of disease, and validate the functional relevance of these changes in the context of proteotoxic stress. While the proteasome shows functional impairment of AR113Q muscle, we speculate that enhancing polyQ AR degradation by the proteasome remains a viable therapeutic strategy. Supporting this notion are several reports leveraging the chaperone machinery to achieve this result [44-46, 50, 56-63]. We propose that alleviating proteasome dysfunction may confer a synergistic rescue with efforts to target the chaperone machinery. This concept is supported by a recent study demonstrating that activation of the transcription factors Nrf1 or Nrf2 by a small molecule leads to significant phenotypic rescue in a transgenic mouse model of SBMA [64]. By combining strategies such as this with proteasome activation and/or chaperone modulation, it may be possible to significantly enhance the selective degradation of polyglutamine proteins, including the polyQ AR.

3.5 Methods

Antibodies and Reagents:

The following primary antibodies were used in our studies: Rabbit anti-AR (N20, Santa Cruz), mouse anti-beta-actin (Sigma), mouse anti-vinculin (Sigma), rabbit anti-PSMA7 (Abcam), rabbit anti-PSMB7 (Cell Signaling), rabbit anti-PSMB5 (Abcam), rabbit anti PSMD11 (Novus), rabbit anti-ADRM1 (Novus), rabbit anti-Nrf1 (C-19, Santa Cruz) (H-285, Santa Cruz), wheat germ agglutinin alexa fluor 488 conjugate (Thermo), mouse anti-tubulin (Sigma). The following drugs and small molecules were used: MLN7243 (Chemietek), RA190 (Calbiochem), epoxomicin (Sigma), MG132 (Sigma), Me4BodipyFL-Ahx3Leu3VS (Boston Biochem), Suc-LLVY-AMC (Enzo Life Sciences).

Mice:

AR113Q and AR21 knock-in mice were derived using exon 1-specific targeting, as previously described [17, 27, 28], and backcrossed to C57BL/6 (≥10 generations). Mice were housed in a specific pathogen free facility, and maintained on a 12-hr light/dark cycle with chow and water ad libitum. Genotyping was performed by polymerase chain reaction (PCR) on ear samples, and primer sequences were as follows: AR fwd: 5′-CCAGAATCTGTTCCAGAGCGTG-3′ (Sigma, 6-FAM labeled), AR rev: 5′-TGTTCCCCTGGACTCAGATG-3′ (Invitrogen). For ASO treatment, mice were injected from 6 weeks of age to 26 weeks of age once per week subcutaneously with an antisense oligonucleotide (50 mg/kg body weight) containing the following sequence: AAGTTGTAGTAGTCGC, as previously described [20]. This 16-mer, 2’,4’-constrained ethyl gapmer ASO is complementary to human and mouse AR transcripts. All

procedures involving mice were approved by the University of Michigan Committee on Use and Care of Animals (PRO00006114) and conducted in accordance with institutional and federal guidelines.

Orchiectomy:

Mice were surgically castrated at 5-6 weeks of age according to previously described methods [55]. Briefly, a 5-mm incision was made in the abdomen at the level of the hind legs. The vas deferens and spermatic cord were separated and ligated with non-absorbable sutures. Following ligation, the testes were removed and the incision was closed using an absorbable suture. Mice were allowed to age to 14 weeks following castration, at which time they were euthanized for further analysis.

RNA-Seq:

Total RNA was extracted using Trizol extraction (Ambion) according to the manufacturer's instructions. Isolated RNAs were reverse transcribed using the High Capacity cDNA Reverse Transcription Kit (Applied Biosystems) according to the manufacturer's recommendations. cDNA was prepared for sequencing using the TruSeq mRNA-Seq sample prep kit according to manufacturer's protocols, and samples were sequenced on an Illumina 2000 platform using the manufacturer's protocols for paired-end, 100-nt sequencing. Samples were multiplexed into pools of six samples each, and each pool was sequenced on one lane of the sequencer. The software package Tuxedo Suite was used for alignment, differential expression analysis, and postanalysis diagnostics. The reference transcriptome UCSC mm10 was used for alignment.

Expression quantitation and differential expression analysis were performed using CuffDiff. Gene and transcripts were identified as differentially expressed based on three criteria: test status = OK, false discovery rate < 0.05, and fold change ≥ 1.5. Analysis was performed by the University of Michigan Bioinformatics core and data has been uploaded to GEO under the accession number GSE106521. Further analysis and visual representation of differentially expressed genes to identify significantly enriched functional categories was performed using GO-Term analysis and PantherDB.

qPCR:

RNA was isolated from tissues at the indicated time points using a TRIzol (Sigma) extraction according to manufacturer's instructions. 2 µg RNA was reverse transcribed using the High Capacity cDNA Reverse Transcription Kit (Applied Biosystems). qPCR was performed using FastStart TaqMan Probe Master Mix (Roche), a 7500 Real-Time PCR SDS System (Applied Biosystems), and gene specific FAM-labeled TaqMan primer/probe mixes (Applied Biosystems). Gene expression was normalized to ZFP146-Vic or Cpsf2-Vic multiplexed within the same well.

Protein Isolation and Western Blot:

Indicated tissue or cells were digested in RIPA buffer (Teknova) containing 1 Complete mini protease inhibitor cocktail (Roche) and 5 mM N-ethylmaleimide (Sigma). Tissue was lysed by mechanical homogenization and cells were lysed by sonication. Muscle lysates were incubated on a rocker at 4ºC for 1h to allow for complete digestion, then cleared by spinning at 12,000*g* for

10 min at 4 ºC. Cell lysates were cleared by spinning at 15,000*g* for 15 mins at 4ºC. Protein concentration was calculated using a DC assay (Bio-Rad). Equal amounts of protein were loaded into NuPage 4-12%, 10 well gels (Invitrogen), and run in 1X MOPS buffer (Invitrogen). Gels were transferred to PVDF membranes using a Semi-Dry Transfer System (BioRad). Blots were blocked for 1h in 5% non-fat dry milk in tris buffered saline (TBS) containing 0.1% Tween and placed into primary antibodies in blocking solution at 4ºC overnight. Goat anti-rabbit HRP (BioRad) and goat anti-mouse horseradish peroxidase (HRP) (BioRad) were used at 1:5000 in 5% non-fat dried milk for 1hr. Blots were quantified using ImageStudio Lite (Licor).

Suc-LLVY-AMC Fluorogenic Cleavage Assay:

To assess proteasome activity, tissue was lysed by steel bead homogenization in Proteasome Activity Buffer (50 mM Hepes pH 7.5, 20 mM KCl, 5 mM $MgCl_2$, 1 mM DTT, 28uM ATP) and assayed at 37ºC for 40 min in the presence or absence of 25 µM MG132. Activity not inhibited by MG132 was considered non-specific and was subtracted from the uninhibited values.

Activity Based Probe Assay:

To asses level of active proteasomes, Me_4BodipyFL-Ahx$_3$Leu$_3$VS was used according to previously described methods [65]. Briefly, tissue was isolated and homogenized in HR buffer (50 mM Tris–HCl (pH 7.4), 5 mM $MgCl_2$, 250 mM sucrose, 1 mM DTT, 2 mM ATP). Protein concentration was determined using the DC assay (BioRad). 40 µg protein was incubated with 1 µM Me_4BodipyFL-Ahx$_3$Leu$_3$VS for 1h at 37ºC. Samples were run on 12% NuPage Bis-Tris gels

(Invitrogen) at 140V for 2hr and imaged using a Typhoon Trio Plus Scanner (Amersham Bioscience).

ADRM1 Deubiquitination:

To reduce ubiquitinated ADRM1, lysate was generated from muscle in cold HR buffer. Tissue was lysed by steel bead homogenization, and 80 µg protein was incubated with 1 µM catalytic domain of USP2 (Boston Biochem) in the presence or absence of 10 µM N-ethylmaleimide (Sigma) at 37ºC for 1h. Lysates were then run on a 12% NuPage Bis-Tris gel and analyzed by western blot.

Skeletal Muscle Imaging:

Muscle was placed in a vessel containing OCT and frozen in methylbutane cooled by dry ice until solid. Tissue was mounted and cryosectioned using a cryocut 1800 cryostat (Leica Biosystems) at 20 µM thickness, rinsed in PBS three times, and fixed in ice cold methanol for 4 min. Tissue sections were again washed with PBS three times, and covered in 10 µg/mL wheat germ agglutinin for 10 min at room temperature. Sections were washed three additional times with PBS and mounted using Vectashield Mounting Media with DAPI (Vector Laboratories). Sections were imaged on a Nikon A-1 confocal microscope.

AR112Q-Expressing PC12 Cells:

To coat plates for cellular experiments with poly-D-lysine (Millipore), the poly-D-lysine was diluted to 100 μg/mL and placed into each well to allow thorough coverage of the bottom surface. Plates were then incubated at 37°C for 1h and subsequently washed with PBS prior to plating. PC12 cells expressing AR10Q or AR112Q under control of the tetOn promotor were used, as previously described [39]. Briefly, cells were grown in media containing 10% charcoal-stripped horse serum (Atlanta Biologicals) and 5% charcoal-stripped fetal bovine serum (Atlanta Biologicals), 1% penicillin-streptomycin solution (Gibco), 0.2% Hygromycin, 0.1% Geneticin.

***Drosophila* Stocks:**

Fly crosses were conducted at 25°C and ~60% humidity in a controlled diurnal environment. The RNAi lines used were from Bloomington *Drosophila* Stock Center: isogenic host strain for attP2 (#36303), attP40 (#36304), RPN 11 (#33662), RPN 13 (#42785), and cnc (#25984, #40854, and #32863). The UAS-ARQ52 transgenic line was a generous gift of Dr. J. Paul Taylor, St. Jude's Children's Research Hospital. GMR-Gal4 was original Bloomington Drosophila Stock #8121.

Fly Lysis and Western Blotting:

Fly heads were dissected from offspring one day after eclosing from their pupal cases and processed for western blots as previously described [66-68]. Heads were collected in sets of 10, then mechanically homogenized in boiling SDS lysis buffer (50 mM Tris pH 6.8, 2% SDS, 10% glycerol and 100 mM dithiothreitol), sonicated for 15 seconds, boiled for 10 min, and

centrifuged at top speed at room temperature for 10 min. Western blots were developed and quantified using a CCD-equipped VersaDoc 5000MP system and Quantity One software (Bio-Rad).

Statistics:

Graphpad Prism 7.0 was used for statistical analysis, with a minimum cutoff of $p<0.05$. Unpaired student's t-test or one-way ANOVA with Tukey's posthoc analysis were used as indicated in the figure legends.

Author Contributions

SRN, ZY, EY GBM and SVT performed experiments. SRN, ZY, GBM, EY, SVT and APL planned experiments and interpreted data. DMR provided a critical reagent. SRN and APL wrote the manuscript, and SRN, DMR, SVT and APL edited the manuscript.

3.6 Acknowledgements

We would like to thank Dr. Shigeo Murata for providing the antibody for DDI-2 [34]. We would also like to acknowledge Dr. Richard McEachin and the University of Michigan Bioinformatics Core for their analysis of RNA-Seq data.

This work was supported by the U. S. National Institutes of Health (R01 NS055746 to A.P.L., T32 GM007863 and T32 GM007315 to S.R.N., R01 NS086778 to S.V.T.).

This work was published in *The Journal of Clinical Investigation* [69].

References

1. Kennedy, W.R., M. Alter, and J.H. Sung, *Progressive proximal spinal and bulbar muscular atrophy of late onset. A sex-linked recessive trait.* Neurology, 1968. **18**(7): p. 671-680.
2. Sobue, G., et al., *X-linked recessive bulbospinal neuronopathy. A clinicopathological study.* Brain : a journal of neurology, 1989. **112 (Pt 1)**: p. 209-232.
3. La Spada, A.R., et al., *Androgen receptor gene mutations in X-linked spinal and bulbar muscular atrophy.* Nature, 1991. **352**(6330): p. 77-79.
4. Giorgetti, E. and A.P. Lieberman, *Polyglutamine androgen receptor-mediated neuromuscular disease.* Cell Mol Life Sci, 2016. **73**(21): p. 3991-9.
5. Mhatre, A.N., et al., *Reduced transcriptional regulatory competence of the androgen receptor in X-linked spinal and bulbar muscular atrophy.* Nature genetics, 1993. **5**(2): p. 184-188.
6. Lieberman, A.P., et al., *Altered transcriptional regulation in cells expressing the expanded polyglutamine androgen receptor.* Human molecular genetics, 2002. **11**(17): p. 1967-1976.
7. Morfini, G., et al., *JNK mediates pathogenic effects of polyglutamine-expanded androgen receptor on fast axonal transport.* Nature neuroscience, 2006. **9**(7): p. 907-916.
8. Szebenyi, G., et al., *Neuropathogenic forms of huntingtin and androgen receptor inhibit fast axonal transport.* Neuron, 2003. **40**(1): p. 41-52.
9. Ranganathan, S., et al., *Mitochondrial abnormalities in spinal and bulbar muscular atrophy.* Human molecular genetics, 2009. **18**(1): p. 27-42.
10. McCampbell, A., et al., *CREB-binding protein sequestration by expanded polyglutamine.* Human molecular genetics, 2000. **9**(14): p. 2197-2202.
11. Kemp, M.Q., et al., *Impaired motoneuronal retrograde transport in two models of SBMA implicates two sites of androgen action.* Human molecular genetics, 2011. **20**(22): p. 4475-4490.
12. Montie, H.L., et al., *Cytoplasmic retention of polyglutamine-expanded androgen receptor ameliorates disease via autophagy in a mouse model of spinal and bulbar muscular atrophy.* Hum Mol Genet, 2009. **18**(11): p. 1937-50.
13. Atsuta, N., et al., *Natural history of spinal and bulbar muscular atrophy (SBMA): a study of 223 Japanese patients.* Brain, 2006. **129**(Pt 6): p. 1446-55.
14. Soraru, G., et al., *Spinal and bulbar muscular atrophy: skeletal muscle pathology in male patients and heterozygous females.* J Neurol Sci, 2008. **264**(1-2): p. 100-5.
15. Rhodes, L.E., et al., *Clinical features of spinal and bulbar muscular atrophy.* Brain, 2009. **132**(Pt 12): p. 3242-51.
16. Malena, A., et al., *Androgen-dependent impairment of myogenesis in spinal and bulbar muscular atrophy.* Acta Neuropathol, 2013. **126**(1): p. 109-21.
17. Yu, Z., et al., *Androgen-dependent pathology demonstrates myopathic contribution to the Kennedy disease phenotype in a mouse knock-in model.* The Journal of clinical investigation, 2006. **116**(10): p. 2663-2672.
18. Monks, D.A., et al., *Overexpression of wild-type androgen receptor in muscle recapitulates polyglutamine disease.* Proc Natl Acad Sci U S A, 2007. **104**(46): p. 18259-64.

19. Palazzolo, I., et al., *Overexpression of IGF-1 in muscle attenuates disease in a mouse model of spinal and bulbar muscular atrophy.* Neuron, 2009. **63**(3): p. 316-28.
20. Lieberman, A.P., et al., *Peripheral androgen receptor gene suppression rescues disease in mouse models of spinal and bulbar muscular atrophy.* Cell Rep, 2014. **7**(3): p. 774-84.
21. Cortes, C.J., et al., *Muscle expression of mutant androgen receptor accounts for systemic and motor neuron disease phenotypes in spinal and bulbar muscular atrophy.* Neuron, 2014. **82**(2): p. 295-307.
22. Giorgetti, E., et al., *Rescue of Metabolic Alterations in AR113Q Skeletal Muscle by Peripheral Androgen Receptor Gene Silencing.* Cell Rep, 2016. **17**(1): p. 125-36.
23. Rocchi, A., et al., *Glycolytic-to-oxidative fiber-type switch and mTOR signaling activation are early-onset features of SBMA muscle modified by high-fat diet.* Acta Neuropathol, 2016. **132**(1): p. 127-44.
24. Li, D., et al., *c-Abl regulates proteasome abundance by controlling the ubiquitin-proteasomal degradation of PSMA7 subunit.* Cell Rep, 2015. **10**(4): p. 484-96.
25. Liu, X., et al., *Interaction between c-Abl and Arg tyrosine kinases and proteasome subunit PSMA7 regulates proteasome degradation.* Mol Cell, 2006. **22**(3): p. 317-27.
26. Isono, E., et al., *Rpn7 Is required for the structural integrity of the 26 S proteasome of Saccharomyces cerevisiae.* J Biol Chem, 2004. **279**(26): p. 27168-76.
27. Yu, Z., et al., *Abnormalities of germ cell maturation and sertoli cell cytoskeleton in androgen receptor 113 CAG knock-in mice reveal toxic effects of the mutant protein.* Am J Pathol, 2006. **168**(1): p. 195-204.
28. Albertelli, M.A., et al., *Replacing the mouse androgen receptor with human alleles demonstrates glutamine tract length-dependent effects on physiology and tumorigenesis in mice.* Mol Endocrinol, 2006. **20**(6): p. 1248-60.
29. Collins, G.A. and A.L. Goldberg, *The Logic of the 26S Proteasome.* Cell, 2017. **169**(5): p. 792-806.
30. Lokireddy, S., N.V. Kukushkin, and A.L. Goldberg, *cAMP-induced phosphorylation of 26S proteasomes on Rpn6/PSMD11 enhances their activity and the degradation of misfolded proteins.* Proc Natl Acad Sci U S A, 2015. **112**(52): p. E7176-85.
31. Steffen, J., et al., *Proteasomal degradation is transcriptionally controlled by TCF11 via an ERAD-dependent feedback loop.* Mol Cell, 2010. **40**(1): p. 147-58.
32. Sha, Z. and A.L. Goldberg, *Reply to Vangala et al.: Complete inhibition of the proteasome reduces new proteasome production by causing Nrf1 aggregation.* Curr Biol, 2016. **26**(18): p. R836-R837.
33. Lehrbach, N.J. and G. Ruvkun, *Proteasome dysfunction triggers activation of SKN-1A/Nrf1 by the aspartic protease DDI-1.* Elife, 2016. **5**.
34. Koizumi, S., et al., *The aspartyl protease DDI2 activates Nrf1 to compensate for proteasome dysfunction.* Elife, 2016. **5**.
35. Nedelsky, N.B., et al., *Native functions of the androgen receptor are essential to pathogenesis in a Drosophila model of spinobulbar muscular atrophy.* Neuron, 2010. **67**(6): p. 936-52.
36. Grimberg, K.B., et al., *Basic leucine zipper protein Cnc-C is a substrate and transcriptional regulator of the Drosophila 26S proteasome.* Mol Cell Biol, 2011. **31**(4): p. 897-909.
37. Verdoes, M., et al., *A fluorescent broad-spectrum proteasome inhibitor for labeling proteasomes in vitro and in vivo.* Chem Biol, 2006. **13**(11): p. 1217-26.

38. Carmony, K.C. and K.B. Kim, *Activity-based imaging probes of the proteasome.* Cell Biochem Biophys, 2013. **67**(1): p. 91-101.
39. Walcott, J.L. and D.E. Merry, *Ligand promotes intranuclear inclusions in a novel cell model of spinal and bulbar muscular atrophy.* The Journal of biological chemistry, 2002. **277**(52): p. 50855-50859.
40. Kuo, C.L. and A.L. Goldberg, *Ubiquitinated proteins promote the association of proteasomes with the deubiquitinating enzyme Usp14 and the ubiquitin ligase Ube3c.* Proc Natl Acad Sci U S A, 2017. **114**(17): p. E3404-E3413.
41. Besche, H.C., et al., *Autoubiquitination of the 26S proteasome on Rpn13 regulates breakdown of ubiquitin conjugates.* EMBO J, 2014. **33**(10): p. 1159-76.
42. Ristic, G., W.L. Tsou, and S.V. Todi, *An optimal ubiquitin-proteasome pathway in the nervous system: the role of deubiquitinating enzymes.* Front Mol Neurosci, 2014. **7**: p. 72.
43. Anchoori, R.K., et al., *A bis-benzylidine piperidone targeting proteasome ubiquitin receptor RPN13/ADRM1 as a therapy for cancer.* Cancer Cell, 2013. **24**(6): p. 791-805.
44. Pratt, W.B., et al., *Targeting Hsp90/Hsp70-based protein quality control for treatment of adult onset neurodegenerative diseases.* Annu Rev Pharmacol Toxicol, 2015. **55**: p. 353-71.
45. Adachi, H., et al., *Heat shock protein 70 chaperone overexpression ameliorates phenotypes of the spinal and bulbar muscular atrophy transgenic mouse model by reducing nuclear-localized mutant androgen receptor protein.* The Journal of neuroscience : the official journal of the Society for Neuroscience, 2003. **23**(6): p. 2203-2211.
46. Adachi, H., et al., *CHIP overexpression reduces mutant androgen receptor protein and ameliorates phenotypes of the spinal and bulbar muscular atrophy transgenic mouse model.* The Journal of neuroscience : the official journal of the Society for Neuroscience, 2007. **27**(19): p. 5115-26.
47. Tokui, K., et al., *DMAG ameliorates polyglutamine-mediated motor neuron degeneration through well-preserved proteasome function in a SBMA model mouse.* Hum Mol Genet, 2008.
48. Waza, M., et al., *17-AAG, an Hsp90 inhibitor, ameliorates polyglutamine-mediated motor neuron degeneration.* Nat Med, 2005. **11**(10): p. 1088-95.
49. Waza, M., et al., *Modulation of Hsp90 function in neurodegenerative disorders: a molecular-targeted therapy against disease-causing protein.* Journal of molecular medicine (Berlin, Germany), 2006. **84**(8): p. 635-46.
50. Wang, A.M., et al., *Activation of Hsp70 reduces neurotoxicity by promoting polyglutamine protein degradation.* Nature chemical biology, 2013. **9**(2): p. 112-118.
51. Sacheck, J.M., et al., *Rapid disuse and denervation atrophy involve transcriptional changes similar to those of muscle wasting during systemic diseases.* FASEB J, 2007. **21**(1): p. 140-55.
52. Rusmini, P., et al., *Aberrant Autophagic Response in The Muscle of A Knock-in Mouse Model of Spinal and Bulbar Muscular Atrophy.* Sci Rep, 2015. **5**: p. 15174.
53. Chua, J.P., et al., *Transcriptional activation of TFEB/ZKSCAN3 target genes underlies enhanced autophagy in spinobulbar muscular atrophy.* Hum Mol Genet, 2014. **23**(5): p. 1376-86.

54. Nath, S.R. and A.P. Lieberman, *The Ubiquitination, Disaggregation and Proteasomal Degradation Machineries in Polyglutamine Disease.* Front Mol Neurosci, 2017. **10**: p. 78.
55. Chua, J.P., et al., *Disrupting SUMOylation enhances transcriptional function and ameliorates polyglutamine androgen receptor-mediated disease.* J Clin Invest, 2015. **125**(2): p. 831-45.
56. Al-Ramahi, I., et al., *CHIP protects from the neurotoxicity of expanded and wild-type ataxin-1 and promotes their ubiquitination and degradation.* The Journal of biological chemistry, 2006. **281**(36): p. 26714-24.
57. Cummings, C.J., et al., *Over-expression of inducible HSP70 chaperone suppresses neuropathology and improves motor function in SCA1 mice.* Human molecular genetics, 2001. **10**(14): p. 1511-8.
58. Glover, J.R. and S. Lindquist, *Hsp104, Hsp70, and Hsp40: a novel chaperone system that rescues previously aggregated proteins.* Cell, 1998. **94**(1): p. 73-82.
59. Hjerpe, R., et al., *UBQLN2 Mediates Autophagy-Independent Protein Aggregate Clearance by the Proteasome.* Cell, 2016. **166**(4): p. 935-49.
60. Jana, N.R., et al., *Co-chaperone CHIP associates with expanded polyglutamine protein and promotes their degradation by proteasomes.* J Biol Chem, 2005. **280**(12): p. 11635-40.
61. Jinwal, U.K., et al., *Chemical manipulation of hsp70 ATPase activity regulates tau stability.* The Journal of neuroscience : the official journal of the Society for Neuroscience, 2009. **29**(39): p. 12079-12088.
62. Miller, V.M., et al., *CHIP suppresses polyglutamine aggregation and toxicity in vitro and in vivo.* J Neurosci, 2005. **25**(40): p. 9152-61.
63. Pratt, W.B., et al., *A model in which heat shock protein 90 targets protein-folding clefts: rationale for a new approach to neuroprotective treatment of protein folding diseases.* Exp Biol Med (Maywood), 2014. **239**(11): p. 1405-13.
64. Bott, L.C., et al., *A small-molecule Nrf1 and Nrf2 activator mitigates polyglutamine toxicity in spinal and bulbar muscular atrophy.* Hum Mol Genet, 2016. **25**(10): p. 1979-1989.
65. de Jong, A., et al., *Fluorescence-based proteasome activity profiling.* Methods Mol Biol, 2012. **803**: p. 183-204.
66. Blount, J.R., et al., *Ubiquitin-binding site 2 of ataxin-3 prevents its proteasomal degradation by interacting with Rad23.* Nat Commun, 2014. **5**: p. 4638.
67. Tsou, W.L., et al., *DnaJ-1 and karyopherin alpha3 suppress degeneration in a new Drosophila model of Spinocerebellar Ataxia Type 6.* Hum Mol Genet, 2015. **24**(15): p. 4385-96.
68. Tsou, W.L., et al., *The deubiquitinase ataxin-3 requires Rad23 and DnaJ-1 for its neuroprotective role in Drosophila melanogaster.* Neurobiol Dis, 2015. **82**: p. 12-21.
69. Nath, S.R., et al., *Androgen receptor polyglutamine expansion drives age-dependent quality control defects and muscle dysfunction.* J Clin Invest, 2018. **128**(8): p. 3630-3641.

CHAPTER 4

MEF2 Impairment Underlies Skeletal Muscle Atrophy in Polyglutamine Disease

4.1 Abstract

Polyglutamine (polyQ) tract expansion leads to proteotoxic misfolding and drives a family of nine diseases. We study spinal and bulbar muscular atrophy (SBMA), a progressive degenerative disorder of the neuromuscular system caused by the polyQ androgen receptor (AR). Using a knock-in mouse model of SBMA, AR113Q mice, we show that E3 ubiquitin ligases which are a hallmark of the canonical muscle atrophy machinery are not induced in AR113Q muscle. Similarly, we find no evidence to suggest dysfunction of signaling pathways that trigger muscle hypertrophy or impairment of the muscle stem cell niche. Instead, we find that skeletal muscle atrophy is characterized by diminished function of the transcriptional regulator Myocyte Enhancer Factor 2 (MEF2), a regulator of myofiber homeostasis. Decreased expression of MEF2 target genes is age- and glutamine tract length-dependent, occurs due to polyQ AR proteotoxicity, and is associated with sequestration of MEF2 into intranuclear inclusions in muscle. Skeletal muscle from R6/2 mice, a model of Huntington disease which develops progressive atrophy, also sequesters MEF2 into inclusions and displays age-dependent loss of MEF2 target genes. Similarly, SBMA patient muscle shows loss of MEF2 target gene expression, and restoring MEF2 activity in AR113Q muscle rescues fiber size and MEF2-regulated gene expression. This work establishes MEF2 impairment as a novel mechanism of

skeletal muscle atrophy downstream of toxic polyglutamine proteins and as a therapeutic target for muscle atrophy in these disorders.

4.2 Introduction

Muscle atrophy is a hallmark of patients with spinal and bulbar muscular atrophy (SBMA), a degenerative disorder of the neuromuscular system. SBMA is caused by a CAG/polyglutamine (polyQ) tract expansion in the androgen receptor (AR), placing it into a family of nine degenerative disorders with similar mutations, including Huntington disease, dentatorubro-pallidoluysian atrophy, and six autosomal dominant spinocerebellar ataxias (type 1, 2, 3, 6, 7, and 17) [1, 2]. PolyQ tract expansion leads to both loss of normal AR function as a transcription factor and ligand-dependent proteotoxicity. These changes ultimately lead to dysregulation of pathways critical for normal cellular function [3-8].

Several lines of evidence have established skeletal muscle tissue as a key contributor to SBMA pathogenesis. SBMA patients develop progressive muscular weakness and concominantly display signs of muscle toxicity, including evidence of myopathy on muscle biopsy and elevated serum creatine kinase levels above what is found in diseases of pure denervation [9-11]. Isolated skeletal muscle satellite cells show impairments in fusion to form myotubes, demonstrating cell-autonomous toxicity in muscle [12]. Knock-in mice expressing polyQ AR under the endogenous mouse promotor develop myopathy months before spinal cord pathology [13]. Transgenic mice overexpressing wild type (WT) AR only in skeletal muscle show hormone-dependent myopathy and motor axon loss; similar effects are seen in mice overexpressing polyQ AR only in muscle [14, 15]. Additionally, overexpression of insulin-like growth factor-1 (IGF-1) in muscle ameliorates the phenotypic severity of SBMA transgenic mice

[16]. The contribution of muscle to the SBMA phenotype is further corroborated by studies demonstrating that knockdown of peripheral polyQ AR or conditional deletion of polyQ AR only in skeletal muscle rescues disease in mice [17, 18].

While skeletal muscle is known to be an important contributor to pathogenesis, little is known about the mechanisms driving muscle atrophy in SBMA. Atrophy is often triggered by induction of a specific program involving upregulation of the E3 ubiquitin ligases MuRF1, Atrogin-1, and MuSA1 as well as the proteasome [19-21]. However, recent analysis of a gene targeted mouse model of SBMA demonstrates age-dependent impairment of proteasome function in muscle, suggesting that polyQ AR-mediated skeletal muscle atrophy may occur through distinct mechanisms [22].

Here, we use a combination of RNAseq analysis and targeted functional assays to explore the pathway leading to skeletal muscle atrophy in SBMA. We identify impaired function of the transcription factor Myocyte Enhancer Factor 2 (MEF2), a well-established modulator of myofiber homeostasis and hypertrophy [23], as a novel contributor to muscle atrophy caused by polyQ AR. We demonstrate that changes in MEF2 function are age- and hormone-dependent and occur as a result of ligand-mediated proteotoxicity. We find that impairment of MEF2 also occurs in skeletal muscle of R6/2 mice, a model of Huntington disease where muscle atrophy is prominent. Finally, we demonstrate that SBMA patient muscle biopsies lose expression of MEF2 target genes, and that restoring MEF2 activity rescues muscle fiber size in vivo. These studies establish MEF2 as a novel therapeutic target which mediates skeletal muscle atrophy in polyglutamine disease.

4.3 Materials and Methods

Mice. AR21Q and AR113Q knock-in mice were generated using exon 1 specific targeting as previously described [13, 24, 25]. Specific pathogen free housing was maintained on a 12 hour light/dark cycle. Chow and water were administered ad libitum. Genotyping was performed with the following primers on ear samples: AR forward: 5′-CCAGAATCTGTTCCAGAGCGTG-3′ (MilliporeSigma, 6-FAM labeled); AR reverse: 5′-TGTTCCCCTGGACTCAGATG-3′ (Invitrogen). AR targeted ASOs were injected subcutaneously (50mg/kg body weight) from 6 to 26 weeks of age once per week. ASOs are made of a 16-mer, 2',4'-constrained ethyl gapmer contain the following sequence: AAGTTGTAGTAGTCGC which is complementary to human and mouse AR transcripts and was detailed previously [18]. All procedures involving mice were approved by the University of Michigan Committee on Use and Care of Animals (PRO00008133) and conducted in accordance with institutional and federal ethical guidelines for animal testing and research.

For R6/2 mice, animal care and procedures were performed in compliance with United Kingdom Home Office regulations (Animals and Scientific Procedures Act 1986) and were approved by the University College London Ethical Review Process Committee. Hemizygous R6/2 mice [26] were bred by backcrossing R6/2 males to (CBA/Ca x C57BL/6J) F1 females (B6/CBAF1/OlaHsd Envigo, UK). Animals were kept on a 12 hour light and dark cycle and room temperature was maintained at 21℃ ± 1℃. All mice had access to moderate environmental enrichment (play tube, wooden chew sticks). Cages were provided with an unlimited supply of water and a high protein chow diet. Mice were genotyped and the *HTT* CAG repeat length was quantified as previously described [27]. The CAG repeat sizes were: 188 ± 1.2 (SD) at 4 weeks,

188 ± 3.06 at 8 weeks and 185 ± 3.37 at 12 weeks of age.

Patient Samples. Anonymized control and patient biopsy samples were obtained from the Neuromuscular Bank of Tissues and DNA samples, Telethon Network of Genetic Biobanks, and the EuroBioBank network.

Orichiectomy. Surgical castration was performed at 5 to 6 weeks as previously described [28]. In brief, an incision no longer than 5 mm was made in the abdomen at the level of the hind legs. Following incision, the vas deferens and spermatic cord were ligated using nonabsorbable sutures. The testes were removed and the incision was closed using absorbable sutures. Mice were aged to 14 weeks, at which point they were euthanized for further analysis.

qPCR. Mouse tissues were lysed in TRIzol for RNA extraction according to manufacturer's instructions. 2µg of RNA were reverse transcribed using the High Capacity cDNA Reverse Transcription Kit (Applied Biosystems). qPCR reactions used FastStart Taqman Probe Master Mix (Roche), a 7500 Real-Time PCR SDS System (Applied Biosystems), and FAM-labeled TaqMan primer/probe mixes specific to the gene of interest (Applied Biosystems). Gene expression in mouse studies was normalized to Cpsf2-Vic multiplexed within the same well.

For patient samples, total RNA was extracted with TRIzol (Thermo Fisher Scientific), and RNA was reverse-transcribed using the iScript Reverse Transcription Supermix (1708841 Bio-Rad) following the manufacturer's instructions. Gene expression was measured by RT-qPCR using the SsoAdvanced Universal Sybr green supermix (1725274 Bio-rad) and the C1000 Touch Thermal

Cycler–CFX96 Real-Time System (Bio-Rad). Human gene expression was normalized to Actin.

Mouse TaqMan Primer/Probes and human primer sequences used are listed below:

Gene	**TaqMan Primer/Probe**
MuRF1 (Trim63)	Mm01185221_m1
Atrogin-1(FBXO32)	Mm00499523_m1
MuSA1 (FBXO30)	Mm01191299_m1
MSTN	Mm01254559_m1
Pax7	Mm01354484_m1
Myf5	Mm00435125_m1
Myog	Mm00446194_m1
PGAM2	Mm01187768_m1
CLCN1	Mm00658624_m1
PFKM	Mm01309576_m1
Myl1	Mm00659043_m1
Myoz1	Mm00469642_m1
Ttn	Mm00621005_m1
Mef2a	Mm01318991_m1
Mef2c	Mm01340842_m1
Cpsf2-VIC	Mm00489754_m1

Table 4.1 List of mouse taqman primers.

Gene	**Forward**	**Reverse**
h_CLCN1 n1	CCCTGGAGGAGCTACAGAA	TTCGAGTTGAAGTCGTGTTCC
h_PFKM n1	CAAAGCCATTGCTGTCTTAACC	GTGAAGATACCAACTCGAACCA
h_Myoz1 n3	CTGATCATGGAACTCACTGGAG	GACAGTTCCTCCAACATCACA
h_Ttn n1	TCGCCCATAAGACACTCC	TGAGCAATGGAGACCTAACA
h_Actin	GGACTTCGAGCAAGAGATGG	AGCACTGTGTTGGCGTACAG

Table 4.2 List of human qPCR primers.

Protein isolation and western blot. Tissues were digested in RIPA buffer (Teknova) containing cOmplete Mini Protease Inhibitor Cocktail (Roche) and 5 mM NEM (MilliporeSigma). Tissue was lysed mechanically using a benchtop tissue homogenizer. Muscle lysates were incubated on a rocker at 4°C for 1 hour to allow for complete digestion, then cleared by spinning at 12,000 *g* for 10 minutes at 4°C. Protein concentration was calculated using the DC assay (Bio-Rad). Equal amounts of protein were loaded into NuPAGE 4%–12%, 10-well gels (Invitrogen) and run in 1× MOPS buffer (Invitrogen). Gels were transferred to PVDF membranes using a Semi-Dry Transfer System (Bio-Rad). Blots were blocked for 1 hour in 5% nonfat dry milk in TBS containing 0.1% Tween and placed into primary antibodies in blocking solution at 4°C overnight. Goat anti-rabbit HRP (Bio-Rad) and goat anti-mouse HRP (Bio-Rad) were diluted at 1:5,000 in 5% nonfat dried milk and incubated for 1 hour at room temperature. Blots were quantified using ImageStudio Lite (Licor).

Skeletal muscle processing. Muscle was harvested from euthanized mice and placed in a vessel containing OCT. The OCT vessel was frozen in methylbutane cooled by dry ice. Tissue was cryosectioned using a Leica CM1900 Cryostat (Leica Biosystems) at 20µm thickness and slides were stored at -80°C.

Immunofluorescence. Slides were removed and thawed at room temperature. Tissue slices were outlined with an ImmunoPen (ImmEdge) and fixed in ice cold methanol for 4 minutes. For

muscle fiber quantification, slides were washed 3 times in PBS and covered in 10µg/mL labeled wheat germ agglutinin (Thermo) for 10 minutes at room temperature. For colocalization studies, slides were washed 3 times in PBS containing 0.1% triton-X (PBS-T) and blocked for 1h at room temperature in 10% Normal Goat Serum in PBS. Slides were then incubated in primary antibody in blocking solution overnight at 4°C. Slides were washed 3 times in PBS-T and incubated in secondary antibody for 1 hour at room temperature in blocking solution. Slides were again washed 3 times in PBS-T and mounted using Prolong Gold with DAPI. Images were taken on a Nikon A1 confocal microscope. Percent of colocalization and muscle fiber size was quantified using automated CellProfiler pipelines and a Zeiss Epifluorescent Microscope.

H&E staining. Slides were fixed in ice cold methanol for 4 minutes. Sections were placed into hematoxylin (modified Mayer's solution) (Abcam) for 1.5 minutes at room temperature. Sections were dipped into distilled water 30 times or until no longer running. Sections were then placed into eosin for 5 minutes at room temperature. Sections were dipped again 30 times into water, followed by 30 times in 70%, 95%, and 100% ethanol. Finally, sections were mounted with DPX mounting solution and imaged. For H&E images, the white balance was adjusted per image on each whole image to ensure true white levels of background using Adobe Photoshop.

Electroporation of mouse muscle. Electroporation was performed according to previous studies In brief, mice at indicated ages were anesthetized using isoflurane in a VIP3000 Isoflurane Matrx by nose cone. Following deep inhaled anesthesia at 2% concentration, the hind limb was shaved

and 30μL of 0.8 U/mL hyaluronidase in sterile saline was injected into the tibialis anterior. Mice were then allowed to recover for two hours, then re-anesthetized and the TA was injected with 50μg total of plasmid DNA. The hindlimb was then coated in ultrasound gel (Medline). Ten 20ms pulses of 175V/cm were then administered to the hindlimb using an ECM 830 Electroporator (BTX Technologies).

Denervation. Under inhaled isoflurane anesthesia, the right sciatic nerve was exposed inferior to the sciatic notch as previously described [29]. The proximal and distal sides were ligated using monocryl 4-0 sutures and 2mm of nerve was cut in between these ligations, preventing axonal regeneration. Tissue was harvested 3 days after surgery for RNA isolation.

Cardiotoxin assay. Mice were injected with cardiotoxin (Millipore, 217503) at 19 weeks of age. One leg was injected with 30μL of 12μM cardiotoxin, while the contralateral leg was injected with saline. Mice were sacrificed at 7d and 14d post injection and the TA muscle was harvested and frozen for processing.

Luciferase assay. Mice were electroporated as described above with a MEF2 promoter-luciferase plasmid and co-transfected with Renilla luciferase as previously described [30]. Muscle was harvested after electroporation, flash frozen in liquid nitrogen, and ground using a pestle and

mortar. Luciferase activity was measured using the dual luciferase reporter assay system (Promega). The amount of luciferase activity was normalized to Renilla luciferase activity.

Antibodies and reagents. The following antibodies were used: Phospho-S6RP (Cell Signaling, 4858), S6RP (Cell Signaling, 2217), Deptor (Cell Signaling, 11816S), REDD1 (Protein Tech, 10638-1-AP), Vinculin (Sigma, V9131), Phospho-SMAD3 (Cell Signaling, 9520S), SMAD3 (Cell Signaling, 9513), MEF2AC (abcam, ab197070), p62 (03-GP62-C), Androgen Receptor (Millipore, PG-21), Wheat Germ Agglutinin Alexa Fluor 594 (Thermo Scientific, W11262), Wheat Germ Agglutinin Alexa Fluor 488 (W11261).

Transcriptome data. Sequencing data were used from the following previously published GEO datasets analyzed as stated: SBMA LABC: GSE106521 [22], SBMA Quadriceps: GSE60691 [31], R6/2 Quadriceps: GSE81367 [32], reanalyzed by DeSeq2 (counts>2 in at least 5 samples, B&H FDR<0.05, FC>1.5), MEF2 KD: GSE61207[33], and Mrf4 KD: GSE67069 [23].

Plasmids. MEF2-VP16 (CA-MEF2) and MEF2ΔDBD-VP16 (DBD-MEF2) were previously characterized and kindly provided by Michael Greenberg [34]. MEF2-Luciferase (RSRF-Luc-2wt) was a gift from Astar Winoto (Addgene plasmid # 31818 ; http://n2t.net/addgene:31818 ; RRID:Addgene_31818) [35]. Tk-Renilla plasmid was from Promega.

Statistics. Statistical analysis was performed in GraphPad Prism using two-tailed unpaired student's t-test for comparisons of two groups and one-way ANOVA with Tukey's multiple comparison test for groups of three or more. A<0.05 was set as the threshold for significance.

4.4 Results

4.4.1 AR113Q Muscle Atrophy is Independent of Ubiquitin-Proteasome Machinery Induction

Skeletal muscle atrophy occurring downstream of denervation, fasting, immobilization, and motor neuron degeneration involves induction of several key E3 ubiquitin ligases and the proteasome [19, 36, 37]. Upregulation of degradative machinery targets sarcomeric proteins to the proteasome and results in fiber size reduction [38]. Three of the best characterized ubiquitin ligases involved in skeletal muscle atrophy are MuRF1, Atrogin-1, and MuSA1 [21, 38, 39]. We confirmed induction of these genes after denervation by comparing mRNA expression levels in control and denervated muscle 3 days following sciatic nerve transection (Fig 4.1A). Next, we examined AR113Q mice, a model of SBMA generated by gene targeting, to determine whether mutant males also exhibit induction of the E3 ubiquitin ligases associated with muscle atrophy. AR113Q mice express a humanized form of AR in which much of the coding sequence of mouse AR exon 1 is replaced by human sequence containing 113 CAG repeats [13, 24]. These mice express endogenous levels of polyQ AR under the control of the mouse AR gene promoter and transcriptional machinery. AR113Q males develop a progressive neuromuscular phenotype which mimics important aspects of the SBMA phenotype (Fig 4.2) [13]. Because the AR gene is on the X chromosome, males are hemizygous for either the mutant or WT allele. In contrast to

denervation, we found no significant induction of any of these E3 ubiquitin ligases in AR113Q quadriceps at 14, 26, and 52 weeks (Fig 4.1B-1D) despite the occurrence of progressive weakness and muscle atrophy (Fig 4.2). In fact, AR113Q males display age-dependent suppression of the MuRF1 and Atrogin-1 genes (Fig 4.1B-1C). These data complement a recent study from our group demonstrating diminished proteasome expression and function in AR113Q muscle and show that SBMA atrophy has several distinctions from other forms of atrophy [22].

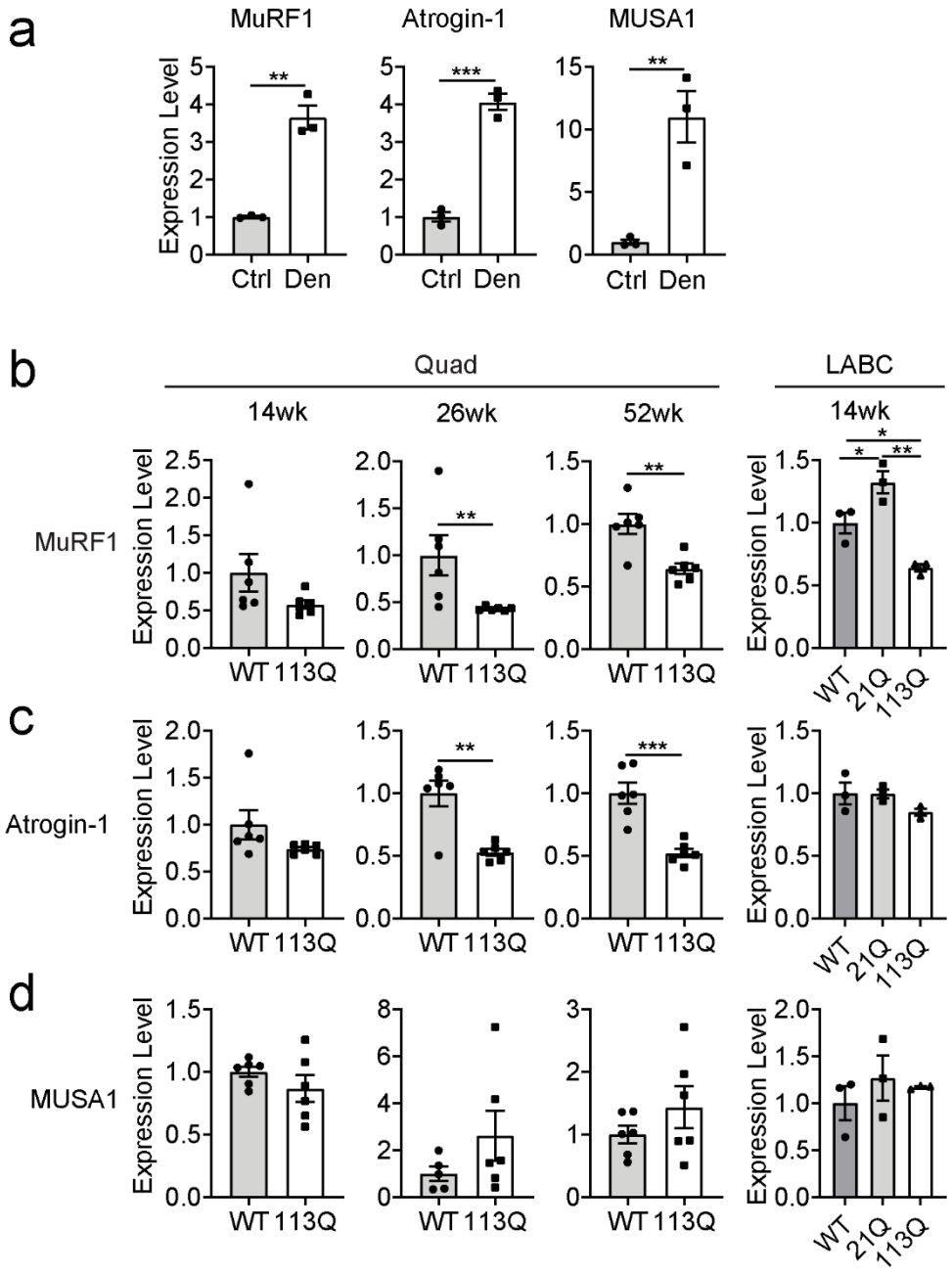

Fig. 4.1 Atrophy-related E3 ubiquitin ligases are not induced in AR113Q skeletal muscle. (A) Relative mRNA expression of FBXO32/Atrogin-1, MuRF1, and MuSA1 in control (ctrl) and denervated (den) mice 3 days following sciatic nerve transection (n=3/group). (B-D) Relative mRNA expression of (B) MuRF1, (C) FBXO32/Atrogin-1, (D) MuSA1 in WT or AR113Q mice in quadriceps (Quad) at 14, 26 and 52 weeks (left, n=6/group) and in LABC at 14 weeks (right, n=3/group). Data are shown as mean ± SEM.*P < 0.05; **P < 0.01; ***P < 0.001 by unpaired t test (quadriceps) or by one-way ANOVA with Tukey's (LABC)

Similar to quadriceps muscle, induction of MuRF1, Atrogin-1, and MuSA1 does not occur in the levator ani/bulbocavernosus muscle (LABC), a pelvic floor muscle which undergoes

severe atrophy due to high levels of AR expression (Fig 4.1B-D, right). We observed no induction of E3 ubiquitin ligases in comparison to either WT or AR21Q males. AR21Q males were generated using the same gene targeting strategy but express a normal CAG repeat length [25] and thereby control for effects of humanizing the mouse AR gene. Previous work has demonstrated that AR21Q mice are phenotypically similar to WT, establishing that the neuromuscular phenotype of AR113Q mice is due solely to polyglutamine tract expansion above the pathogenic threshold [13]. Collectively, these analyses demonstrate that AR113Q mice lack induction of the classical, ubiquitin-proteasome system (UPS)-based muscle atrophy machinery and suggest that alternative mechanisms underlie muscle atrophy in this disease.

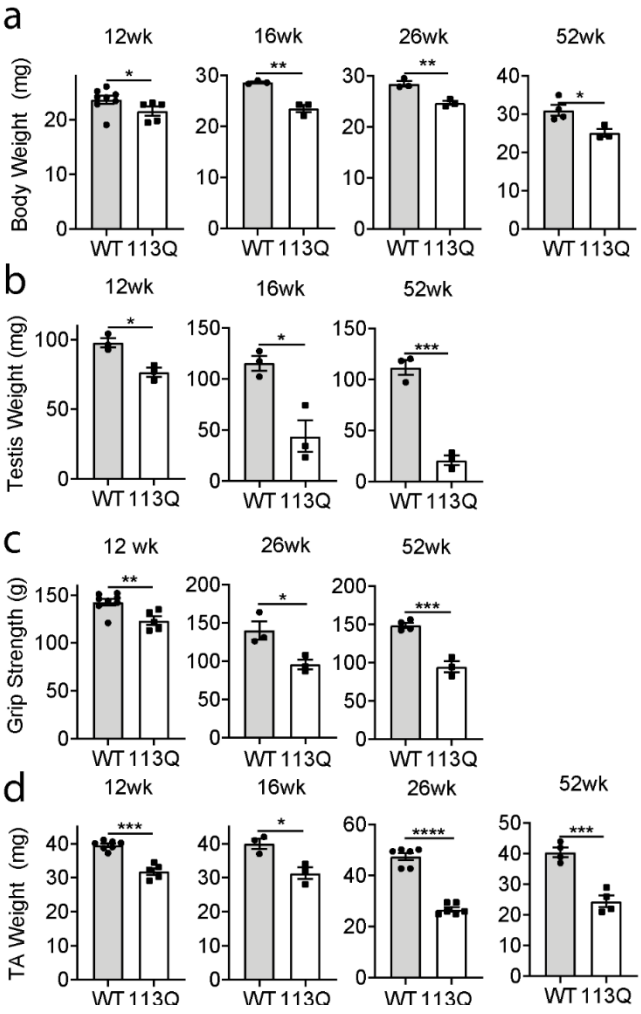

Fig. 4.2 AR113Q mice show a progressive neuromuscular phenotype. Age-dependent changes in (A) body mass (12wk: n=8v5, 16wk: n=3v3, 26wk: n=3v3, 52wk n=4v3), (B) testis mass (n=3v3), (C) grip strength (12wk: n=8v5, 26wk: n=3v3, 52wk: n=4v3), and (D) tibialis anterior mass. (12wk: n=7v5, 16wk: n=3v3, 26wk: n=6v6, 52wk: n=4v4). Data are mean ± SEM.*P < 0.05; **P < 0.01; ***P < 0.001, ****P<0.0001 by unpaired t-test.

4.4.2 Hypertrophic Signaling is Increased in SBMA Muscle

We next sought to determine whether impaired signaling to stimulate muscle hypertrophy contributes to AR113Q atrophy. Two major signaling pathways, regulated by mTOR and myostatin, modulate skeletal muscle hypertrophy (Fig 4.3A) [30]. As reduced mTOR activity is a

well-established hallmark of muscle atrophy [38, 40, 41], we hypothesized that mTOR signaling may be impaired in SBMA and contributes to reduction of muscle fiber size. We examined phosphorylation of S6RP, a well-established mTORC1 target, in 14 week LABC. In contrast to expectation, we found significant upregulation of mTOR signaling in AR113Q muscle (Fig 4.3B), similar to a previous report [42]. This signal was ablated by administration of rapamycin to WT and AR113Q mice for two weeks, demonstrating specificity for mTOR activation (Fig 4.3B). We next sought to determine if upstream regulators of mTOR were differentially affected in AR113Q mice. Two well characterized mTOR inhibitors are Deptor [43] and REDD1 [44, 45]. AR113Q muscle displays significant reduction in levels of both Deptor and Redd1 proteins,

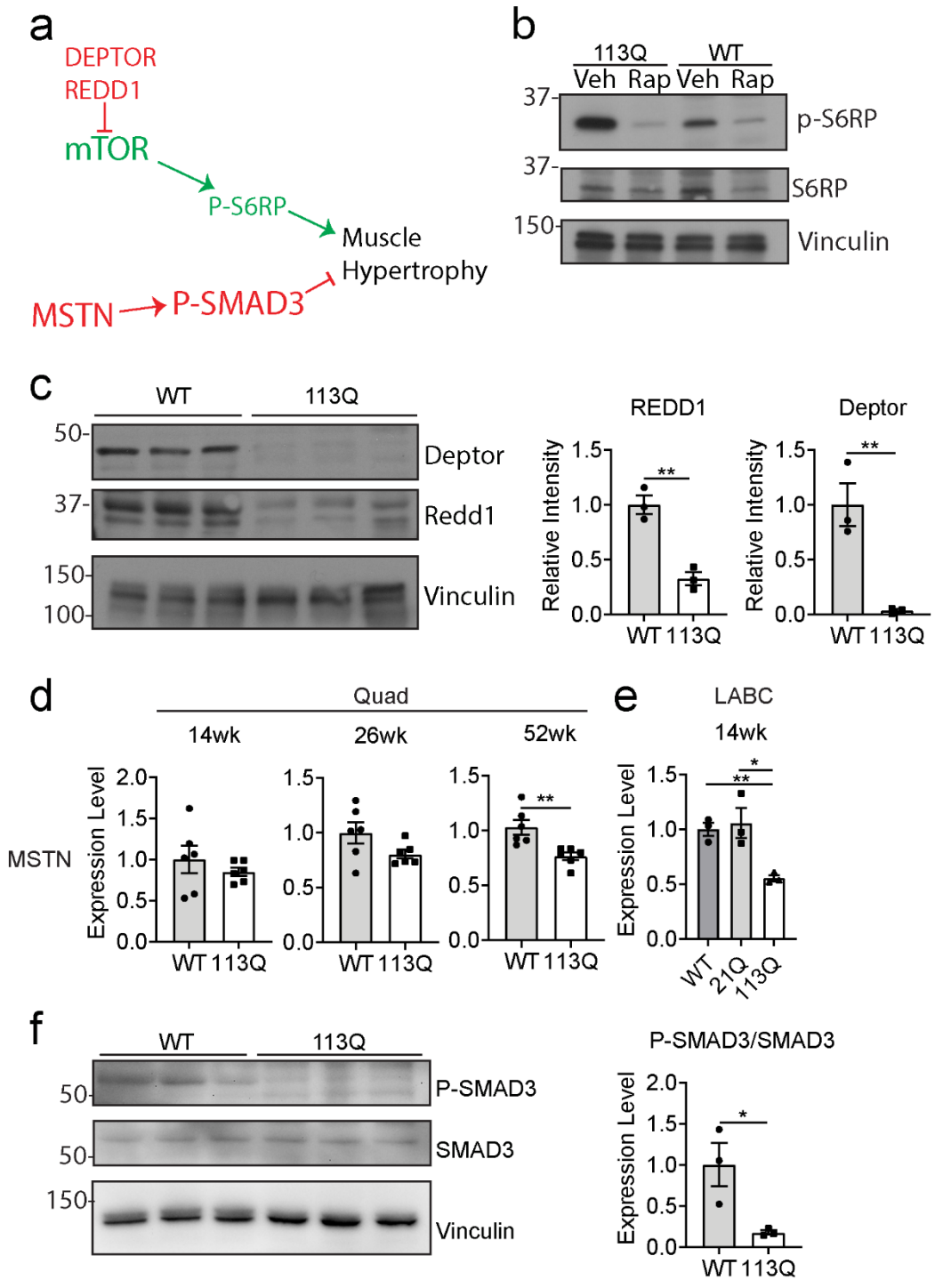

Fig. 4.3 Activity of signaling pathways that influence fiber size in AR113Q muscle. (A) Schematic of signaling pathways which regulate muscle regeneration and hypertrophy (inhibitory in red, stimulatory in green). (B) Levels of phospho-S6RP in WT vs AR113Q LABC at 14 weeks, following two week treatment with vehicle (Veh) or rapamycin (Rap) I.P. (C) Relative levels of Deptor and REDD1 proteins in WT vs AR113Q LABC at 14 weeks (n=3/group). Data are mean ± SEM.**P < 0.01 by unpaired t test. (D, E) Relative mRNA expression of myostatin (MSTN) in WT or AR113Q quadriceps at 14, 26, and 52 weeks (D, n=6/group) and LABC at 14 weeks (E, n=3/group). (D) Data are mean ± SEM. * P<0.05, **P < 0.01 by unpaired t test. (E) Data are mean ± SEM. *p<0.05, **p<0.01 by one-way ANOVA. (F) Levels of phospho-SMAD3 in WT and AR113Q quadriceps at 26 weeks (n=3/group). Data are mean ± SEM. * P<0.05 by unpaired t test

demonstrating that loss of inhibitors coincides with significant mTOR activation (Fig 4.3C).

These results demonstrate that mTOR signaling is activated to favor hypertrophy in AR113Q muscle and led us to examine whether other effectors of muscle hypertrophy are dysregulated in disease.

Myostatin is known to be a potent inhibitor of skeletal muscle hypertrophy [46]. To determine whether myostatin induction plays a role in AR113Q muscle atrophy, we performed qPCR on 14, 26, and 52 week quadriceps. We observed no change in myostatin expression in the quadriceps at early time points and significant suppression of myostatin expression in 52 week quadriceps (Fig 4.3D) and 14 week LABC (Fig 4.3E). To support the notion that myostatin signaling is diminished in AR113Q muscle, we examined the level of phospho-SMAD3, a downstream effector of myostatin. We detected significantly decreased phospho-SMAD3 in AR113Q muscle, supporting the conclusion that myostatin signaling is suppressed (Fig 4.3F). As both myostatin and mTOR signaling changed to favor hypertrophy rather than atrophy in mutant muscle, we conclude that alterations in these pathways do not underlie AR113Q skeletal muscle pathology.

4.4.3 Muscle Regeneration is Intact in SBMA Muscle

We next asked whether the cells that replenish muscle, satellite cells and myoblasts, are dysfunctional in AR113Q males. We performed qPCR for markers of muscle satellite cells, Pax7 and Myf5 [47, 48], and the myoblast marker myogenin (Myog) (Fig 4.4A). For all of these markers, we saw increases in expression as early as 14 weeks, suggesting that these cell populations are present in AR113Q skeletal muscle (Fig 4.4B). Moreover, the induction of Pax7

and Myf5 expression was significant compared to AR21Q, demonstrating that upregulation of satellite cell markers is dependent on glutamine tract expansion.

We sought to determine whether satellite cell dysfunction and impaired regeneration after injury contributes to AR113Q muscle atrophy. To accomplish this, we injected cardiotoxin (CTX) into the tibialis anterior muscle, leading to severe muscle damage and fiber destruction [49, 50]. In WT mice, muscle fibers are replenished to their original size by satellite cells 12-14 days after CTX administration [50, 51]. Significant destruction of muscle fibers was present in both WT and AR113Q mice at 7 days post CTX injection (Fig 4.4D), and both WT and AR113Q mice successfully regenerated muscle fibers by 14 days post injection (Fig 4.4E). Following regeneration, fibers trended larger for WT mice and were slightly, but significantly larger (6%) for AR113Q mice than their respective original sizes (Fig 4.4F, left), demonstrating that AR113Q mouse satellite cells remain functional. Although fibers successfully regenerated to their original size, subtle changes in satellite cell function were suggested by the reduction in nuclei per fiber in SBMA mouse muscle (Fig 4.4F, right). Similar changes have been reported in primary satellite cell cultures from SBMA patients [12]. As these defects do not prevent fiber regeneration in vivo post-injury by the muscle stem cell population, we conclude that they are unlikely to significantly contribute to AR113Q atrophy. Having determined that UPS-based degradation, impaired hypertrophic signaling, and regenerative capability do not account for reduced muscle fiber size in AR113Q mice, we sought out alternative factors which may contribute to muscle atrophy in disease.

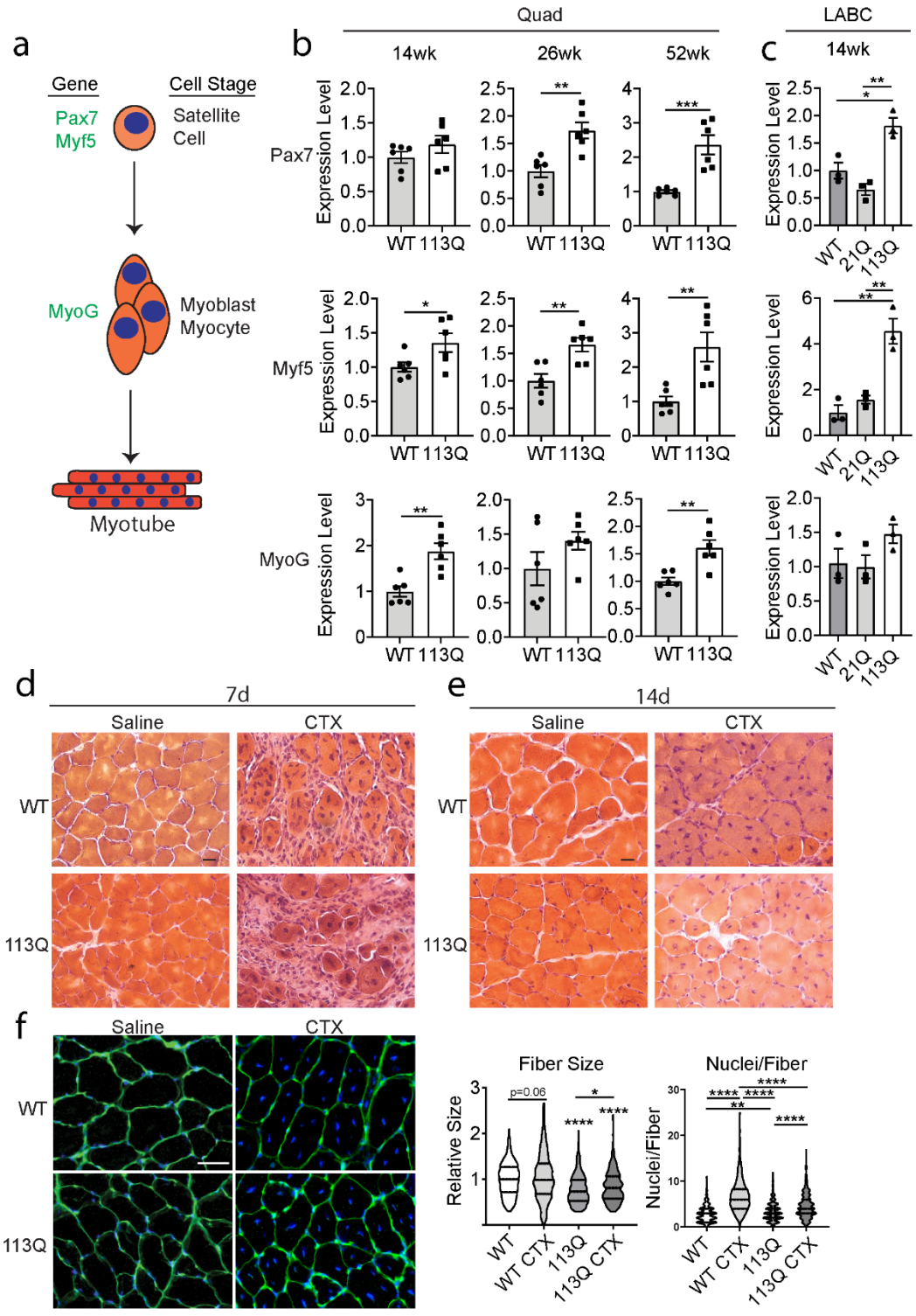

Fig. 4.4 Myoregeneration is intact in AR113Q muscle. (A) Schematic of examined markers of muscle satellite cells (PAX7, Myf5) and myoblasts/myocytes (MyoG). (B, C) Relative mRNA expression of PAX7 (top), Myf5 (middle) and MyoG (bottom) in WT and AR113Q quadriceps at 14, 26, and 52 weeks (B, n=6/group) and in WT, AR21Q, and AR113Q LABC at 14 weeks (C, n=3/group). (D-F) Tibialis anterior of WT or AR113Q mice were injected with cardiotoxin (CTX) or saline and examined by H&E stain at 7d (D) or 14d (E) post injection. Scale bar = 20µm. (F) Muscle fibers were stained with WGA and DAPI at 14d post injection. Fiber size and nuclei/fiber quanitified and displayed as a violin plot (n=3 mice/group, 3 images/mouse, >100 fibers/mouse). Scale bar = 50µm. *P<0.05, **P < 0.01, ****P<0.0001 by unpaired t test (B) or one-way ANOVA with Tukey's (C and F)

GO: Cellular Component Analysis - Quad					
	ID	**p-value**	**q-val Bonf.**	**Query List Hits**	**Genome Hits**
1	Contractile fiber part	1.18E-34	9.91E-32	64	244
2	Contractile fiber	1.041E-33	8.75E-31	65	261
3	Myofibril	2.328E-31	1.96E-28	61	248
4	Sarcomere	1.037E-30	8.71E-28	58	228
5	I Band	2.496E-26	2.10E-23	45	158

Table 4.3. GO Term Analysis of AR113Q Quad. Toppgene GO Term: Cellular Component Analysis was performed on an RNAseq data set of differentially expressed genes in the quadriceps of WT and AR113Q mice (n=3/group, FDR<0.05, FC>1.5 bidirectionally). The top 5 enriched categories are listed.

Transcription Factor Binding Site Analysis - Quad					
	ID	**p-value**	**q-val Bonf.**	**Query List Hits**	**Genome Hits**
1	CTAWWWATA V$RSRFC4 Q2	1.26E-11	7.60E-09	45	298
2	V$MEF2 02	8.148E-09	4.91E-06	31	197
3	V$RSRFC4 01	3.031E-08	1.83E-05	31	208
4	YTATTTNR V$MEF2	2.416E-07	1.46E-04	56	558
5	V$RSRFC4 Q2	2.641E-07	1.59E-04	27	182

Table 4.4. Transcription factor binding site analysis of AR113Q Quad. ToppGene Transcription Factor Binding Site analysis was performed on an RNAseq data set of differentially expressed genes in the quadriceps of WT and AR113Q mice (n=3/group, FDR<0.05, FC>1.5 bidirectionally). The top 5 enriched transcription factor binding site categories are listed.

Transcription Factor Binding Site Analysis - LABC					
	ID	**p-value**	**q-val Bonf.**	**Query List Hits**	**Genome Hits**
1	V$MEF2 02	1.34E-10	8.22E-08	75	197
2	CAGGTG V$E12	3.09E-10	1.90E-07	466	1956
3	V$MEF2 03	3.30E-09	2.03E-06	72	198
4	V$MEF2 Q6 01	6.03E-09	3.70E-06	74	208
5	CTAWWWATA V$RSRFC4 Q2	6.14E-09	3.77E-06	97	298

Table 4.5. Transcription factor binding site analysis of AR113Q LA/BC. ToppGene Transcription Factor Binding Site analysis was performed on an RNAseq data set of differentially expressed genes in the LABC of WT and AR113Q mice (n=3/group, FDR<0.05, FC>1.5 bidirectionally). The top 5 enriched transcription factor binding site categories are listed.

Gene Set Name	# Genes in Set (K)	# Overlap (k)	k/K	p-value	FDR q-value
CAGGTG_E12_Q6	2485	155	0.0624	1.26E-43	7.73E-41
TGGAAA_NFAT_Q4_01	1896	133	0.0701	1.23E-42	3.80E-40
CAGCTG_AP4_Q5	1524	111	0.0728	6.28E-37	1.29E-34
GGGAGGRR_MAZ_Q6	2274	136	0.0598	3.96E-36	6.09E-34
AACTTT_UNKNOWN	1890	122	0.0646	1.77E-35	2.18E-33
YTATTTTNR_MEF2_02	697	73	0.1047	2.69E-34	2.76E-32
CTAWWWATA_RSRFC4_Q2	361	54	0.1496	1.98E-33	1.74E-31
GGGCGGR_SP1_Q6	2940	150	0.051	3.20E-32	2.46E-30
TGACCTY_ERR1_Q2	1043	82	0.0786	1.43E-29	9.75E-28
TTGTTT_FOXO4_01	2061	116	0.0563	2.18E-28	1.34E-26
GCANCTGNY_MYOD_Q6	924	74	0.0801	3.02E-27	1.69E-25
MEF2_02	228	38	0.1667	1.25E-25	6.39E-24
RSRFC4_Q2	214	36	0.1682	1.70E-24	8.07E-23
RSRFC4_01	245	38	0.1551	1.84E-24	8.08E-23
TATAAA_TATA_01	1296	83	0.064	6.03E-24	2.47E-22

Table 4.6. GSEA analysis of transcription factor enrichment for differentially expressed genes in an RNAseq data set of the SBMA quadriceps (n=3/group, FDR<0.05, FC>1.5 bidirectionally). MEF2 categories are highlighted in light blue.

4.4.4 The Transcription Factor MEF2 is Impaired in AR113Q Muscle

Using an RNAseq data set generated from AR113Q mouse quadriceps at 14 weeks [28] and GO Term: Cellular Component analysis of differentially expressed genes, we identified that all of the top 5 enriched categories are related to sarcomere structural genes (Table 4.3). We performed transcription factor binding site analysis using ToppGene to nominate transcription factors that could account for this loss of sarcomere gene transcription. Strikingly, we found that binding sites for the transcription factor Myocyte Enhancer Factor 2 (MEF2) account for 5 of the top 5 and 4 of the top 5 hits when analyzing differentially expressed genes in the quadriceps and LABC, respectively (Table 4.4-4.5). Gene Set Enrichment Analysis (GSEA) also showed MEF2 binding sites accounting for 5 of the top 15 transcription factor binding sites, and as the only transcription factor with multiple hits (Table 4.6). These results were unexpected, as MEF2 mRNA expression (Fig 4.5A) and protein level (4.5B) were not altered. RNAseq data also showed no significant change in expression of any *Mef2* family gene (Table 4.7). To test whether MEF2 activity is impaired in AR113Q muscle, we electroporated a plasmid containing a MEF2 promoter site upstream of luciferase into mouse hindlimb muscle. Luciferase activity was examined 48 hours post-electroporation and normalized to co-transfected, constitutively expressed Renilla luciferase. We found significant reduction of MEF2 activity in AR113Q muscle (Fig 4.6A) without a difference in Renilla luciferase activity (Fig 4.5C), consistent with impaired MEF2 activity in vivo. We next compared differentially expressed genes in AR113Q muscle to a published data set of MEF2A targets in C2C12 cells which were identified by RNAseq and confirmed by MEF2A ChIP-Exo [33]. Strikingly, ~20% of identified MEF2 targets were altered in AR113Q quadriceps and ~40% of targets in AR113Q LABC (Fig 4.6B). We further compared differentially expressed genes in AR113Q muscle to another data set in which

the MEF2 inhibitor Mrf4 was knocked down in mouse muscle and expression analysis was performed in the context of activated MEF2 [23]. We found that ~10% of all genes that changed upon Mrf4 knockdown were altered in AR113Q quadriceps; similarly, ~30% were altered in AR113Q LABC (Fig 4.6C). Notably, knockdown of AR113Q in vivo using peripherally administered AR-targeted antisense oligonucleotides rescues changes in MEF2 target genes (Fig 4.6D) [18]. Importantly, this intervention diminishes expression of polyQ AR in peripheral tissues but not CNS [18], indicating that MEF2 impairment occurs independent of polyQ AR actions in lower motor neurons. To validate changes in MEF2 regulated genes in an independent cohort of mice, we examined expression of several MEF2 targets (genes found in MSigDB, MEF2-ChIP-Seq, or Mrf4 KD data sets) known to play an important role in skeletal muscle in AR113Q quadriceps at 14, 26, and 52 weeks. These studies demonstrated a significant decrease in target gene expression that often progressed with age (Fig 4.6E).

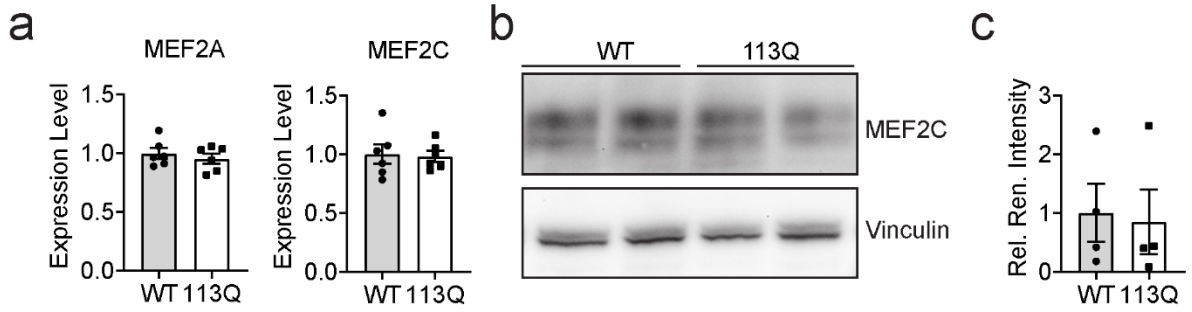

Fig. 4.5 MEF2 mRNA expression and protein level does not change in AR113Q mice. (A) Expression of MEF2A (left) and MEF2C (right) was determined in WT vs AR113Q mice at 26 weeks (n=6v6). (B) MEF2C protein was examined by western blot in WT and AR113Q mice (n=2/group). (C) Renilla luciferase activity was measured between WT and AR113Q mice (n=4v4). Data are shown as mean ± SEM.

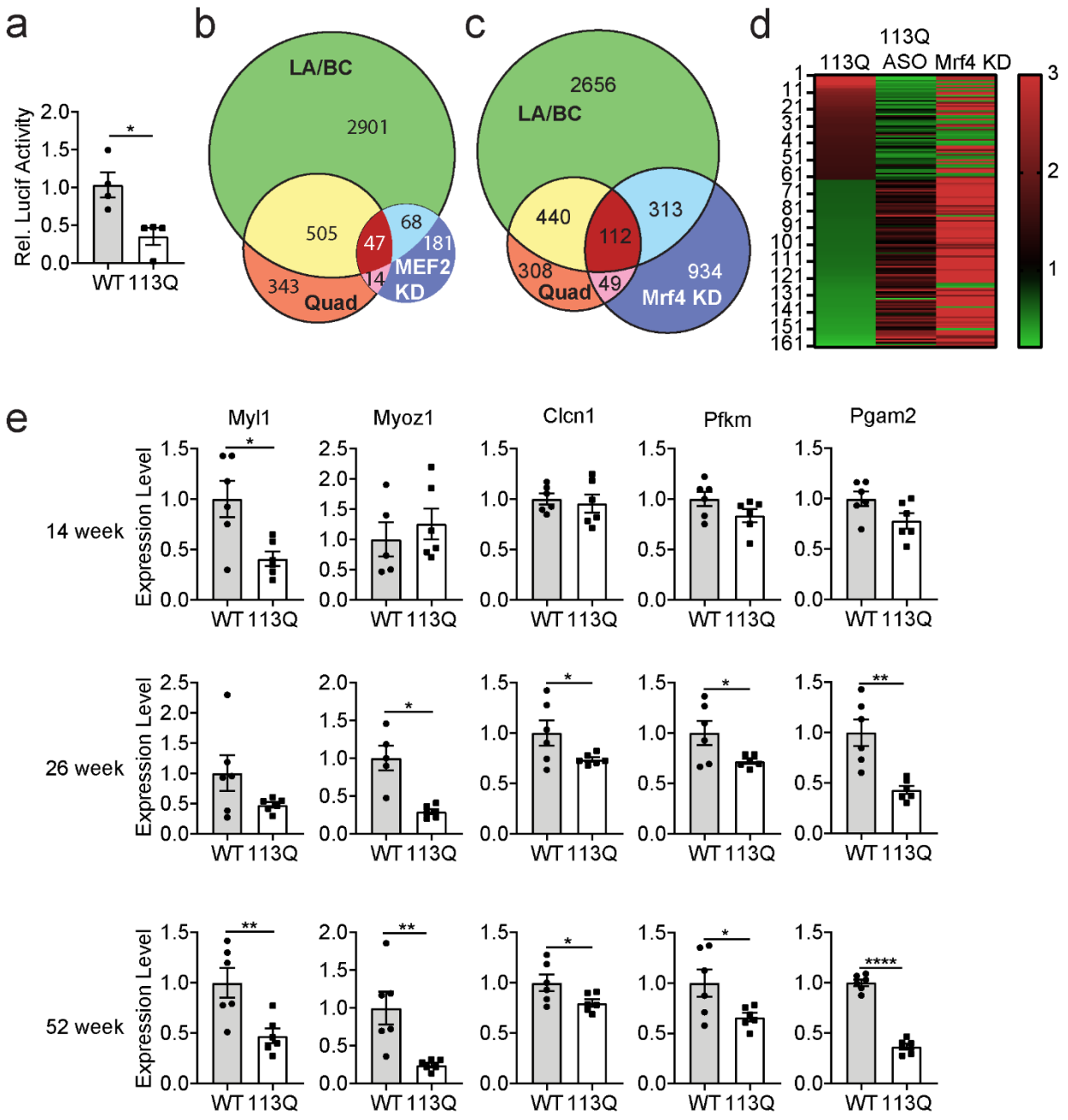

Fig. 4.6 Diminished MEF2 activity in AR113Q muscle. (A) Tibialis anterior of 26 week WT and AR113Q mice were co-transfected with MEF2-luciferase and constitutively expressed Renilla luciferase. (n=4/group). Data are mean ± SEM.*P < 0.05 by unpaired t test. (B) Differentially expressed genes (AR113Q vs WT) were compared to MEF2 target genes identified by gene knockdown (KD) and validated by ChIP-exo. P = 6.21e-26 by hypergeometric test for Quad overlap with MEF2 KD and P = 2.67e-27 by hypergeometric test for LABC overlap with MEF2 KD. (C) Differentially expressed genes (AR113Q vs WT) were compared to effects of Mrf4 KD. P= 2.12e-68 for LABC overlap with Mrf4 KD and P= 5.20e-36 for Quad overlap with Mrf4 KD (D) Heatmap showing fold change of 161 overlapping genes between AR113Q Quad and Mrf4 KD. Three comparisons to WT are displayed: AR113Q Quad, AR113Q Quad from mice treated with antisense oligonucleotides, and tibialis anterior from WT mice following Mrf4 KD. (E) Relative expression of MEF2 targets PFKM, Ryr1, Myl1, CLCN1, Myoz1 and PGAM2 was measured in WT and AR113Q mice at 14 (left), 26 (middle), and 52 (right) weeks in quadriceps (n=5-6/group). Data are shown as mean ± SEM.*P < 0.05; **P < 0.01; ***P < 0.001, ****P<0.0001 by unpaired t test

4.4.5 Diminished MEF2 Target Expression is Caused by Hormone- and Polyglutamine Length-Dependent Gain of Function.

Expansion of the AR's polyQ tract leads to partial loss of its normal function as a transcriptional regulator. In addition, the mutant protein undergoes hormone-dependent misfolding and aggregation resulting in gain of function changes crucial to the neuromuscular phenotype. To determine whether loss of MEF2 targets is dependent on the polyglutamine tract expansion, we compared gene expression in WT, AR21Q, and AR113Q muscle. AR21Q mice are phenotypically similar to WT mice, demonstrating that the neuromuscular phenotype is solely due to the polyQ expansion [25]. We found that loss of MEF2 target gene expression, like the neuromuscular phenotype, is dependent on the expanded glutamine tract and not the humanized sequence of exon 1 (Fig 4.8A).

We next sought to establish whether impaired MEF2 function is due to loss of AR activity or hormone-dependent proteotoxicity. To determine this, we castrated WT males at 5-6 weeks and allowed them to age to 14 weeks. This manipulation eliminates testosterone production and abrogates AR signaling. We found that castration does not alter expression of MEF2 regulated genes (Fig 4.8B) suggesting that loss of AR signaling does not impair MEF2 function. This conclusion is corroborated by the observation that ASO treatment rescues expression of MEF2 targets (Fig 4.6D). As ASOs diminish AR levels, changes due to loss of function are exacerbated by treatment while those due to gain of function proteotoxicity are ameliorated. The finding that MEF2 targets are rescued by ASO administration supports the notion that loss of MEF2 function is due to polyglutamine mediated toxicity.

Next, we castrated AR113Q males. Castration prevents hormone dependent misfolding and aggregation of polyQ AR and abrogates the neuromuscular phenotype of AR113Q mice

[13]. We found that castration also rescues expression of MEF2 target genes (Fig 4.8C) indicating that, like the motor phenotype, MEF2 impairment results from hormone-dependent proteotoxicity. Together, these results demonstrate that MEF2 impairment occurs in a gain of function, polyQ tract-dependent manner.

AR113Q misfolding is associated with the formation of intranuclear inclusions in skeletal muscle nuclei [13]. We performed immunofluorescence using a MEF2A/C antibody to determine whether MEF2 is also mislocalized in AR113Q muscle. We identified robust colocalization of MEF2 with intranuclear p62 puncta, a marker of inclusions formed by polyQ AR (Fig 4.8D). Similar staining was observed using antibodies against MEF2A and MEF2C (Fig 4.7A). These data demonstrate MEF2 sequestration into intranuclear inclusions in mutant muscle. Consistent with the notion that MEF2 has properties that confer a high potential for co-aggregation, several prediction pipelines identified significant intrinsic disorder in the transactivating domain of MEF2C (Supp Fig

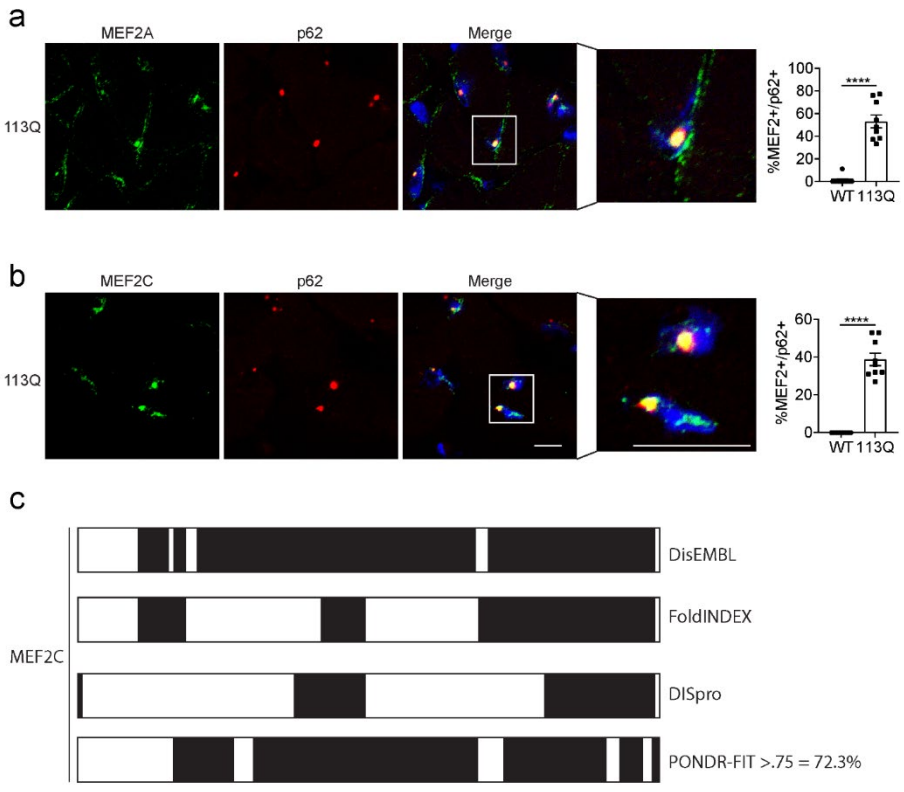

Fig 4.7 MEF2A and MEF2C antibodies show sequestration to intranuclear aggregates. (A, B) AR113Q LABC at 14 weeks was stained for MEF2A (A), MEF2C (B) and p62. Co-localization with p62 quantified at right. (n=3v3 mice, 3 images/mouse), ****P<0.0001 by unpaired t-test. Scale bar = 10µm. (C) MEF2 sequence is marked black for portions suggestive of intrinsic disorder using DisEMBL, FoldINDEX, DISpro, and PONDR-FIT pipelines. Disorder was found by all pipelines in the transactivating domain.

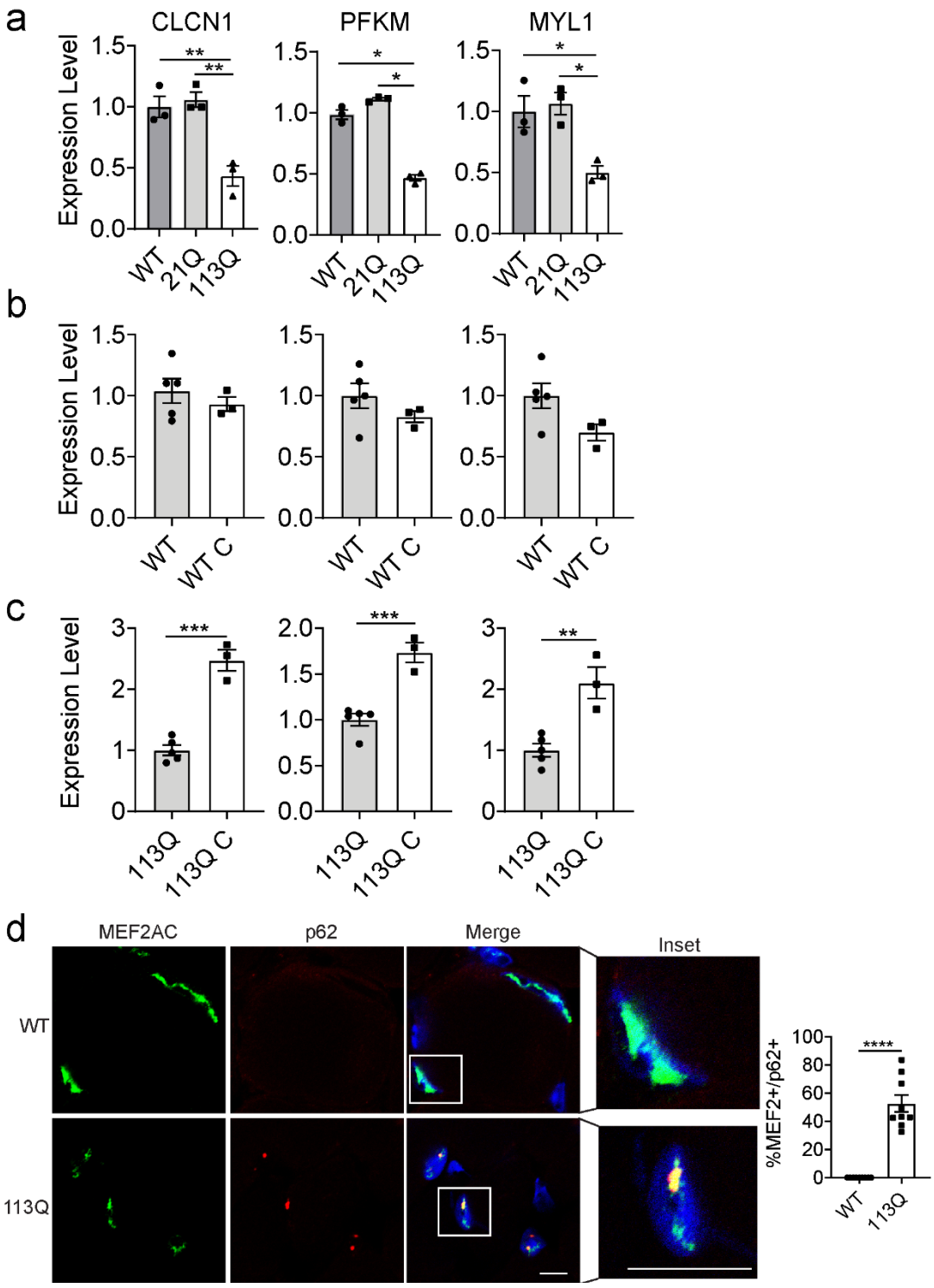

Fig. 4.8 AR113Q muscle shows hormone- and Q tract length-dependent MEF2 impairment and sequestration. (A-C) Relative mRNA expression of MEF2 targets was measured in the LABC of (A) WT, AR21Q, and AR113Q mice at 14 weeks of age. (n=3/group), (B) WT mice compared to WT mice castrated at 6 weeks and allowed to age to 14 weeks (WT C). (n=3-5/group), and (C) AR113Q mice compared to AR113Q mice castrated at 6 weeks and allowed to age to 14 weeks (AR113Q C) (n=3-5/group) (D) Co-localization of p62 and MEF2A/C in LABC of WT and AR113Q mice at 14 weeks of age, quantified at right (n=3 mice/group). Data are shown as mean ± SEM. Scale bar = 10μm. *P < 0.05; **P < 0.01; ***P < 0.001, ****P<0.0001 by unpaired t test (A, B, D) or one-way ANOVA with Tukey's (C)

4.7B).

4.4.6 Polyglutamine Huntingtin Sequesters MEF2 in Skeletal Muscle and Decreases MEF2 Target Gene Expression.

As our findings suggest that polyQ expansion underlies MEF2 impairment and sequestration, we hypothesized that these mechanisms are similarly active in other models of polyQ disease that exhibit skeletal muscle atrophy. To test this hypothesis, we studied R6/2 mice. These mice express an N-terminal fragment of polyQ huntingtin (HTT), develop age-dependent skeletal muscle atrophy, and form intranuclear inclusions in skeletal muscle [32, 52]. We utilized a previously published RNAseq data set of R6/2 quadriceps to determine whether polyQ HTT also alters MEF2 target gene expression. This analysis revealed 2,715 differentially expressed genes between WT and R6/2 muscle. We found significant overlap between differentially expressed genes from R6/2 quadriceps and effects of MEF2 (Fig 4.9A) and Mrf4 (Fig 4.9B) knockdown. Notably, knockdown of Mrf4, a MEF2 inhibitor, shows changes opposite to those observed in R6/2 quadriceps, supporting the concept of impaired MEF2 activity downstream of polyQ HTT (Fig 4.9C). We confirmed diminished expression of MEF2 target genes in an independent cohort of R6/2 mice by qPCR. We found progressive changes, with 3 targets showing diminished expression at 4 weeks, 4 targets at 8 weeks, and all 6 targets at 12 weeks of age (Fig 4.9D). Moreover, using immunofluorescence we found significant sequestration of MEF2 into skeletal muscle inclusions, with MEF2 colocalizing to ~85% of p62 positive inclusions (Fig 4.9E).

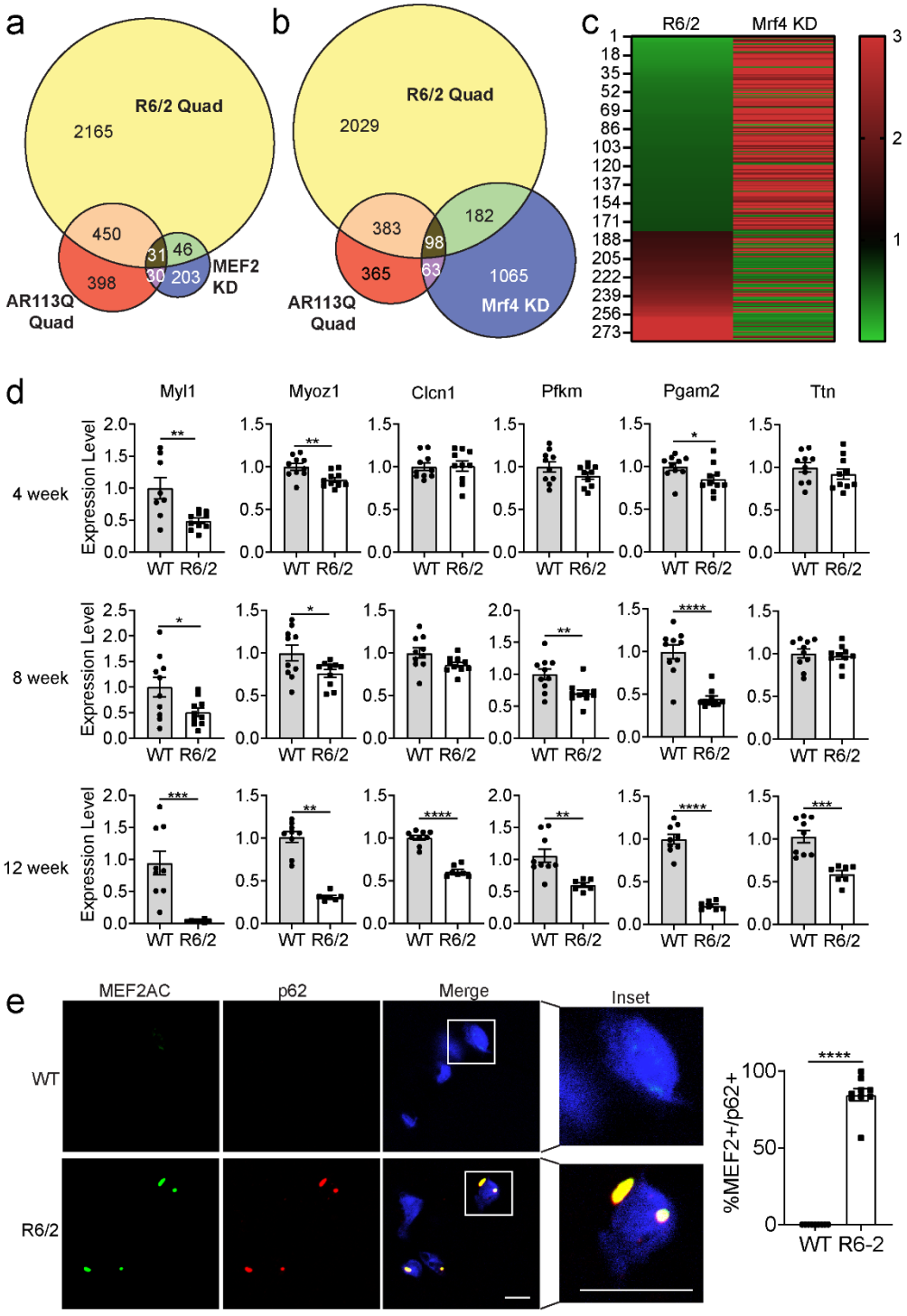

Fig. 4.9 Diminished MEF2 function and sequestration in R6/2 muscle. (A) Differentially expressed genes in R6/2 quadriceps were compared to known MEF2 targets and AR113Q quad. Overlap is shown by Venn diagram. P = 9.27e-07 for MEF2 KD vs R6/2 overlap (B) Differentially expressed genes in R6/2 quadriceps were compared to effects of Mrf4 KD. Overlap is shown by Venn diagram. P = 6.69e-09 for Mrf4 KD vs R6/2 overlap. (C) Heatmap showing fold change of 280 overlapping genes in R6/2 Quad and Mrf4 KD. Two comparisons to WT are displayed: R6/2 quadriceps and tibialis anterior following Mrf4 KD. (D) R6/2 mice were examined for gene expression changes in quadriceps at 4, 8, and 12 weeks of age (n=8-10/group for 4, 8wk, n=9 WT 12 week, n=7 R6/2 12 week). (E) Co-localization of p62 and MEF2A/C in quadriceps of WT and R6/2 mice at 12 weeks of age, quantified at right. Data are shown as mean ± SEM. Scale bar = 10μm. *P < 0.05; **P < 0.01; ***P < 0.001, ****P<0.0001 by unpaired t test

4.4.7 SBMA Patients Show Loss of MEF2 Target Expression, and Replacing MEF2 Rescues AR113Q Muscle Atrophy.

We sought to determine whether changes in expression of MEF2 target genes also occur in SBMA patients. To accomplish this, we performed qPCR on a cohort of SBMA skeletal muscle biopsies. We found significant reduction of these targets in patients versus controls (Fig 4.12) without loss of MEF2 expression (Fig 4.10), suggesting that MEF2 impairment is a conserved disease mechanism. To determine the extent to which loss of MEF2 function contributes to AR113Q muscle atrophy, we tested whether adding back constitutively active MEF2 (CA-MEF2) would rescue muscle fiber size [23, 34, 53]. This CA mutant consists of the MEF2 DNA binding domain fused to the VP16 transactivating domain and estrogen receptor hormone binding domain; nuclear translocation and activity of this mutant is controlled by tamoxifen (Fig. 4.11). [23, 34]. In addition to its constitutively active nature, this construct has significantly less predicted disorder suggesting less propensity for co-aggregation (Fig. 4.11B). At 19 weeks of age, after AR113Q mice show significant muscle atrophy (Fig 4.11), we electroporated CA-MEF2 into tibialis anterior (TA) muscle of one hind limb. The contralateral TA was electroporated with VP16-MEF2 containing a deletion in the DNA binding domain (DBD-MEF2), thereby preventing transcriptional activity [23, 34]. Importantly, DBD-MEF2 does not alter muscle fiber size [23]. Following electroporation, mice were administered tamoxifen every other day for 7 days prior to harvesting muscle. We found a 24% increase in muscle fiber size owing to expression of CA-MEF2 in AR113Q muscle (Fig 4.12B-D). Electroporated CA-MEF2 was predominantly diffuse within the nucleus of skeletal muscle and did not colocalize with p62+ intranuclear inclusions (Fig. 4.11C). Notably, this rescue of muscle

fiber size is accompanied by increased expression of MEF2 target genes, including the same genes reduced in SBMA patients (Fig 4.12E). Strikingly, restoration of MEF2 activity also rescued expression of critical genes mediating metabolic dysfunction in SBMA, an important disease phenotype characterized by diminished carbohydrate metabolism (Fig 4.12F) [29, 42]. Taken together, these results demonstrate loss of MEF2 targets in SBMA patient muscle and rescue of muscle atrophy by restoring MEF2 activity and target gene expression in AR113Q mice.

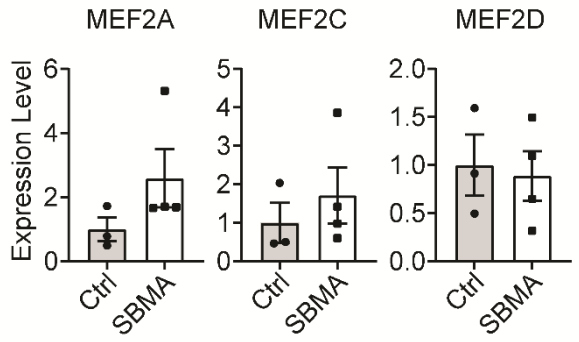

Fig. 4.10 MEF2 expression is not significantly altered in SBMA patient muscle biopsies. SBMA patient muscle biopsies were examined for expression of MEF2A, MEF2C, and MEF2D (n=3v4). Values not significant by unpaired t-test

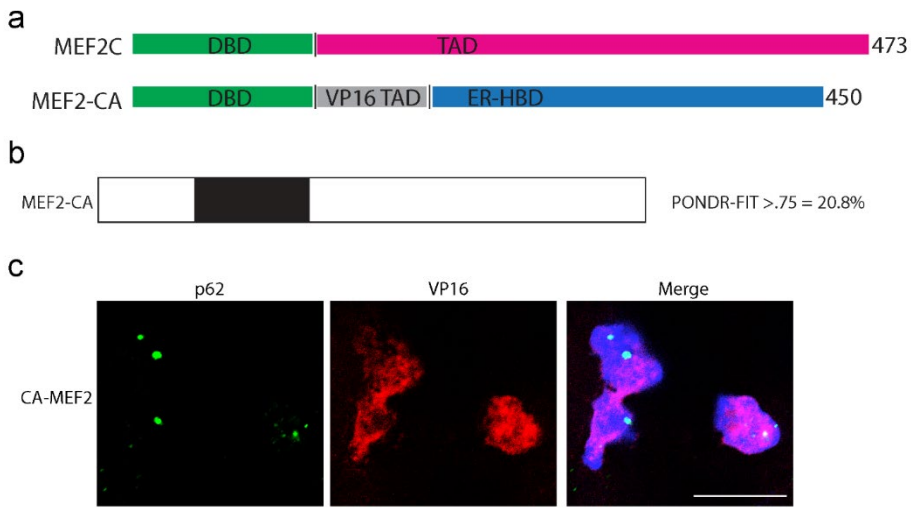

Fig. 4.11 CA-MEF2 has less intrinsic disorder and does not colocalize with intranuclear p62 pucta. (A) Diagram of the differences between WT MEF2C and MEF2-CA (DBD = DNA binding domain, TAD = transactivating domain, ER= Estrogen Receptor, HBD = Hormone Binding Domain). (B) PONDR analysis of intrinsic disorder of MEF2-CA construct. (C) Staining of AR113Q muscle at 19wks showing diffuse VP16 signal and intranuclear p62 puncta. Scale bar = 12.5µm.

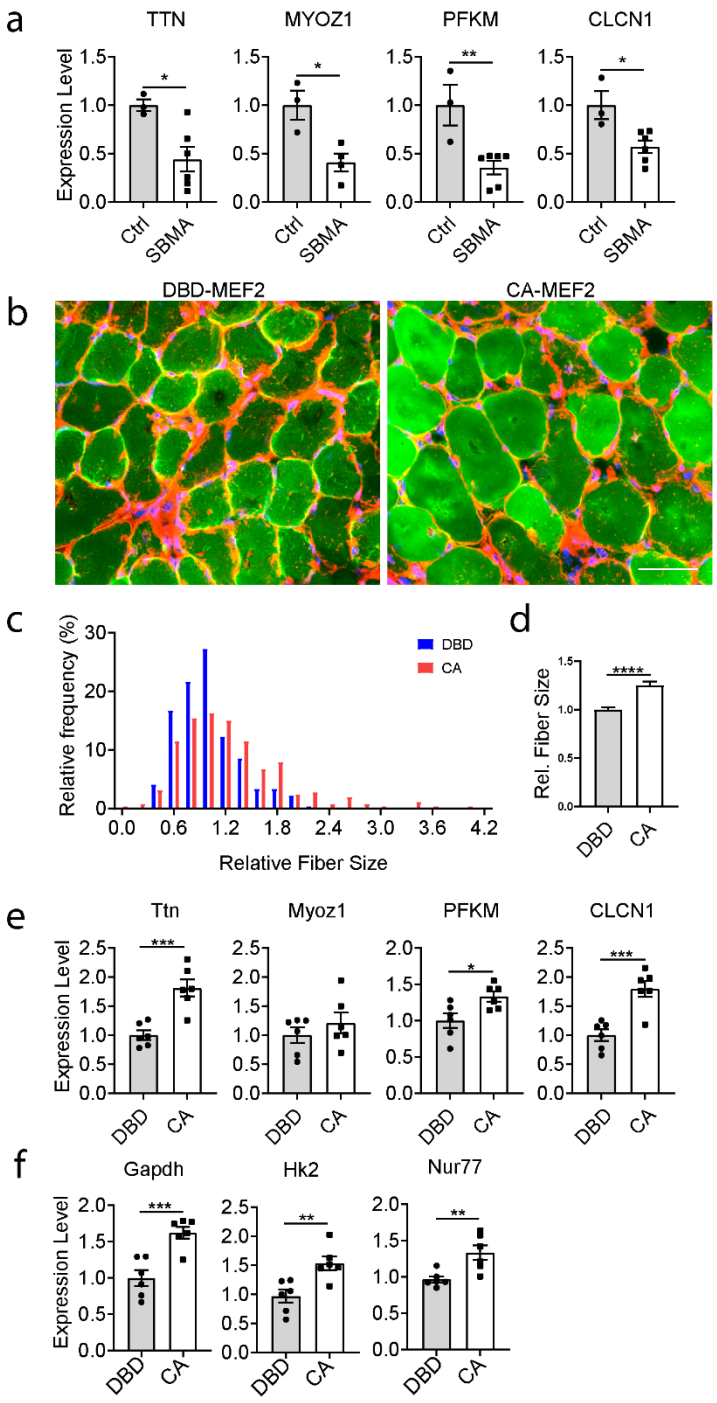

Fig. 4.12 SBMA muscle shows decreased expression of MEF2 target genes, and CA-MEF2 rescues AR113Q muscle atrophy. (A) SBMA patient muscle biopsies were examined for expression of MEF2 targets CLCN1 (n=3v6), Myoz1 (n=3v4), PFKM (n=3v6), and TTN (n=3v6) by qPCR. (B-D) AR113Q mice were transfected with CA-MEF2 in one leg and DBD-MEF2 in the contralateral leg. Each plasmid was co-transfected with GFP for fiber identification. After 24h, mice were injected with tamoxifen every other day for 7 days. (B) Tibialis anterior was harvested and analyzed. Scale bar = 50µm. Quantification of cross sectional area of transfected fibers (n=3mice/group, 3 images/mouse, n>50 fibers/mouse) is shown as a histogram (C) and mean ± SEM (D), ****P<0.0001 by unpaired t test. (E,F) AR113Q muscle expressing DBD-MEF2 and CA-MEF2 was examined for expression levels of (E) MEF2 targets altered in SBMA patients Ttn, MyoZ1, Pfkm, Clcn1 and (F) genes that regulate metabolism including Gapdh, Hk2, and Nur77 (n=6 mice/group). Data are mean ± SEM.*P < 0.05; ***P < 0.001 by unpaired t test

4.5 Discussion

We demonstrate a novel mechanism of skeletal muscle atrophy mediated by toxic proteins with expanded polyQ tracts, resulting in impaired function of the transcriptional regulator MEF2. The MEF2 family of transcription factors consists of four members, with *Mef2a*, *Mef2c*, and *Mef2d* most abundantly expressed in skeletal muscle (Table S4). Prior research demonstrates that MEF2A, -C, and -D bind the same consensus sequence [54], and that they are capable of compensating for knockout of one but not all 3 *Mef2* genes in satellite cells, suggesting redundant function of MEF2 family members in skeletal muscle [55]. Similar compensation of MEF2 family members has been demonstrated in the CNS, suggesting that functional redundancy is conserved between organ systems [56]. *Mef2c* expression is known to make important contributions to sarcomere integrity and maintenance [57]. Supporting this notion, MEF2 proteins regulate the expression of a large number of genes encoding structural proteins of the sarcomere [23, 33], and skeletal muscle specific deletion of *Mef2c* leads to rapid deterioration of myofibers and disorganized sarcomeres [57]. Additional studies have demonstrated that postnatal growth is impaired by skeletal muscle specific *Mef2c* deletion in mice [58]. Moreover, activation of MEF2 by silencing of the repressor *Mrf4* or by overexpression of the constitutively active form, drives skeletal muscle hypertrophy in vivo, defining MEF2 as a key regulator of muscle hypertrophy [23]. In support of this role, NCoR1 knockout in mouse skeletal muscle also leads to MEF2 activation and skeletal muscle hypertrophy [59]. Additional studies have confirmed a role for MEF2 in cardiac [60] and smooth muscle hypertrophy [61], suggesting a conserved role between muscle types. Together, these studies have established MEF2 as a critical regulator of muscle homeostasis.

Here, we show that diminished MEF2 function occurs in atrophic muscles of SBMA mice (Figs. 4.6,4.8), Huntington disease mice (Fig. 4.9), and SBMA patients (Fig 4.12A). Evidence supporting this conclusion includes diminished activity of a MEF2-luciferase reporter in AR113Q muscle (Fig. 4.6A) and decreased expression of MEF2 regulated genes in AR113Q (Fig. 4B-E) and R6/2 mice (Fig. 4.9A-D) as well as in SBMA patients (Fig. 4.12A). Expression of CA-MEF2 rescues AR113Q muscle atrophy and target gene expression (Fig 4.12B-E), indicating the importance of these changes to disease pathogenesis and suggesting that targeting MEF2 function may be a novel and unexplored therapeutic avenue. Notably, impaired MEF2 activity occurs without concurrent alterations in the activity of the canonical UPS-mediated atrophy pathway (Fig 4.1) [22], disruption of signaling pathways that influence muscle hypertrophy (Fig. 4.3), or significant impairment of the muscle stem cell niche (Fig. 3). As such, toxic polyglutamine proteins trigger muscle atrophy through a distinct and previously uncharacterized mechanism.

MEF2 activity is influenced by post-translational modifications, including acetylation and phosphorylation, which can enhance DNA binding and activity [62-64]. Several proteins have been identified as inhibiting MEF2 activity, either by direct binding or localization to MEF2 binding sites, including HDAC4 [65], Mrf4 [23], and NCoR1 [59]. Interestingly, MEF2 expression and nuclear translocation are not altered in AR113Q muscle, but its nuclear localization is disrupted by sequestration into intranuclear inclusions, suggesting that co-aggregation is a final consequence of aberrant interaction with polyQ AR. Similar findings are observed in R6/2 muscle (Fig 6), where the HDAC4-myogenin axis has been shown to be re-expressed [66]. This sequestration may reflect the fact that the MEF2C transactivating domain is intrinsically disordered and prone to aggregation (Supp Fig 4.7C). These findings align with our

observation that MEF2 impairment is mediated by polyQ AR proteotoxicity rather than loss of function (Fig 4.8). Whether sequestration of MEF2 into morphologically visible inclusions is necessary for functional impairment is uncertain; it is possible that its aberrant association with soluble polyQ species in the nucleus may also disrupt activity and that sequestration into protein aggregates is the end stage of this process.

Although MEF2 represents a promising therapeutic target, limitations remain in leveraging this pathway in patients. While MEF2 is able to restore fiber size in atrophic muscle of adult SBMA mice, whether this effect is sustained during long-term treatment is not yet known. Further, because MEF2 plays key roles in skeletal [23], cardiac [60], and smooth muscle [61] as well as in the nervous system [34, 53, 67, 68], therapeutically targeting MEF2 specifically in skeletal muscle remains a significant challenge. To overcome these limitations, we propose that in addition to direct modulation of MEF2, a strategy by which mutant AR is targeted to prevent aggregation and sequestration of MEF2, such as by administration of antisense oligonucleotides [18] or modulation of the HSP70/90 chaperone machinery [69, 70] may be synergistic as a long-term therapeutic.

The sequestration and functional impairment of transcriptional regulators, including cAMP response element-binding protein (CBP) [71], specific protein-1 (Sp1) [72, 73], and TAFII130 [72], has been implicated in neuronal dysfunction in polyQ disease. Our data suggest that a similar mechanism disrupts activity of MEF2, a critical regulator of sarcomere maintenance, to trigger skeletal muscle pathology. As MEF2 is also strongly implicated in activity-dependent neuronal survival [34, 53, 67, 68], we hypothesize that this mechanism of MEF2 sequestration and loss of function may additionally contribute to CNS pathology in polyQ diseases. It is intriguing to speculate that disease-specific disruptions of certain transcriptional

regulators may contribute to cell type vulnerability. In this regard, our observation of impaired MEF2 function in skeletal muscle provides both new mechanistic insight and identification of a therapeutic target for polyQ-mediated muscle atrophy.

Author Contributions:

SRN, MLL, ZY, CM, and KMV performed experiments contained in this study. STJ, ECED, GS, GB, DMR, and MP provided critical reagents and samples. SRN and APL wrote and edited the manuscript. SRN, APL, MP, STJ, CM, GB, and MP edited the manuscript.

This chapter is currently in revision for publication.

References

1. Lieberman, A.P., V.G. Shakkottai, and R.L. Albin, *Polyglutamine Repeats in Neurodegenerative Diseases.* Annu Rev Pathol, 2019. **14**: p. 1-27.
2. Pratt, W.B., et al., *Targeting Hsp90/Hsp70-based protein quality control for treatment of adult onset neurodegenerative diseases.* Annu Rev Pharmacol Toxicol, 2015. **55**: p. 353-71.
3. Mhatre, A.N., et al., *Reduced transcriptional regulatory competence of the androgen receptor in X-linked spinal and bulbar muscular atrophy.* Nature genetics, 1993. **5**(2): p. 184-188.
4. Lieberman, A.P., et al., *Altered transcriptional regulation in cells expressing the expanded polyglutamine androgen receptor.* Human molecular genetics, 2002. **11**(17): p. 1967-1976.
5. Ranganathan, S., et al., *Mitochondrial abnormalities in spinal and bulbar muscular atrophy.* Human molecular genetics, 2009. **18**(1): p. 27-42.
6. Montie, H.L., et al., *Cytoplasmic retention of polyglutamine-expanded androgen receptor ameliorates disease via autophagy in a mouse model of spinal and bulbar muscular atrophy.* Hum Mol Genet, 2009. **18**(11): p. 1937-50.
7. Nedelsky, N.B., et al., *Native functions of the androgen receptor are essential to pathogenesis in a Drosophila model of spinobulbar muscular atrophy.* Neuron, 2010. **67**(6): p. 936-52.
8. Scaramuzzino, C., et al., *Protein arginine methyltransferase 6 enhances polyglutamine-expanded androgen receptor function and toxicity in spinal and bulbar muscular atrophy.* Neuron, 2015. **85**(1): p. 88-100.
9. Atsuta, N., et al., *Natural history of spinal and bulbar muscular atrophy (SBMA): a study of 223 Japanese patients.* Brain, 2006. **129**(Pt 6): p. 1446-55.
10. Soraru, G., et al., *Spinal and bulbar muscular atrophy: skeletal muscle pathology in male patients and heterozygous females.* J Neurol Sci, 2008. **264**(1-2): p. 100-5.
11. Rhodes, L.E., et al., *Clinical features of spinal and bulbar muscular atrophy.* Brain, 2009. **132**(Pt 12): p. 3242-51.
12. Malena, A., et al., *Androgen-dependent impairment of myogenesis in spinal and bulbar muscular atrophy.* Acta Neuropathol, 2013. **126**(1): p. 109-21.
13. Yu, Z., et al., *Androgen-dependent pathology demonstrates myopathic contribution to the Kennedy disease phenotype in a mouse knock-in model.* The Journal of clinical investigation, 2006. **116**(10): p. 2663-2672.
14. Monks, D.A., et al., *Overexpression of wild-type androgen receptor in muscle recapitulates polyglutamine disease.* Proc Natl Acad Sci U S A, 2007. **104**(46): p. 18259-64.
15. Ramzan, F., et al., *Distinct Etiological Roles for Myocytes and Motor Neurons in a Mouse Model of Kennedy's Disease/Spinobulbar Muscular Atrophy.* J Neurosci, 2015. **35**(16): p. 6444-51.
16. Palazzolo, I., et al., *Overexpression of IGF-1 in muscle attenuates disease in a mouse model of spinal and bulbar muscular atrophy.* Neuron, 2009. **63**(3): p. 316-28.

17. Cortes, C.J., et al., *Muscle expression of mutant androgen receptor accounts for systemic and motor neuron disease phenotypes in spinal and bulbar muscular atrophy.* Neuron, 2014. **82**(2): p. 295-307.
18. Lieberman, A.P., et al., *Peripheral androgen receptor gene suppression rescues disease in mouse models of spinal and bulbar muscular atrophy.* Cell Rep, 2014. **7**(3): p. 774-84.
19. Lecker, S.H., et al., *Multiple types of skeletal muscle atrophy involve a common program of changes in gene expression.* FASEB J, 2004. **18**(1): p. 39-51.
20. Bodine, S.C. and L.M. Baehr, *Skeletal muscle atrophy and the E3 ubiquitin ligases MuRF1 and MAFbx/atrogin-1.* Am J Physiol Endocrinol Metab, 2014. **307**(6): p. E469-84.
21. Bodine, S.C., et al., *Identification of ubiquitin ligases required for skeletal muscle atrophy.* Science, 2001. **294**(5547): p. 1704-8.
22. Nath, S.R., et al., *Androgen receptor polyglutamine expansion drives age-dependent quality control defects and muscle dysfunction.* J Clin Invest, 2018. **128**(8): p. 3630-3641.
23. Moretti, I., et al., *MRF4 negatively regulates adult skeletal muscle growth by repressing MEF2 activity.* Nat Commun, 2016. **7**: p. 12397.
24. Yu, Z., et al., *Abnormalities of germ cell maturation and sertoli cell cytoskeleton in androgen receptor 113 CAG knock-in mice reveal toxic effects of the mutant protein.* Am J Pathol, 2006. **168**(1): p. 195-204.
25. Albertelli, M.A., et al., *Replacing the mouse androgen receptor with human alleles demonstrates glutamine tract length-dependent effects on physiology and tumorigenesis in mice.* Mol Endocrinol, 2006. **20**(6): p. 1248-60.
26. Mangiarini, L., et al., *Exon 1 of the HD gene with an expanded CAG repeat is sufficient to cause a progressive neurological phenotype in transgenic mice.* Cell, 1996. **87**(3): p. 493-506.
27. Sathasivam, K., et al., *Identical oligomeric and fibrillar structures captured from the brains of R6/2 and knock-in mouse models of Huntington's disease.* Hum Mol Genet, 2010. **19**(1): p. 65-78.
28. Chua, J.P., et al., *Disrupting SUMOylation enhances transcriptional function and ameliorates polyglutamine androgen receptor-mediated disease.* J Clin Invest, 2015. **125**(2): p. 831-45.
29. Giorgetti, E., et al., *Rescue of Metabolic Alterations in AR113Q Skeletal Muscle by Peripheral Androgen Receptor Gene Silencing.* Cell Rep, 2016. **17**(1): p. 125-136.
30. Schiaffino, S., et al., *Mechanisms regulating skeletal muscle growth and atrophy.* FEBS J, 2013. **280**(17): p. 4294-314.
31. Chua, J.P. and A.P. Lieberman, *Pathogenic mechanisms and therapeutic strategies in spinobulbar muscular atrophy.* CNS Neurol Disord Drug Targets, 2013. **12**(8): p. 1146-56.
32. Bondulich, M.K., et al., *Myostatin inhibition prevents skeletal muscle pathophysiology in Huntington's disease mice.* Sci Rep, 2017. **7**(1): p. 14275.
33. Wales, S., et al., *Global MEF2 target gene analysis in cardiac and skeletal muscle reveals novel regulation of DUSP6 by p38MAPK-MEF2 signaling.* Nucleic Acids Res, 2014. **42**(18): p. 11349-62.
34. Flavell, S.W., et al., *Activity-dependent regulation of MEF2 transcription factors suppresses excitatory synapse number.* Science, 2006. **311**(5763): p. 1008-12.

35. Woronicz, J.D., et al., *Regulation of the Nur77 orphan steroid receptor in activation-induced apoptosis.* Mol Cell Biol, 1995. **15**(11): p. 6364-76.
36. Leger, B., et al., *Human skeletal muscle atrophy in amyotrophic lateral sclerosis reveals a reduction in Akt and an increase in atrogin-1.* FASEB J, 2006. **20**(3): p. 583-5.
37. Sacheck, J.M., et al., *Rapid disuse and denervation atrophy involve transcriptional changes similar to those of muscle wasting during systemic diseases.* FASEB J, 2007. **21**(1): p. 140-55.
38. Cohen, S., J.A. Nathan, and A.L. Goldberg, *Muscle wasting in disease: molecular mechanisms and promising therapies.* Nat Rev Drug Discov, 2015. **14**(1): p. 58-74.
39. Sartori, R., et al., *BMP signaling controls muscle mass.* Nat Genet, 2013. **45**(11): p. 1309-18.
40. Ohanna, M., et al., *Atrophy of S6K1(-/-) skeletal muscle cells reveals distinct mTOR effectors for cell cycle and size control.* Nat Cell Biol, 2005. **7**(3): p. 286-94.
41. Bodine, S.C., et al., *Akt/mTOR pathway is a crucial regulator of skeletal muscle hypertrophy and can prevent muscle atrophy in vivo.* Nat Cell Biol, 2001. **3**(11): p. 1014-9.
42. Rocchi, A., et al., *Glycolytic-to-oxidative fiber-type switch and mTOR signaling activation are early-onset features of SBMA muscle modified by high-fat diet.* Acta Neuropathol, 2016. **132**(1): p. 127-44.
43. Peterson, T.R., et al., *DEPTOR is an mTOR inhibitor frequently overexpressed in multiple myeloma cells and required for their survival.* Cell, 2009. **137**(5): p. 873-86.
44. Brugarolas, J., et al., *Regulation of mTOR function in response to hypoxia by REDD1 and the TSC1/TSC2 tumor suppressor complex.* Genes Dev, 2004. **18**(23): p. 2893-904.
45. Sofer, A., et al., *Regulation of mTOR and cell growth in response to energy stress by REDD1.* Mol Cell Biol, 2005. **25**(14): p. 5834-45.
46. McPherron, A.C., A.M. Lawler, and S.J. Lee, *Regulation of skeletal muscle mass in mice by a new TGF-beta superfamily member.* Nature, 1997. **387**(6628): p. 83-90.
47. Crist, C.G., D. Montarras, and M. Buckingham, *Muscle satellite cells are primed for myogenesis but maintain quiescence with sequestration of Myf5 mRNA targeted by microRNA-31 in mRNP granules.* Cell Stem Cell, 2012. **11**(1): p. 118-26.
48. Gunther, S., et al., *Myf5-positive satellite cells contribute to Pax7-dependent long-term maintenance of adult muscle stem cells.* Cell Stem Cell, 2013. **13**(5): p. 590-601.
49. Attia, M., et al., *Muscle satellite cells are functionally impaired in myasthenia gravis: consequences on muscle regeneration.* Acta Neuropathol, 2017.
50. Park, S.Y., et al., *Stabilin-2 modulates the efficiency of myoblast fusion during myogenic differentiation and muscle regeneration.* Nat Commun, 2016. **7**: p. 10871.
51. Hardy, D., et al., *Comparative Study of Injury Models for Studying Muscle Regeneration in Mice.* PLoS One, 2016. **11**(1): p. e0147198.
52. Cha, J.H., et al., *Altered brain neurotransmitter receptors in transgenic mice expressing a portion of an abnormal human huntington disease gene.* Proc Natl Acad Sci U S A, 1998. **95**(11): p. 6480-5.
53. Mao, Z., et al., *Neuronal activity-dependent cell survival mediated by transcription factor MEF2.* Science, 1999. **286**(5440): p. 785-90.
54. Yu, Y.T., et al., *Human myocyte-specific enhancer factor 2 comprises a group of tissue-restricted MADS box transcription factors.* Genes Dev, 1992. **6**(9): p. 1783-98.

55. Liu, N., et al., *Requirement of MEF2A, C, and D for skeletal muscle regeneration.* Proc Natl Acad Sci U S A, 2014. **111**(11): p. 4109-14.
56. Majidi, S.P., et al., *Chromatin Environment and Cellular Context Specify Compensatory Activity of Paralogous MEF2 Transcription Factors.* Cell Rep, 2019. **29**(7): p. 2001-2015 e5.
57. Potthoff, M.J., et al., *Regulation of skeletal muscle sarcomere integrity and postnatal muscle function by Mef2c.* Mol Cell Biol, 2007. **27**(23): p. 8143-51.
58. Anderson, C.M., et al., *Myocyte enhancer factor 2C function in skeletal muscle is required for normal growth and glucose metabolism in mice.* Skelet Muscle, 2015. **5**: p. 7.
59. Yamamoto, H., et al., *NCoR1 is a conserved physiological modulator of muscle mass and oxidative function.* Cell, 2011. **147**(4): p. 827-39.
60. Dadson, K., et al., *Adiponectin is required for cardiac MEF2 activation during pressure overload induced hypertrophy.* J Mol Cell Cardiol, 2015. **86**: p. 102-9.
61. Li, C., et al., *Increased IGF-IEc expression and mechano-growth factor production in intestinal muscle of fibrostenotic Crohn's disease and smooth muscle hypertrophy.* Am J Physiol Gastrointest Liver Physiol, 2015. **309**(11): p. G888-99.
62. Molkentin, J.D., L. Li, and E.N. Olson, *Phosphorylation of the MADS-Box transcription factor MEF2C enhances its DNA binding activity.* J Biol Chem, 1996. **271**(29): p. 17199-204.
63. Zhao, M., et al., *Regulation of the MEF2 family of transcription factors by p38.* Mol Cell Biol, 1999. **19**(1): p. 21-30.
64. Ma, K., et al., *Myocyte enhancer factor 2 acetylation by p300 enhances its DNA binding activity, transcriptional activity, and myogenic differentiation.* Mol Cell Biol, 2005. **25**(9): p. 3575-82.
65. Cohen, T.J., et al., *The deacetylase HDAC4 controls myocyte enhancing factor-2-dependent structural gene expression in response to neural activity.* FASEB J, 2009. **23**(1): p. 99-106.
66. Mielcarek, M., et al., *HDAC4-myogenin axis as an important marker of HD-related skeletal muscle atrophy.* PLoS Genet, 2015. **11**(3): p. e1005021.
67. Andzelm, M.M., et al., *A Late Phase of Long-Term Synaptic Depression in Cerebellar Purkinje Cells Requires Activation of MEF2.* Cell Rep, 2019. **26**(5): p. 1089-1097 e3.
68. Flavell, S.W., et al., *Genome-wide analysis of MEF2 transcriptional program reveals synaptic target genes and neuronal activity-dependent polyadenylation site selection.* Neuron, 2008. **60**(6): p. 1022-38.
69. Wang, A.M., et al., *Activation of Hsp70 reduces neurotoxicity by promoting polyglutamine protein degradation.* Nature chemical biology, 2013. **9**(2): p. 112-118.
70. Eftekharzadeh, B., et al., *Hsp70 and Hsp40 inhibit an inter-domain interaction necessary for transcriptional activity in the androgen receptor.* Nat Commun, 2019. **10**(1): p. 3562.
71. Steffan, J.S., et al., *The Huntington's disease protein interacts with p53 and CREB-binding protein and represses transcription.* Proc Natl Acad Sci U S A, 2000. **97**(12): p. 6763-8.
72. Dunah, A.W., et al., *Sp1 and TAFII130 transcriptional activity disrupted in early Huntington's disease.* Science, 2002. **296**(5576): p. 2238-43.
73. Li, S.H., et al., *Interaction of Huntington disease protein with transcriptional activator Sp1.* Mol Cell Biol, 2002. **22**(5): p. 1277-87.

CHAPTER 5

Distinguishing Myopathic and Neuropathic Change in SBMA

5.1 Introduction

Thus far, this thesis has examined the evidence supporting the role of skeletal muscle dysfunction in spinobulbar muscular atrophy (SBMA). In chapter 1, I described the manifestations and pathophysiology of SBMA. In chapter 2, I discussed the role of protein quality control in polyglutamine disease. In chapter 3, I outlined the surprising finding that the proteasome is impaired in SBMA and that this contributes to the age-dependent phenotype. In chapter 4, I followed up on the unexpected finding of proteasome impairment in the context of muscle atrophy by defining an alternate atrophy pathway at work in SBMA. In this final chapter, I will attempt to address the question "Is SBMA correctly categorized as a neurodegenerative disease?" To address this question, I sought an unbiased method to compare the global changes in gene expression occurring in SBMA muscle to those occurring in myopathy and neuropathy. Leveraging transcriptomic datasets of polyglutamine disease and models of myopathy and neuropathy, similarities and differences were quantitatively and qualitatively assessed. This analysis provides a springboard for discussion of the broad implications of my thesis work and potential future directions.

5.2 Methods

RNAseq data was accessed from the following GEO accession numbers: AR113Q Quad, KRKR, and ASO (GSE60691), AR113Q LABC (GSE106521), R6/2 Quadriceps (GSE81367), Denervation Soleus (GSE58669), and mdx/mTR (GSE127929). These datasets were then aligned and counts were quanitified by Dr. Hui Jiang (University of Michigan, School of Public Health). Following alignment, count matrices were analyzed for differential expression compared to their individual controls using DESeq2. Genes were considered differentially expressed based on the following criteria: FC>1.5, FDR<0.05. Venn diagrams were generated using Interactivenn. Heat maps and spearman correlation matrices were generated using Prism.

5.3 Datasets Included in Comparative Transcriptomic Analysis

In order to compare SBMA to myopathy, an RNAseq dataset generated from the mdx-mTR Duchenne's Muscular Dystrophy (DMD) mouse model was used [1]. These mice contain mutations in dytrophin-1 as in Duchenne's patients, as well as a mutation in telomerase which potentiates the disease phenotype. Dystrophin-1 is a key structural component of the membrane of myotubules, mutation of which leads to loss of myofiber structural integrity and damage to the muscle with use.

To model neuropathic change, RNA sequencing data from denervated muscle (3 days post sciatic nerve transection) was used. This muscle is structurally intact but has lost communication with the central nervous system resulting in paralysis [2]. This leads to a well-characterized rapid induction of the atrophy pathway as mentioned previously in this thesis.

These datasets were compared against two skeletal muscle data sets generated in our lab from previously described AR113Q knock-in mice at 14 weeks of age [3-5]. One data set is from the quadriceps, which is early symptomatic at this time point, and one is from the levator ani/bulbocavernosus muscle (LABC), which is severely atrophic due to a high level of androgen receptor expression. Using the aforementioned data sets allow for comparison between early changes in SBMA muscle as well as the changes which remain through severe stages of atrophy and are consistent across multiple muscles.

In order to focus on changes downstream of polyglutamine protein expression in muscle, we included the quadriceps of 12 week old R6/2 mice, which overexpress an N-terminal fragment of polyglutamine Huntingtin. These mice develop age progressive muscle atrophy accompanied by polyglutamine inclusions and misfolding [6]. Importantly, these mice develop this phenotype without any androgen receptor loss of function. This allows us to be sure that changes are due to polyglutamine protein expression and not androgen receptor loss of function.

RNA sequencing data was included from AR113Q knock-in mice in which androgen receptor was mutated to promote DNA binding and transactivation (KRKR). The modification of two lysines to arginine prevents SUMOylation, a ubiquitin like post-translational modification

which impairs AR transactivation [5]. This mutation leads to increased action of polyglutamine androgen receptor as a hormone-dependent transcriptional regulator and rescues loss of function effects.

Finally, RNA-seq data was included from AR113Q mice treated with antisense oligonucleotides from 6 to 14 weeks of age [4]. These mice have significantly diminished expression of androgen receptor in the periphery, leading to rescue of the neuromuscular phenotype and gain of function changes downstream of the polyglutamine expansion while exacerbating changes which occur due to loss of function.

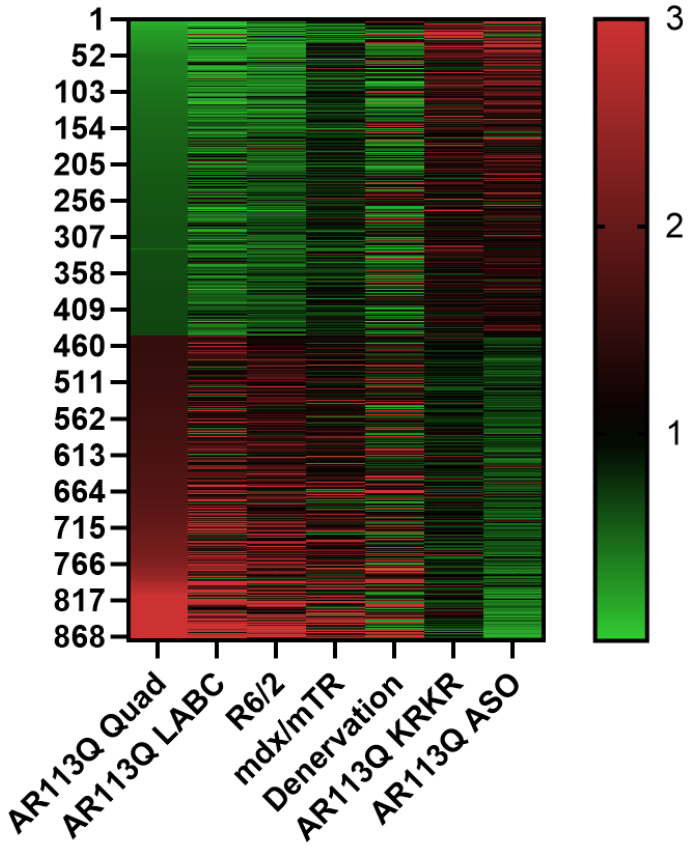

Figure 5.1. Heat map of RNAseq data sets. A comparison of transcriptomic changes between mice expressing polyglutamine proteins, muscular dystrophy, and denervation. AR113Q = SBMA knock-in mouse, R6/2 = polyQ huntingtin transgenic mouse, mdx/mTR = Duchenne's Muscular Dystrophy mouse model.

5.4 Examining Transcriptome Overlap Between Multiple Causes of Muscle Dysfunction

All datasets were analyzed using DESeq2 to quantify differential expression and fold change [7]. To determine similarity between sets, we compared genes significantly altered in the SBMA quadriceps at a timepoint of early symptom onset in SBMA across all other data sets (Figure 1). Confirming a conserved network of changes downstream of polyglutamine androgen receptor in muscle, we saw a high degree of concordance between the LABC and the Quadriceps of

AR113Q mice (Lane 1 and 2, Figure 5.1). This degree of concordance was maintained for the quadriceps muscle of the R6/2 mouse, demonstrating that it is the polyglutamine tract and not androgen receptor context that drives the vast majority of these changes.

As expected, we saw a significant reversal of these gene changes upon treatment with antisense oligonucleotides which diminish polyQ AR expression. This finding demonstrates that most transcriptome changes are dependent on the mutant protein and not due to loss of function, which would be exacerbated by ASO administration. Surprisingly, we saw a less robust but noticeable rescue of many of these changes in gene expression in the AR113Q KRKR mouse. We suggest that forcing the androgen receptor to transactivate and regulate gene expression leads to less toxic gain of function by the mutant protein and an ASO-like effect in these mice.

5.5 Comparing SBMA to DMD and Denervation as Models of Myopathy and Neuropathy

Next, we sought to use these data to quantify correlations between our data sets and establish the degree of similarity between genes changing in polyglutamine mice and those occurring in models of myopathy and neuropathy. To accomplish this, we compared the above datasets to the mdx-mtr mouse, a model of myopathic change due to an intrinsic muscle defect, and denervated muscle, a model for neuropathic change in muscle due to loss of nerve input.

To determine similarities, we performed a Spearman Log-Rank Correlation test across these data sets (Figure 5.2). This analysis supported our impressions of the heatmaps, as described above. We found high correlation coefficients between AR113Q quadriceps, LABC, and R6/2 quadriceps. In support of ASOs rescuing disease at a transcriptomic level, we saw a negative correlation coefficient when comparing ASOs to all 3 polyglutamine affected muscles. Intriguingly, this negative correlation holds up strongly for even the R6/2 mouse, which expresses polyQ Htt rather than AR, demonstrating that the glutamine tract is the most important factor for toxicity in the muscle. We also saw a significant negative correlation with the KRKR mouse, which partially rescues

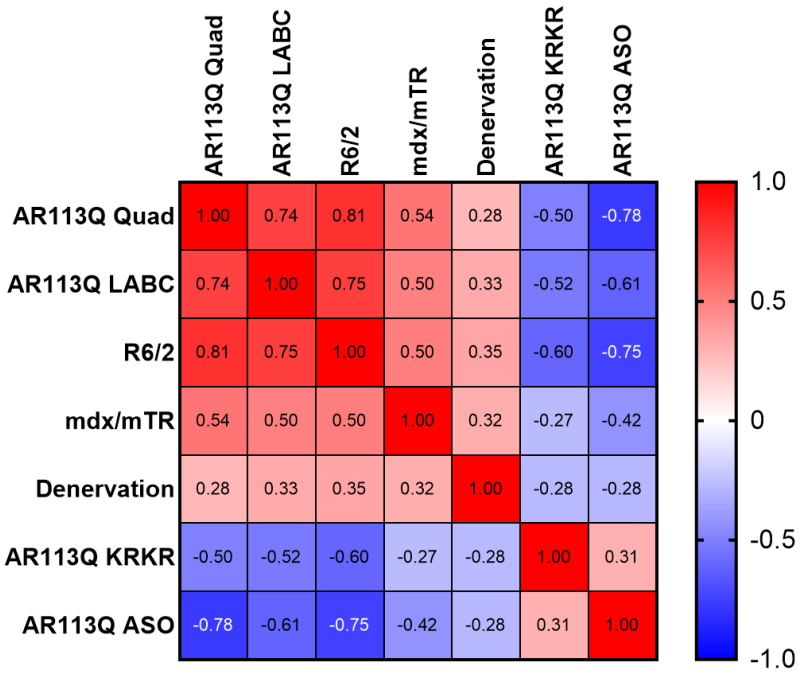

Figure 5.2. Spearman Log-Rank correlation of RNAseq datasets.

the phenotype by promoting AR transactivation. This finding further supports our hypothesis that promoting normal function of AR may lower the amount of toxic gain of function.

5.6 Comparing Polyglutamine Disease Transcriptomic Change to mdx/mTR and Denervation

When comparing our models of myopathy and neuropathy to polyglutamine protein expressing mice, we found a positive correlation for both. However, the correlation was stronger (.50-.54, p=1.68e-55 to 2.74e-68) for the model of myopathy than for the model of neuropathy (.28-.35, p=1.12e-17 to 1.18e-22). These results support the idea that intrinsic muscle defects may play an important role in SBMA. They also indicate that SBMA shows features of both myopathic and neuropathic change at a transcriptomic level.

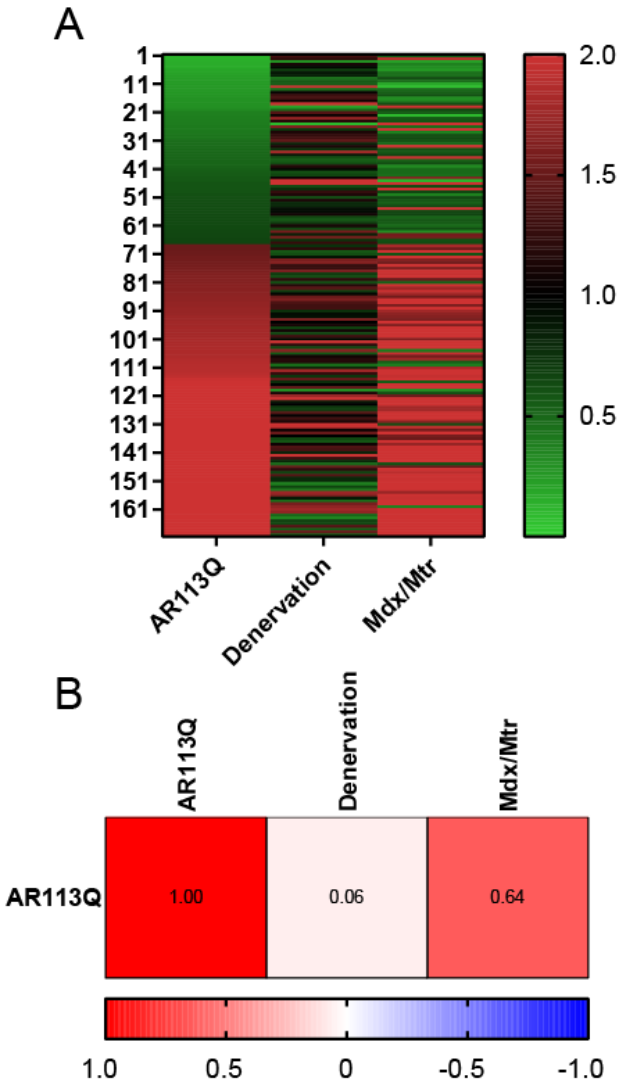

Figure 5.3. Genes unique to myopathy and AR113Q muscle. A. Heat map of genes uniquely differentially expressed (FDR<0.05, FC>1.5) in AR113Q and mdx/mTR mice. B. Spearman log-rank correlation of differentially expressed genes.

To further assess the relationship of SBMA to models of myopathy or neuropathy, we examined genes uniquely altered in both the AR113Q quadriceps and either mdx/mTR or denervation models. 170 genes were differentially expressed in mdx/mTR and AR113Q quadriceps and not in denervation (Figure 5.3A). Performing a Spearman correlation matrix on this subset of genes, we found a strong correlation (.64, p = 2.06e-21) between AR113Q and mdx/mTR, indicating these changes are predominantly in the same direction and of similar magnitude (Figure 5.3B). Performing the same analysis for AR113Q and denervated mice, we found 245 genes differentially expressed uniquely in both (Figure 5.4A). However, the directionality of the gene expression changes was less correlated (.21, p=0.001). Unexpectedly, the mdx/mTR mouse had a stronger correlation (.35, p=1.15e-8) even amongst this set of genes, despite the fact that they did not reach the threshold for differential expression. This data collectively supports the original hypothesis that AR113Q mice are more similar at a transcriptomic level with myopathic than neuropathic change.

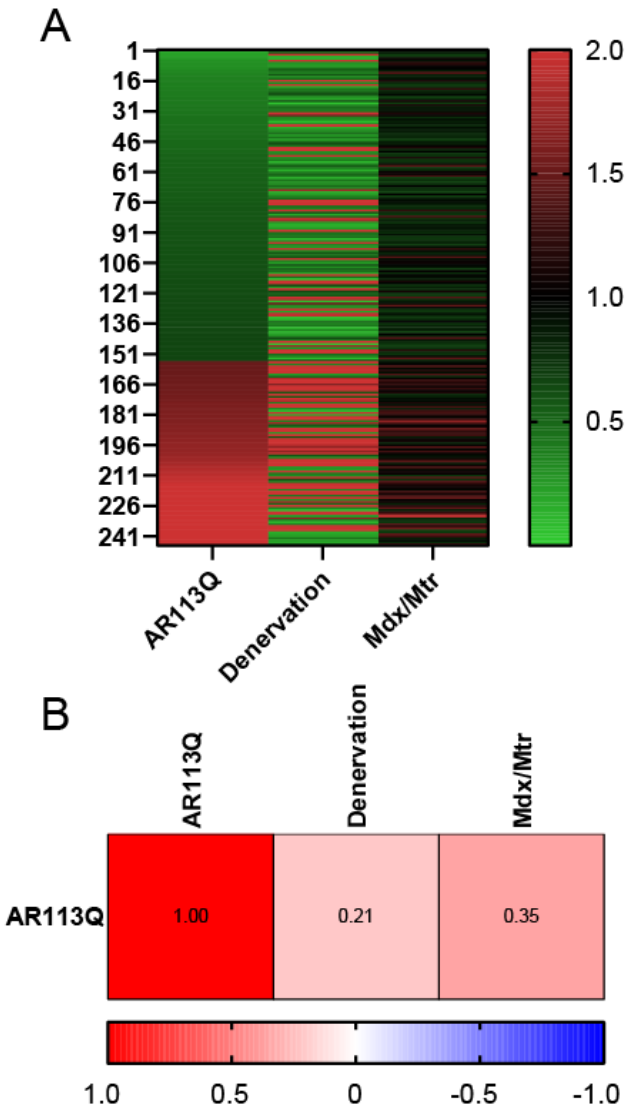

Figure 5.4. Genes unique to denervation and AR113Q muscle. A. Heat map of genes uniquely differentially expressed (FDR<0.05, FC>1.5) in AR113Q and denervated mice. B. Spearman log-rank correlation of differentially expressed genes.

Finally, we sought to establish what pathway level changes occur downstream of polyglutamine proteins in muscle. To do this, we filtered for genes significantly changing (FDR<0.05) in all three data sets of polyQ mice (AR113Q quad, AR113Q LABC, R6/2) and that are rescued by ASO treatment of AR113Q mice (Figure 5.5). We identified 213 genes meeting these criteria. We split these genes into two categories: those going down in polyQ disease and

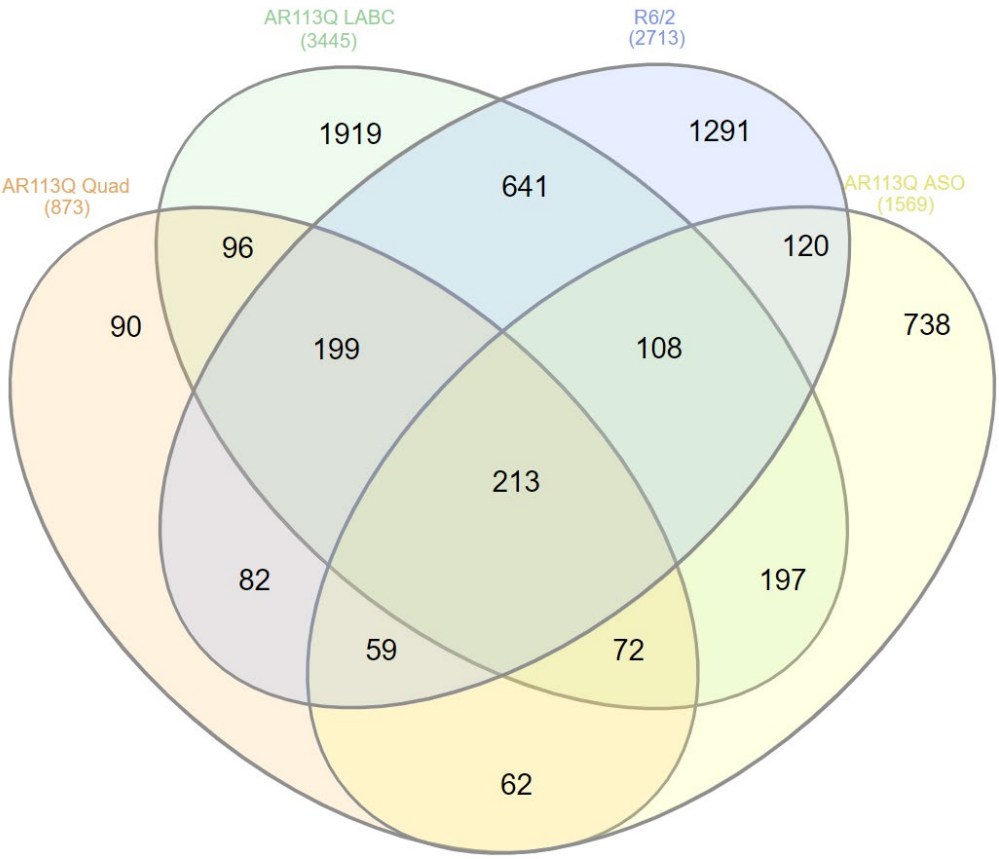

Figure 5.5. Defining gain of function changes in skeletal muscle downstream of polyglutamine proteins. Differentially expressed genes in skeletal muscle of AR113Q Quad, AR113Q LABC, R6/2 Quad, and AR113Q Quad treated with antisense oligonucleotides were examined for overlap.

those going up. We ran both lists through GO Term analysis using GSEA to determine what categories are significantly altered by polyQ proteins in muscle. By analyzing downregulated genes, we found that all five of our top five hits related to genes of muscle contraction and the sarcomere, reinforcing the last chapter's conclusion that loss of MEF2 targets is a major change

downstream of polyglutamine proteins in muscle (Figure 5.6). For upregulated genes, we found that three out of the top five hits were related to exocytosis and secretion. This is a currently uncharacterized change in SBMA. This raises the possibility that polyglutamine proteins lead to increased secretion and exocytosis from skeletal muscle. As several studies have demonstrated that exocytosis is a key mechanism for communication with the liver, pancreas, and brain, it is possible that these pathways may be altered in some way by polyglutamine proteins and should be addressed by future studies.

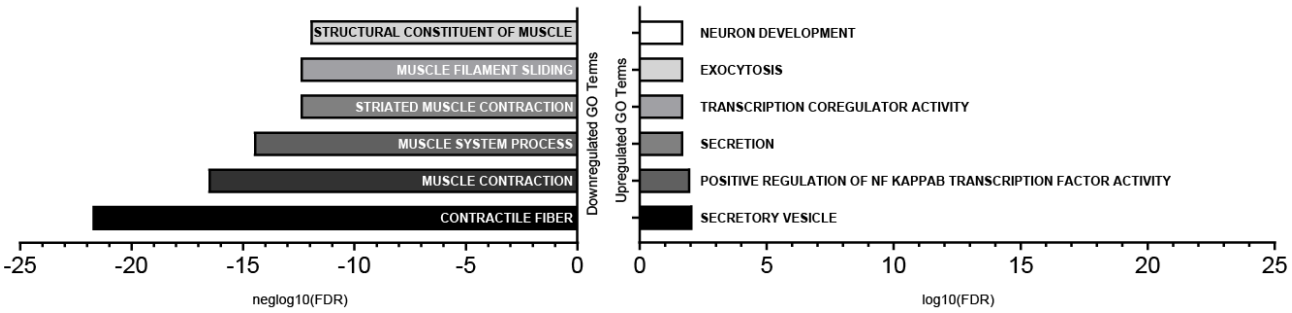

Figure 5.6. GO Term analysis of polyQ gain of function genes. Upregulated genes are on the right and downregulated genes are on the left.

5.7 Conclusions and Future Directions

The data presented across chapters 3-5 support the surprising finding in SBMA that muscle plays a key role in pathogenesis of disease and define a paradigm shift in which canonical pathways of muscle atrophy are suppressed in SBMA and MEF2 impairment plays a key role in progression. As demonstrated by leveraging ASO treatment in SBMA mice, changes within skeletal muscle represent a primary target for therapeutics and warrant further study. Though great progress is being made in skeletal muscle physiology, several key questions remain unaddressed. It is currently unknown whether the alterations in skeletal muscle drive the later

onset neurological phenotype, or if these represent two independently progressive sites of toxicity. The finding of increased transcriptional expression of genes associated with exocytosis is exciting as it represents a possible mechanism for communication between skeletal muscle and other organ systems such as the CNS and warrants further exploration. The recent discovery that up to half of SBMA patients show signs of steatosis or steatohepatitis supports communication between the skeletal muscle, CNS, and the liver. Finally, while we have shown MEF2 activation is a potential therapeutic strategy in SBMA, whether this is viable in the long term is not known. Additionally, no well-characterized MEF2 activating small molecules have been described. I propose that follow-up studies should focus on characterizing three key areas: 1) Clarifying the mechanism of communication between skeletal muscle and neurons, 2) Further characterization of MEF2's therapeutic potential in long term treatment, and 3) Defining additional and complementary mechanisms of skeletal muscle wasting in SBMA. By better understanding these key areas, we can enable the development of targeted therapeutics for muscle wasting downstream of polyglutamine proteins.

References

1. Sacco, A., et al., *Short telomeres and stem cell exhaustion model Duchenne muscular dystrophy in mdx/mTR mice.* Cell, 2010. **143**(7): p. 1059-71.
2. Macpherson, P.C., P. Farshi, and D. Goldman, *Dach2-Hdac9 signaling regulates reinnervation of muscle endplates.* Development, 2015. **142**(23): p. 4038-48.
3. Yu, Z., et al., *Androgen-dependent pathology demonstrates myopathic contribution to the Kennedy disease phenotype in a mouse knock-in model.* The Journal of clinical investigation, 2006. **116**(10): p. 2663-2672.
4. Giorgetti, E., et al., *Rescue of Metabolic Alterations in AR113Q Skeletal Muscle by Peripheral Androgen Receptor Gene Silencing.* Cell Rep, 2016. **17**(1): p. 125-36.
5. Chua, J.P., et al., *Disrupting SUMOylation enhances transcriptional function and ameliorates polyglutamine androgen receptor-mediated disease.* J Clin Invest, 2015. **125**(2): p. 831-45.
6. Bondulich, M.K., et al., *Myostatin inhibition prevents skeletal muscle pathophysiology in Huntington's disease mice.* Sci Rep, 2017. **7**(1): p. 14275.
7. Love, M.I., W. Huber, and S. Anders, *Moderated estimation of fold change and dispersion for RNA-seq data with DESeq2.* Genome Biol, 2014. **15**(12): p. 550.